



Chilean Senate Ratifies Agreement with ESO

Riccardo Giacconi, Director General of ESO

On 5 September 1996, the Senate of the Republic of Chile (Second Chamber of the Parliament) approved the Interpretative, Supplementary and Modifying Agreement to the Convention of 1963, which regulates the relations between the European Southern Observatory and its host country, the Republic of Chile.

Following formal approval by the ESO Council, it is expected that instruments of ratification could be exchanged before the end of this year.

The completion of this process is a reason for great mutual satisfaction as the new Agreement consolidates the already existing good relationship between ESO and the Government of Chile, and heralds a new era of cooperation with benefits for both parties.

The ratification of this Agreement is of particular value for ESO, now engaged at Cerro Paranal in the construction of the largest telescope of the world, because it signifies a pillar of stability for the future activities of this Organisation in Chile and thus for the development and operation of the VLT observatory into the next century. The European astronomical community now has full security that it can continue to pursue its front-line scientific investigations in Chile.

At the same time the Chilean astronomers will have privileged access

within up to 10 per cent of observing time on all present and future ESO telescopes in Chile. They also will have membership on all ESO scientific and technical committees. Chilean and European scientific communities will henceforth share the important scientific discoveries which will be made with the VLT facility at Cerro Paranal.

By this Agreement the ESO regulations for local Chilean staff will be modified to incorporate the principles of Chilean legislation regarding collective bargaining and freedom of association. This new regulation will be drafted in consultation with a representative of the Chilean Government as well as local staff representatives.

Concerning ESO's juridical immunity on all of the territory of Chile, the Government of Chile has indicated to ESO that these immunities are clearly stipulated in the 1963 Convention and that it is applicable to all properties and possessions of the Organisation, wherever they are located in Chile. Those properties, according to the Convention, should only be used by the Organisation in Chile for scientific and official purposes. The Acuerdo reconfirms these immunities and their validity for both, Paranal and La Silla Observatories. The issue of ownership of the Paranal site had been settled earlier in the year by the Chilean

government in direct negotiation with the private claimants.

As part of this Agreement ESO will continue and increase its contributions to the development of Chilean astronomy and the educational and cultural development of local communities. ESO is indebted to the Government of Chile and especially to the Minister of Foreign Relations, Don José Miguel Insulza, and all those who have worked towards this Agreement and its ratification by the Chilean Parliament.

I wish also to recognise the contribution of all those at ESO who played a role in bringing this about. The ESO negotiating committee included both previous and present Presidents of the ESO Council, Professor Franco Pacini and Dr. Peter Creola, as well as many members of the Council. We are particularly indebted to Mr. Daniel Hofstadt who has played a continued and significant role in the improvement of the Chile-ESO relations.

Together with all our partners in Europe and Chile, ESO can continue enthusiastically in this new and exciting scientific adventure of building the Very Large Telescope. All humanity without regard of national boundaries, will benefit from the wealth of new knowledge in the origin and evolution of the physical universe in which we live, which this powerful new observatory will bring about.

The M1 Cell-M3 Tower of the VLT Design Overview and Manufacturing Progress

S. STANGHELLINI, ESO

Introduction

The primary mirror cell and the primary support system of the VLT have to fulfil stringent requirements. The thin meniscus blank demands a high-precision support system and good structural stiffness. Despite its moderate thickness, the weight of the primary mirror exceeds 23 tons. To be compatible with the overall VLT telescope design, which has been optimised to give a high first eigenfrequency of the tube, the design of the M1 cell must be a light but stiff structure. In addition, the primary mirror support system has to be able to cope with the inevitable deflection associated with the large dimensions. Preliminary studies showed that a space frame of approximately 10 tons weight, together with an appropriate hydraulic support system, would be suitable to support the primary mirror of the VLT.

The M1 cell forms part of the sub-assembly called M1 Cell-M3 Tower, and comprises, in addition to the primary cell and tertiary mirror supporting tower, the safety and handling support system of the primary mirror, the cooling system for the primary mirror, and the complete control electronics.

In April 1993, following preliminary feasibility studies, ESO awarded competitive design and development contracts to two European consortia, leading to a complete design of the M1 Cell-M3 Tower, and to a reduced scale mock-up of the M1 support system with actual size prototypes. The design of the French consortium composed of GIAT Industries – Branche Gitech, and SFIM Industries was finally selected by ESO, and a contract for the construction of this unit was awarded to the same consortium in February 1995. The major characteristics are described here, together with the summary of the manufacturing status.

M1 Cell Design and Construction

The design of the M1 cell is based on the possibilities offered by laser cutting and welding technology of which GIAT Industries is a leader in Europe. The technology allows the manufacture of very complicated structures starting from thin metal sheets. It is possible to obtain large beams with very thin walls and internal reinforcements which is not

possible when using standard profiles. This possibility is extensively exploited in the M1 cell design to generate the variable section profiles used in the 12 radial rafters, and the complicated structures on which the mirror supports are mounted. The various faces of the structural beams and boxes are cut out from selected metal sheets in the desired shape by a computer guided infrared laser beam. The precision of the cuts is

such that, after manually pre-assembling the beams, it is possible to weld them in an automatic mode along the seam without any fillet material. A minimum amount of heat is introduced into the metal, and the residual stresses are low, which is advantageous for the dimensional stability.

In summary, the laser technology results in the following advantages for the design and the construction:

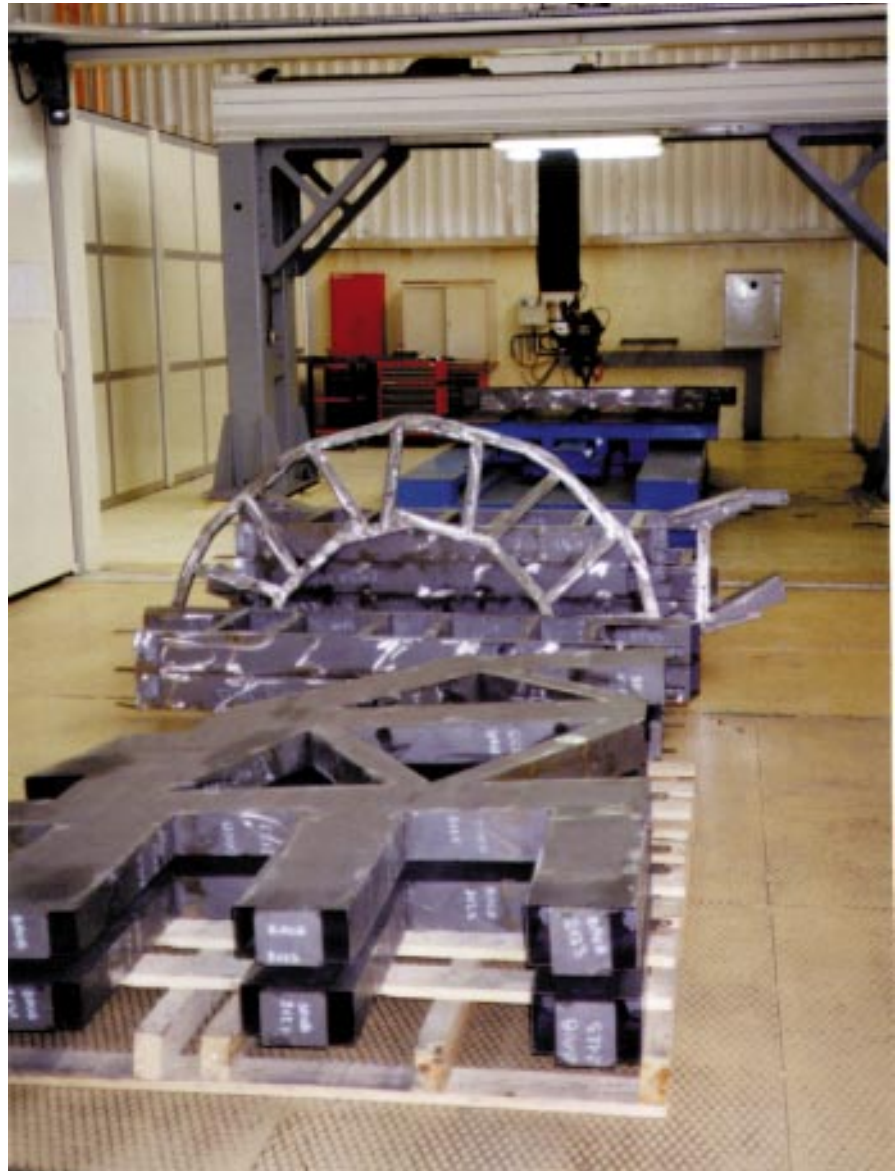
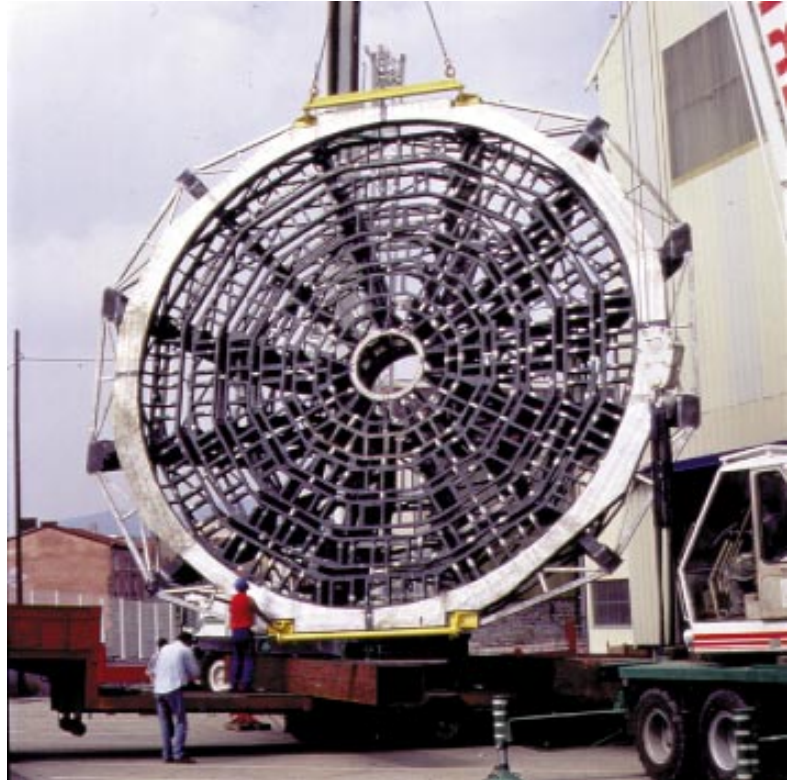


Figure 1: GIAT laser welding shop with preassembled parts of the cell.



Figures 2a and 2b: The M1 cell.

- absence of complex structural nodes requiring complicated cuts and welding,
- optimum utilisation of the steel with the use of thin sheets and tapered sections,
- excellent dimensional stability,
- larger internal space for the installation of equipment and better access than in a conventional space frame structure,

- the laser cutting and welding process, being computer controlled, is more economical for building four units of the M1 cells than standard construction methods. (See Fig.1.)

The M1 cell resembles a truncated cone with the upper surface having a diameter of approximately 10 m, and a thickness of 2.8 m. There are twelve tapered radial rafters, each of which extends from one of the attachment points

to the telescope at the edge to three annular belts (rings) at the centre. Two of these belts are used for the M3 tower and its rotating stage, and the third for the Cassegrain instrumentation. All the assemblies have internal reinforcements to stiffen the thin walls. The top surface of the M1 cell is made of 7 concentric rings which have been manufactured using laser technology and are used for mounting the axial and lateral

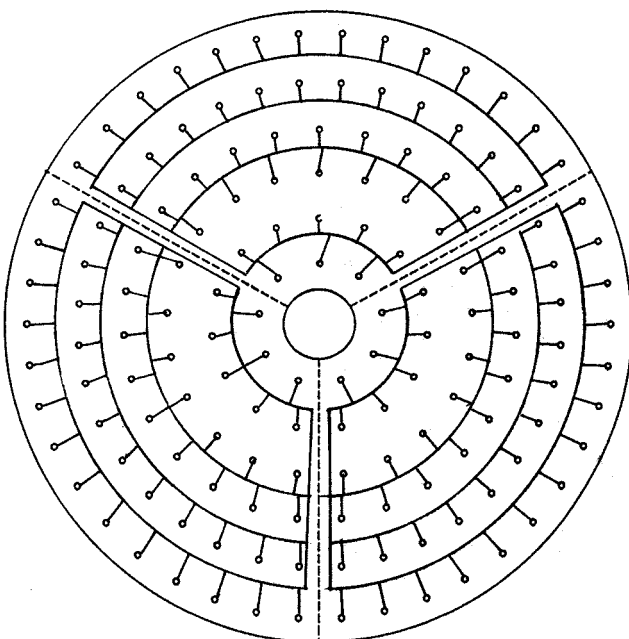


Figure 3a: Topology of axial support hydraulic circuits.



Figure 3b: Passive axial support prototype.

supports. The most external ring is used as base for the lateral M1 supports, while the 6 internal rings, resembling ladders, are used for the M1 axial supports, and for the safety and handling system supports. The thickness of the plates used in the ladders and their cross sections are variable, increasing from the centre to the periphery. (See Figs. 2a and 2b.)

The axial supports are positioned in the cut-outs of the ladders by interfaces allowing the fine adjustment of the support position. The position of the cross beams connecting the rafters and contributing to the general stiffness of the M1 cell has been optimised, as far as possible, to leave free space for the various pieces of electromechanical equipment. These include the electronic cabinets of the M1 Cell-M3 Tower and the Cassegrain instrumentation, and the various hydraulic components of the M1 hydraulic support system. It is worth mentioning here that the final mass of the M1 cell is approximately 10.5 tons, while its first elastic mode, once fully loaded and mounted onto the telescope exceeds 14 Hz. Its stiffness is such that the rigid displacement of the primary mirror when moving from zenith to horizon is only a few tenths of a millimetre.

The M1 Support System

The axial support system comprises 150 axial support points on 6 concentric rings, which combine a passive hydraulic pad and an electromechanical force actuator. The hydraulic pads, connected in three hydraulic sectors, act like astatic levers, supporting the mirror weight while removing the gravity deflection. The force actuators are used for active optics correction by adding or subtracting a force to the fraction of the mirror weight carried by each hydraulic pad. The lateral support system acts at the outer rim of the mirror by means of passive hydraulic pads.

The axial force is applied to load spreaders at the mirror back by means of a dedicated flexure, which also exercises a safety function against overload. The lateral supports use the same hydraulic pad design as the axial ones, but the load is carried by means of a special lever connected to the mirror by a cardan joint.

A considerable effort has been spent on the definition and the testing of the passive supports. The version finally selected makes use of two hydraulic chambers, one supporting the weight of the mirror, the other compensating the hydrostatic pressure generated when the telescope is tilted. The passive axial support is largely astatic to cope with the M1 cell deflection, and free from dangerous friction or hysteresis. The stiffness of the support is such that the

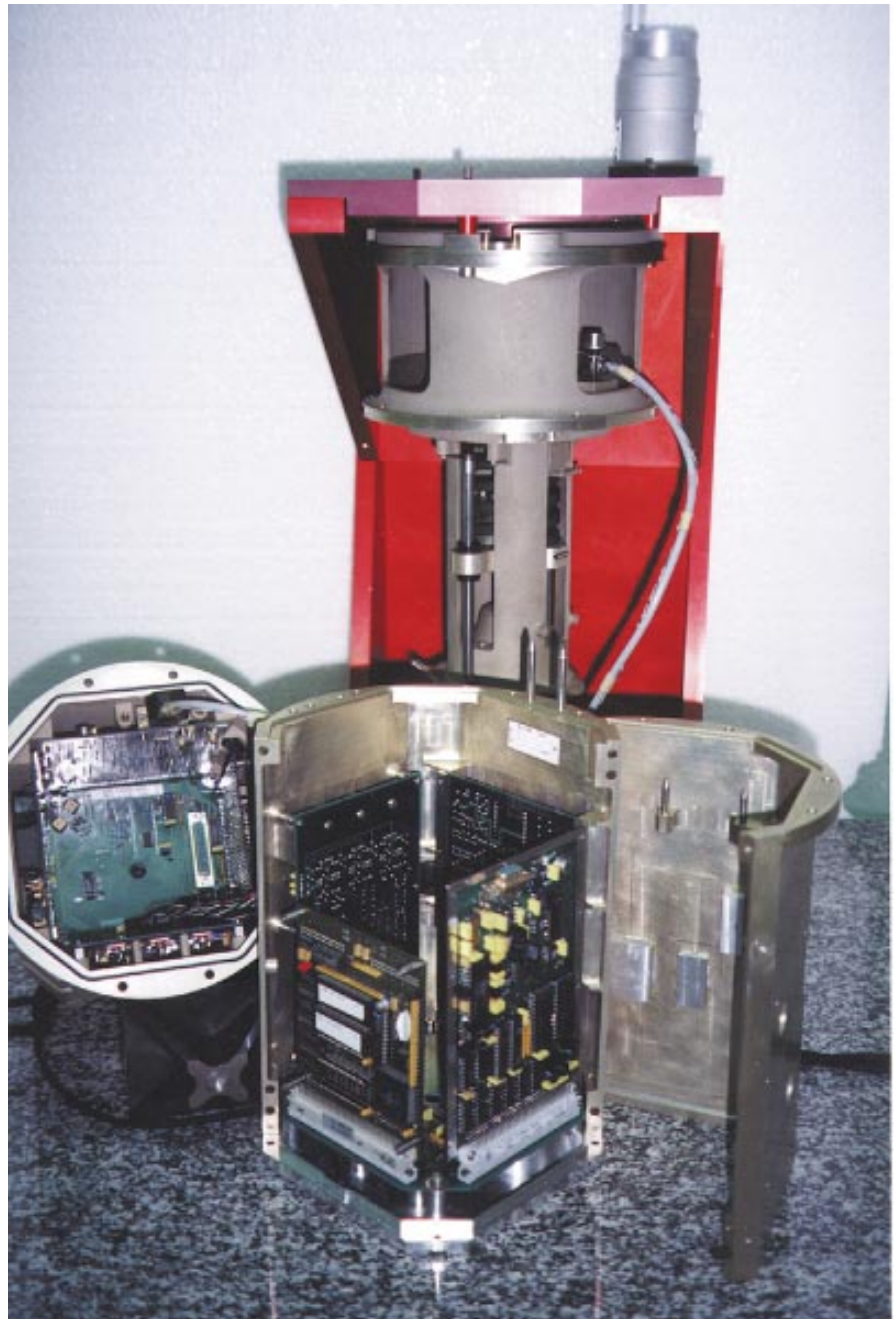


Figure 4: Active axial force actuator.

first rigid axial mode of the primary mirror M1 on its supports exceeds 25 Hz, which is important for the dynamics of the telescope and for the resistance to wind buffeting.

During the design phase, much attention was dedicated to the study of the topology of the hydraulic circuits of the passive supports. The topology, together with the pipe diameter and the viscosity of the fluid used, influences the dynamics of the active correction and the resistance to wind buffeting on the primary. A good compromise was sought to be able to perform active optics correction with fast settling time as well as to be able to damp the effect of wind on the primary. A parallel connection between the passive supports was chosen together with the possi-

bility of adapting the degree of connection between the hydraulic sectors to match the prevailing wind condition. The selected topology was chosen on the basis of dynamic simulations which included the dynamics of the mirror and of the M1 cell. (See Figs. 3a and 3b.)

As most of the wind energy is located in frequencies above 1 Hz, it is interesting in case of wind to reduce the bandwidth of the system to below this frequency. This is done by means of remotely operated valves installed in the external circumferential pipes which slow the movement of the oil as occurring during astigmatic deflection of the primary. In the event of wind excitation, this has the effect of stiffening the primary mirror by coupling it in the astig-

matic mode to the M1 cell for high temporal frequencies without violating the principle of a kinematic mount.

Given the moderate thickness of the blank, the force actuators used for active optics correction must be extremely accurate. Their force resolution is 0.05 N as determined by the minimum amount of astigmatism which must be corrected. The required force range of 500 N pull and 800 N push force depends on various factors, including the final polishing accuracy of the primary mirror, the effort required to bend the primary mirror to Cassegrain shape, and the active optics forces.

Each of the 150 force actuators has its own microcomputer to control its function and to communicate with the Local Control Unit of the M1 Cell-M3 Tower by means of a dedicated bus. This minimises the cabling and increases the reliability of the system. The individual actuators are composed of an electromechanical part and an electronic part. The electromechanical part generates a force by the compression of a spring and transmits it to the shaft of the passive hydraulic support through a load cell of high resolution and linearity. The electronic boards are assembled inside a mechanical casing ensuring thermal conduction and electromagnetic shielding. The few watts of power dissipated are transferred by heat pipes from the casing to the M1 cold plate to minimise heat dissipation to the surrounding (see Fig. 4).

The M1 Safety and Handling Support System

The behaviour of the M1 cell during an earthquake is influenced by the dynamics of the telescope structure. Response spectra analyses carried out with the complete telescope model have shown that a dedicated safety support system must be used in case of earthquake to restrain safely the primary mirror. The system uses radial and axial elastomer pads, mounted onto hydraulic jacks, which are pressurised if an earthquake is detected by an independent accelerometer.

The axial pads mounted below the primary mirror can also be used to lift the primary mirror above the M1 cell when removal is necessary for periodical recoating. This is done when the M1 cell with the primary mirror has been transported to the maintenance building using a special transportation carriage. Once the mirror has been lifted from its support system, an overhead handling crane installed in the Mirror Maintenance Building takes the primary and places it in the coating plant.

Primary Mirror Cooling

To reduce the mirror seeing, the primary mirror can be cooled to allow the temperature of the mirror to be as close as possible to the temperature of the ambient air at the beginning of the night and to follow its evolution during the night. The cooling is performed by means of a radiation cold plate located just below the M1 mirror and mounted on the M1 cell. The cold plate is realised by means of rolled aluminium plates on which copper tubes are fixed by brazing. The cooling fluid is provided through the telescope structure. The cold plate located approximately 20 cm away from the rear surface of the mirror is supported on the M1 cell by elastic dampers to avoid any vibration. The cold cavity between mirror and cold plate is closed by a soft rubber seal without contact to the mirror. Small fans in the cavity can be operated to move the air around mylar obstacles to avoid stratification and improving the cooling. Temperature sensors are fixed to the cold plate and to the M1 in order to control the cooling process.

Given the statistical distribution of the air temperature of the clear nights during the year at Paranal, it is expected that the M1 cooling system used in conjunction with the air conditioning in the enclosure and temperature prediction models will allow the temperature of the front mirror surface to be maintained within $-1.0^{\circ}\text{C} / +0.2^{\circ}\text{C}$ from ambient for over 80 % of the total observation time.

The M3 Tower

The tertiary mirror of the VLT is installed on a tower which is attached to the M1 cell. The mechanical system of the M3 tower allows the focus of the telescope to be selected. The M3 tower is divided in two parts. The lower part, containing the rotating stage to shift between the Nasmyth A and B, is mounted on the M1 cell. The upper removable part extends through the central hole of the primary mirror and is connected to a flange of the rotating stage. The rotating stage makes use of a pre-stressed bearing and a worm gear drive.

A sophisticated control law copes with the friction in the system and ensures a good repeatability of the positioning. Once in the desired position, the tower is locked with a pneumatic brake. This solution, in conjunction with the use of aluminium for the superior part, allows considerable stiffness to be attained and assures the stability of the M3 position. The first elastic mode of the tower exceeds 20 Hz.

Given the dimensions of the VLT and the obvious difficulty of gaining access to the tertiary mirror, a motorised support system for the tertiary mirror has been included to fine tune its position remotely. In addition, the M3 can be moved outside the beam by a remotely operated stowing mechanism to allow the use of the Cassegrain focus. An Atmospheric Dispersion Compensator, when required by the Cassegrain instrumentation, can be installed inside the lower part of the rotating stage.

Manufacturing Status

The first M1 cell has now been completed. The cell was assembled on a dedicated jig at the St-Chamond factory of GIAT. The laser welded subassemblies, after having been annealed, were assembled from top to bottom on the jig and manually welded together. The manual welds were shot peened to avoid any risk of cracking. Once completely assembled, the M1 cell was turned and the various interfaces and reference points measured with the help of theodolites. Finally the flanges of the M3 tower and of the Cassegrain rotator adapter were machined. The M1 cell was then sand blasted and painted.

The second M1 cell is now in production. Most of the laser subassemblies have already been produced and assembly will start as required by the delivery plan.

Two M3 towers have been manufactured in parallel. The first one is ready to be integrated in the M1 cell while the second unit is used to perform parallel testing of the LCU. The support system of the primary mirror is now in serial production. The force actuators are produced by SFIM Industries in Paris while the passive supports are produced by GIAT in Tarbes. The first batch of supports is now available to start the system integration in the GIAT assembly hall at St-Chamond. The cold plate of the primary mirror and the heat pipes to cool the force actuator are also in production.

A complete cycle of testing is foreseen in Europe for the M1 Cell-M3 Tower. The testing foresees the use of a concrete dummy primary mirror to check the complete functionality. To install the mirror in the M1 cell, the M1 Handling Tool, to be eventually installed in the Mirror Maintenance Building in Chile, will be used. The tool has been designed by GIAT and its installation in the assembly hall is presently underway.

Stefano Stanghellini
e-mail: sstanghe@eso.org

VLT Systems Engineering Group Moving Ahead

T. ANDERSEN, ESO

Large projects require participation of many specialists working in different fields. Though highly capable, it is not possible for each of these specialists to have a complete overview of the project. Hence, in large projects like the VLT, there is a trend towards installing a separate systems engineering group to assist the programme manager in keeping a technical overview.

The task of systems engineering for the VLT was initially performed by staff of the Telescope Department. However, to further strengthen the organisation of the VLT, a separate Systems Engineering Group was set up at the beginning of 1995. At present, the group has five members that are all specialised in system analysis or synthesis.

Finite Element Computations

Execution of finite-element calculations is one important working field of the group. Many VLT contractors carry out calculations of this nature for subsystems. However, to ensure correct modelling, it is necessary to supply simplified computer models of the interfacing structure. It is also necessary to combine models from subcontractors to ensure that the performance of the complete telescope will be satisfactory.

Such combined models tend to become large with many thousands of degrees of freedom. Hence, it is often required to reduce model size by applying superelements or condensation techniques. Figure 1 shows a finite element model of the complete telescope. The model is based on various submodels received from contractors.

The model has over 100 000 degrees of freedom. Since it is a formidable task to solve 100 000 equations, reduction techniques have been applied to reduce

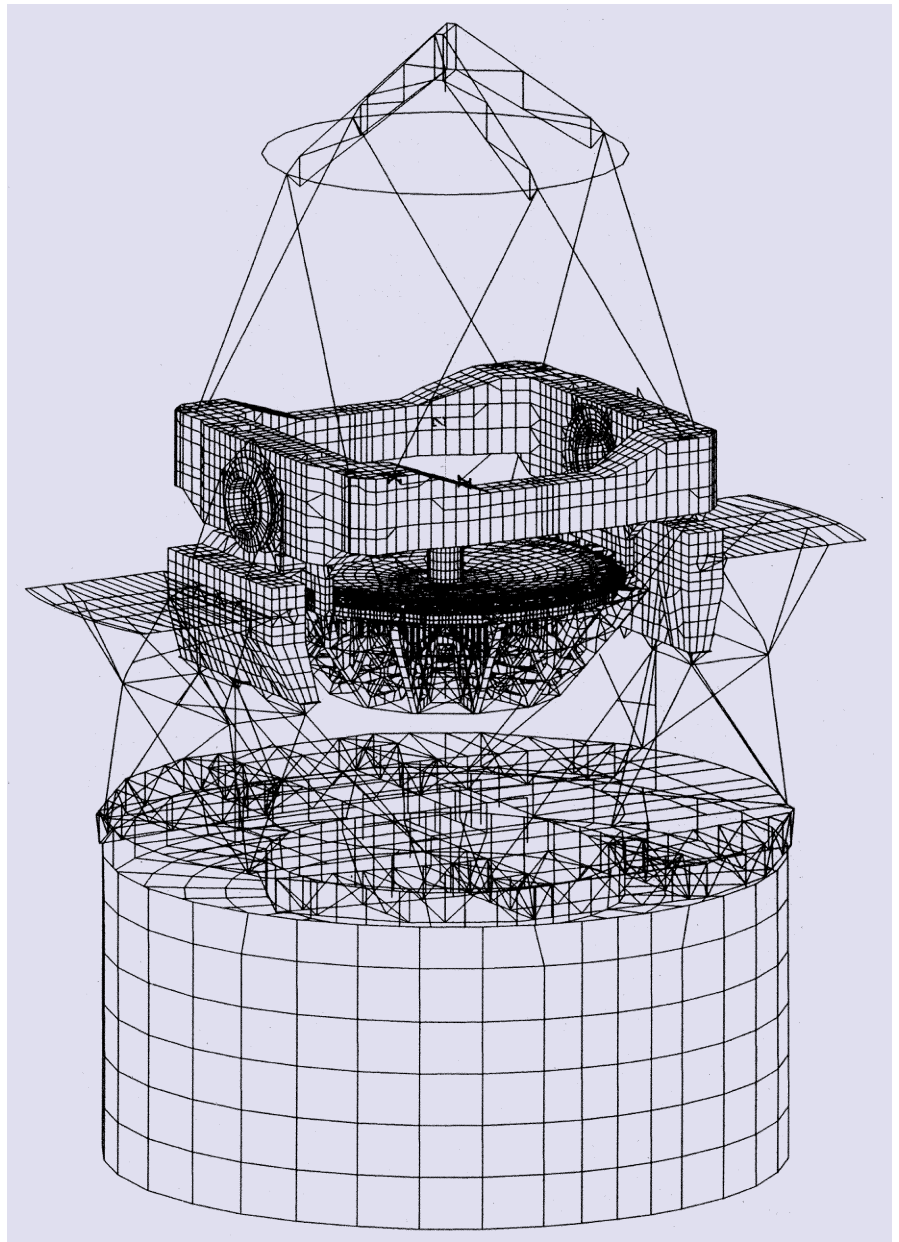


Figure 1. Finite-element model of a unit telescope of the VLT. The model has over 100,000 degrees of freedom.

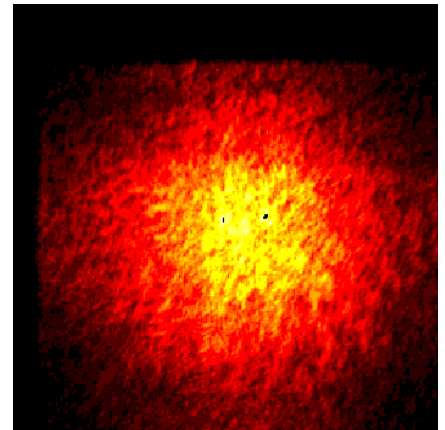
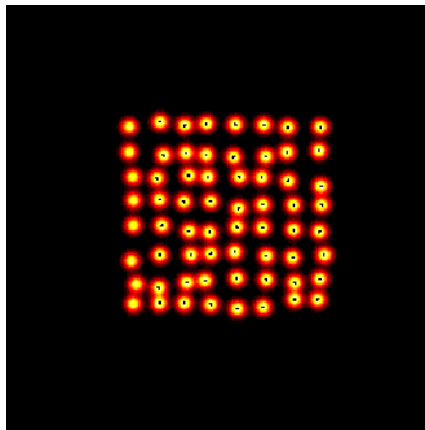
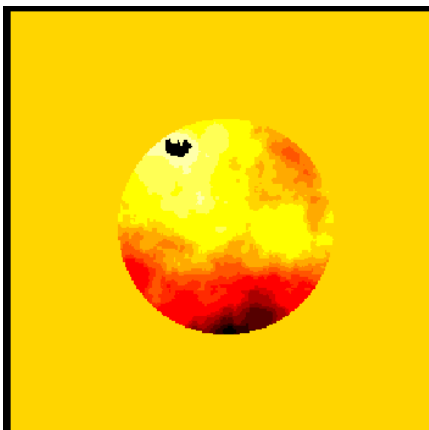


Figure 2. Atmospheric phase screen (left), Shack-Hartmann pattern in wavefront sensor (middle), and final star image (right).

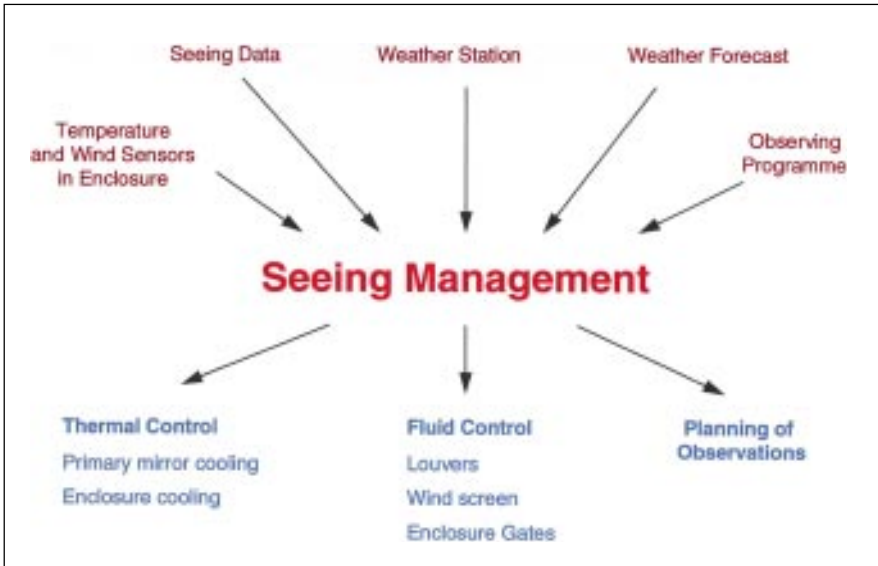


Figure 3. The philosophy of seeing management for the VLT.

the number of degrees of freedom to about 40,000 before solving the equations.

Simulation Models

It is essential to be able to predict accurately the VLT performance, and to study the effect of changes or malfunctions. To achieve this, a simulation model including optics, structural dynamics, mirror support system, atmosphere, detectors, and active optics has been set up. The computer model simulates telescope performance in the time domain.

The simulation model has been applied to study a number of different effects, in particular those related to performance of the active optics system under wind load. Some representative results are shown in Figure 2.

Currently, a simulation model of the VLT Interferometer system is being developed. The model will include optics, disturbances from atmosphere and tunnel turbulence, star characteristics, detector dynamics, fringe sensor, control loops and structural dynamics. The model should be ready in about one year. Ultimately, it will interface to a scientific module that will permit evaluation of VLT scientific performance.

Seeing Management

Although seeing can normally not be controlled freely, it can be strongly influenced by a proper thermal and fluid dynamical control. A diagram depicting the seeing management philosophy is shown in Figure 3.

A thermal computer model of the VLT has been set up to study possible control strategies. Also, a strategy for establishing optimal cooling of the telescope and primary mirror has been established.

Currently, implementation of the model in the VLT control system is in preparation.

A strategy for the control of the wind screen, louvers, and hatches has been formulated. For different wind speeds and pointing angles with respect to wind, a decision table has been derived. This is illustrated in Figure 4, showing the settings of wind screen, louvers and hatches for different situations.

Configuration Control

A large number of documents and drawings have been issued for the VLT. During design, manufacture and installation of the telescopes it is inevitable

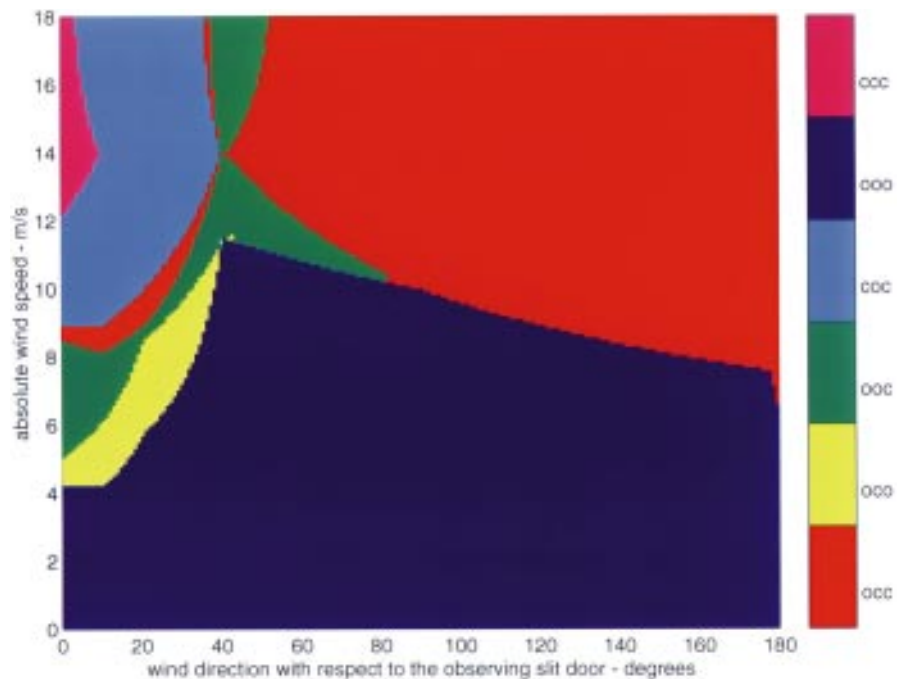


Figure 4. Diagram showing setting of ventilation doors, louvers, and wind screen as a function of angle to wind and wind speed. Letter code: First character=ventilation doors, second character=louvers, third character=wind screen. O=open, C=closed.

that changes or corrections are introduced. To assist in contract management and to preserve integrity in the documentation material, configuration control must be performed at an appropriate level.

Procedures have been set up for the handling of changes and waivers. Further, support related to failure reports is given to the Quality Assurance manager.

Not least due to the great distance between Paranal and Garching, it was found essential to establish a computerised tool for configuration control. The functionality of this tool has recently been specified and suitable ways of implementation are being studied. It is the intention to have a first version of the tool in place before testing of the first telescope in Milano. Besides the tasks dealt with above, it would provide for electronic problem reporting and a daily log book. Access via the Web is foreseen for authorised users.

Finally, complete drawing libraries will be set up both on Paranal and in Garching.

Integration and Commissioning

Systems engineering has participated actively in the planning of integration and commissioning on Paranal. Systems engineering will participate in these activities and will provide a link between the engineering groups in Garching and Paranal.

Other Activities

Systems engineering is giving support to various teams at ESO related to

engineering activities in the definition phase, or modifications and upgrades to existing systems. One example is a possible implementation of a nutating sub-reflector for the SEST. Development of such a facility is presently contracted to a subcontractor.

Conclusion

VLT Systems Engineering has now been fully set up and is in operation. It is expected that VLT Systems Engineering will play an important role during commissioning. Finally, Systems Engineer-

ing is seen as the nucleus for possible new large projects of ESO.

Torben Andersen
e-mail: tanderse@eso.org

KODAK Technical Pan 4415 Film at the ESO Schmidt Telescope

BO REIPURTH, ESO

For the past 25 years the ESO Schmidt telescope has operated with photographic plates, first using the Ila emulsions, and later the finer-grained IIIaJ and IIIaF emulsions. For a number of reasons, we have now discontinued the use of emulsions on glass plates and have changed to a new film-based emulsion. Firstly, prices for our large 30 cm × 30 cm plates have been increasing in recent years, and are now close to 100 US dollars per plate. Secondly, Kodak has for extended periods had difficulties delivering plates, and the continued production of large glass plates has been in doubt. Finally, and most importantly, reports from the United Kingdom Schmidt Telescope Unit on the astronomical use of Kodak's Tech-Pan 4415 film have been very positive. Consequently, one of our plateholders has been redesigned at La Silla for the use of film, and we are now in the final stages of an extended period of testing this new system.

Kodak Tech-Pan 4415 film is a black-and-white panchromatic negative film with extended red sensitivity. It has a fairly uniform spectral sensitivity at all visible wavelengths, and extends out to 690 nm, which makes it particularly useful for work at H α . In fact, solar astronomers doing H α photographs of the surface of the Sun were the first to exploit this emulsion for astronomical purposes. Night time astronomical use of the 4415 emulsion was pioneered by amateur astronomers, and it remained exclusively in amateur use until the UKSTU undertook a major study of its astronomical applications a few years ago (e.g. Parker et al., 1994). The film is extremely fine grained, with grains of about half the size of the IIIa emulsions, allowing much higher resolution. The sensitivity is very high for a photographic emulsion, and a DQE of 4–5% has been estimated for hypered emulsions.

As for most photographic emulsions, the best results for astronomical purposes with the 4415 emulsion are achieved when it is hypered. Tests at La Silla have shown that optimum results are achieved when the film is baked at

70°C and soaked in a flow of Nitrogen for 30 minutes followed by Hydrogen for 6 hours. After exposure the film is developed in D19 at 20°C for 8 minutes.

Glass plates have the advantage that they are stiff, and our plateholders have employed a simple mechanical pressure

along the edges of the plates to bend them to the shape of the precisely machined mandrel. A similar method will not work for a film, so Wolfgang Eckert designed at La Silla a set of fine interconnected grooves in the mandrel, which, when connected to a vacuum

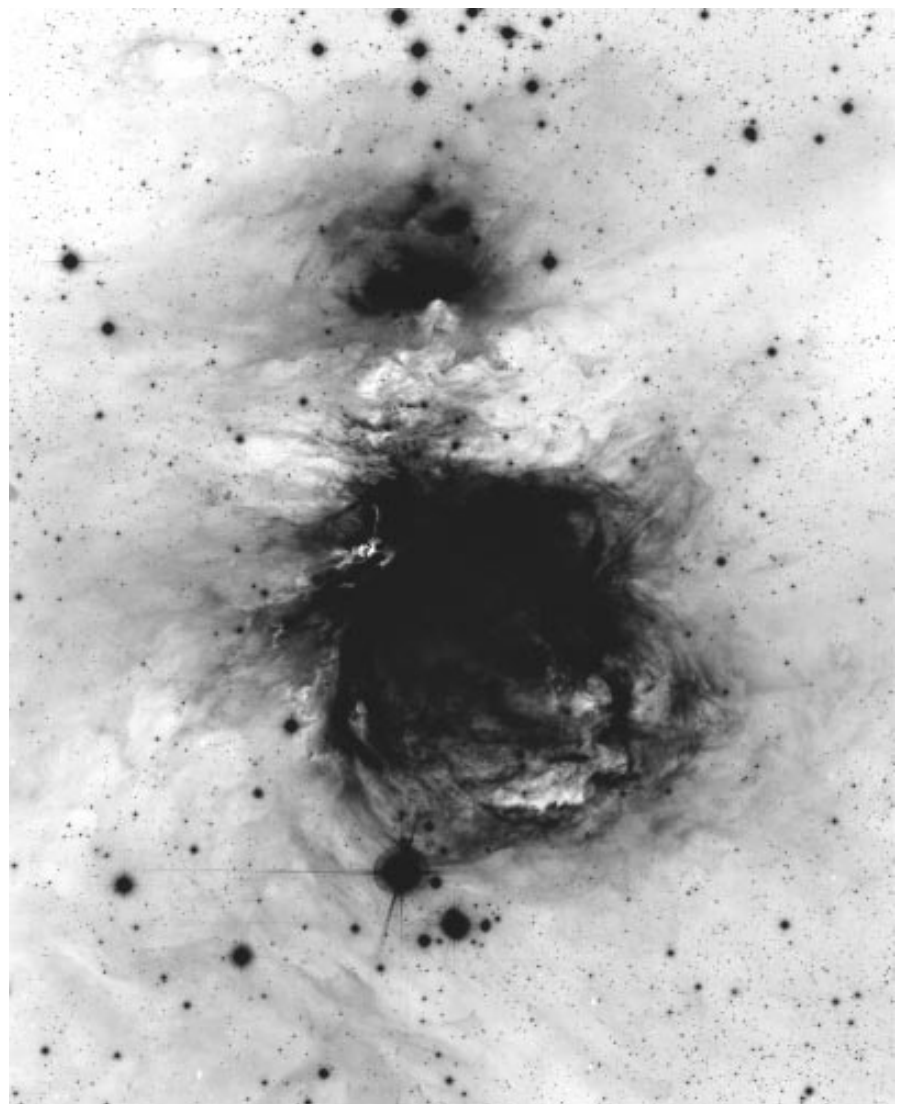


Figure 1: Part of an ESO Schmidt exposure of 150 minutes duration using the new Kodak Tech-Pan 4415 film-based emulsion and an RG 630 filter, showing the Orion Nebula.

pump, will hold the film firmly against the surface of the mandrel. The contact between film and mandrel is so tight that even a small dust grain will show up as a tiny deformation in the smooth film surface. The image quality is uniformly excellent across the film, with the exception of a small region in one corner, and we are currently looking into how to correct this.

In addition to its sensitivity and resolution, the Tech-Pan 4415 film has a number of practical advantages. One is cost, since the price of a 30 cm × 30 cm film currently is about 10 US dollars, almost a factor of ten lower than for the glass plates used up to now. Other advantages are the ability of storing hypered emulsions for longer periods without degradation, and the ease of transport. In the future, films will be mailed directly from La Silla to the users, without the delay of sending them via Garching, as was done for the glass plates.

The arrival of film at the ESO Schmidt telescope and the end to the use of emulsions on glass plates has, however, two disadvantages. The principal one is that we, at least for now, cannot take blue exposures that can be photometrically calibrated. To create a band-pass similar to B or V we would in the past select an appropriate filter that defines the blue limit and an appropriate emulsion that defines the red limit. However, the 4415 emulsion always has a red limit of 690 nm. We have looked into the possibility of purchasing a special B-band and V-band filter set, but for the very large size that we require, prices are exorbitant. Another problem with our blue filters is that they have red leaks. These red leaks were not of any consequence for our old glass-based emulsions with their more limited wavelength range, but

they overlap with the extended red sensitivity of the 4415 emulsion. A possible exception to the above comments is our UG1 filter (300 nm–400 nm), where the contamination of red light appears to be small. The red leak of UG1 starts at 670 nm, and the tail of the 4415 emulsion sensitivity reaches out to 690 nm. We have tried to qualitatively estimate the effect of this impurity by exposing a 4415 emulsion through the UG1 filter and our objective prism. It turns out that for only the very brightest stars do the resulting spectra show a small and very weak red spectral component. This suggests that the red contamination is small, and that the UG1 filter can be used to make ultraviolet/blue exposures for projects where high photometric accuracy is not critical.

The second disadvantage is that it is not clear that films have the same structural stability as glass, and consequently high-precision astrometry is not recommended with film. The thick (178 μm) ester base that supports the emulsion has nonetheless great strength, and with a sufficiently fine grid of astrometric reference stars, it is likely that good results can be achieved, although a specific study is required to establish this.

Figure 1 shows part of an exposure on 4415 film centred on the Orion Nebula. The exposure was 150 minutes through a RG 630 filter, which transmits in particular the H α emission of the region. The delicate large-scale structure of the HII region is remarkably well detected, and provides an example of data which can only be produced with a wide-field instrument like a Schmidt camera. Other recent studies that are now being carried out with the new 4415 emulsion include surveys for microlensing events towards the Galactic Bulge, light curves

of RR Lyrae stars in a nearby galaxy, studies of large tidal tails of globular clusters, variability of young X-ray sources around molecular clouds, searches for new Trojan asteroids, and large-scale structure of the bright comets Hyakutake and Hale-Bopp. Also, using the objective prism, a major systematic survey is in progress, which identifies new young H α emission stars in all the star forming dark clouds along the southern galactic plane; more than 1000 new pre-main sequence stars have already been discovered this way.

The ESO Schmidt telescope, with its large 5° by 5° field, continues to be a unique facility for the ESO community, and with the introduction of a modern, fine-grained and highly sensitive emulsion like the 4415 Tech-Pan emulsion, users are now able to conduct large-scale surveys that are deeper and have better resolution than in the past.

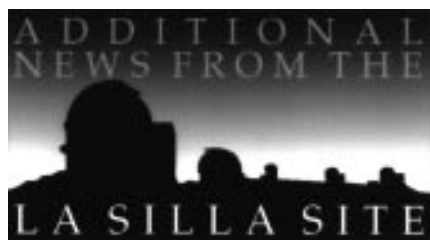
Acknowledgements

I am grateful to Quentin A. Parker of the United Kingdom Schmidt Telescope Unit for supplying very useful information on the progress of 4415 film use at the UKSTU in the early phases of this work. I also thank Lucky Achmad and night assistants Guido and Oscar Pizarro, who carried out the extensive hypering and development tests.

References

Parker, Q.A., Philipps, S., Morgan, D.H., Malin, D.F., Russell, K.S., Hartley, M., Savage, A.: 1994, in *Astronomy from Wide-Field Imaging*, IAU Symposium No. 161, eds. H.T. MacGillivray et al., p.129.

Bo Reipurth
breipur@eso.org



The La Silla News Page

The editors of the La Silla News Page would like to welcome readers of the fifth edition of a page devoted to reporting on technical updates and observational achievements at La Silla. We would like this page to inform the astronomical community of changes made to telescopes, instruments, operations, and of instrumental performances that cannot be

reported conveniently elsewhere. Contributions and inquiries to this page from the community are most welcome. (P. Bouchet, R. Gredel, C. Lidman)

News from the 3.6-m Upgrade Project

L. PASQUINI, U. WEILENMANN; ESO La Silla

1. Introduction

The objective of the 3.6-m Upgrade Project is to improve performance and operations of the 3.6-m telescope, and

to put this telescope into the front line for the first decade of the next century. In order to reach this goal, several points have to be investigated to firmly establish the real telescope capabilities,

namely:

- (i) Image quality and seeing,
- (ii) M1 degradation and
- (iii) Telescope pointing and mechanical behaviour.

In the course of the last year, these studies have been carried out and the first results obtained were presented at the ESO UC/STC in April 1996.

Some of the early reports have been reported in *The Messenger* (Gilliotte, 1996; Guisard, 1996; No. 83). The document presented at the UC/STC is available in the 3.6-m+CAT www page.

The 3.6-m Upgrade, in addition to the refurbishment of the telescope, also foresees an upgrade of the present instrumentation and instrument control, according to a plan which follows the suggestions of the 'La Silla 2000 Committee' (Andersen, 1996). The instrumentation plan is given in Table 1.

At first, the status of the Upgrade Project shall be briefly illustrated and thereafter detailed information will be given on the two important issues of the main mirror aluminisation and image quality analysis.

2. The Status of the Upgrade Project

The Upgrade Project has been divided in smaller sub-projects, called work components (WC). An overview is given in Table 2. Activity has been already started in 15 WC's, most of the requirement specifications have passed review by this time and are ready for the conceptual design.

The definition of the TCS GUI (graphical user interface) (WC1) is one of the major tasks. The aim is to develop one single standard user interface that shall be available for all telescopes at La Silla in the future. There is a lot of experience accumulated at La Silla for building the human-machine interface, and an attempt is made to receive from the review as much input as possible. The TCS software (WC2) will be VLT compatible to the largest extent possible, the difference is found at the level of the servos and the interface to existing subsystems which are not subject to upgrade.

The conceptual design for the modification of the Cassegrain adapter and the calibration unit (WC6) is already well advanced. Most of the opto-mechanical functions will be refurbished, but without building a new adapter. Great care shall be taken in order to limit heat dissipation in the adapter. The guide-probe field will be ~ 36' and the unvignetted field for EFOSC2 6' x 6'. The new calibration unit will be housed in two intermediate flanges which are required because of (i) the different front focal distance of EFOSC2 and (ii) the new position of the focal plan. The unit consists of an integrating sphere in the upper flange with fiber-fed calibration sources located outside the adapter, both for space reasons and also to prevent heat dissipation. The same calibration unit will also be available for the CES fiber link (WC 45). A

Table 1: Base Line Instrumentation

Instrument	In Operation	Decommissioned
EFOSC 1	Now	June 1997
EFOSC 2	October 1997	July 1999
CASPEC	Now	January 2000
ADONIS	Now	January 2001
TIMMI 2	January 1999	January 2003
CES Very High Res.	January 1998	January 2003

VLT-standard technical CCD is employed for the guide-probe and centre field and it shall have a position accuracy of < 1". A second CCD will be used for image analysing and for the slit view option. First it was planned to use the same CCD, but optical and mechanical constraints oblige us to choose an approach with two CCDs.

The auxiliary functions (WC 5) are already well advanced and due for review, further work has to be closely co-ordinated with the Cassegrain adapter and the calibration unit, as these functions are controlled from the same subsystem.

The upgrade of EFOSC2 includes WC 11 for the GUI, WC 15 for the instrument modification like new grisms, polarimetry mode, Lyot stop, MOS wheel and the mechanical interface to the telescope, and WC 17 for the MOS star plates punching machine. EFOSC2 shall be controlled by modern instrument control SW (ICS), similar to EMMI at the NTT.

The same applies for CASPEC (WC 12), but there is no instrument

modification foreseen here. CASPEC will be later in the pipeline, as priority has been given to EFOSC2.

The Cassegrain/CES fiber link (WC 45) and the Image Slicer/Focal Enlarger (WC 53) are in the preliminary design phase. For the very high-resolution option it is foreseen to seek the collaboration with an interested institute. Two minor work components are: (i) the modification of the F/35 infrared top end, to increase the adjustment range for the coma correction. This implementation will take place already in October, and: (ii) the installation of pneumatic sensors on the lateral support pads of the main mirror for diagnostic purposes.

For TIMMI 2, an external institute (University Observatory Jena) made an interesting proposal to ESO and they could provide this instrument by the 1st Quarter of 1999. TIMMI 2 shall fulfil the important role to serve as a test bench for the VLT-VISIR instrumentation. A memorandum of understanding is presently being prepared.

Table 2: Work Components for the 3.6-m Upgrade Project

WC	Description	Status
1, 2	TCS: Graphical User Interface and Control SW	Requ. Specs.
4	Autoguider with technical CCD	Requ. Specs.
5	Auxiliary Systems Functions	Prelim. Design
6	Modification of F/8 Cassegrain Adapter and new Calibration	Unit Design Review
11, 15	EFOSC 2: Instrument Control Software and Instrument Modification	Requ. Specs.
17	MOS Starplate Punching Machine	Requ. Specs.
12	CASPEC: Instrument Control Software	Requ. Specs.
19	F/35: Top End Modification	Prelim. Design
31, 32	Image Quality & Seeing and Structural Analysis of Telescope	Study
35	Hydraulic and Pneumatic Sensors for Pressure Monitoring	Study
45, 53	CES: Fiber Adapter and Image Slicer	Prelim. Design
-	TIMMI 2 (external provider)	Negotiations
-	CES: Very Long Camera (external provider)	Negotiations

3. Report on the Technical Time in June 1996

J. FLUXÁ, S. GUISARD, G. IHLE; ESO

Although a lot of the work is still in the requirement specification phase (see Table 2), a few urgent interventions were needed, and the study of some of the

relevant telescope aspects had to be completed.

In the two last weeks of June the main mirror aluminisation was per-

formed (somewhat in advance to the normal schedule), and the opportunity was taken to perform some of the work, in particular in the area of thermal and mechanical control of the telescope and of the image quality problem. This report summarises these actions:

3.1 Installation of Water Cooled Electronic Racks in the Cassegrain Cage

The heat produced by the racks inside the Cassegrain cage can be as high as 1KW and is dissipated below the primary mirror cell, resulting in an increase of the mirror temperature always above ambient temperature. Getting rid of this major heat source was essential to improve both, dome and mirror seeing. Water cooled racks have now been installed which house the electronics for the control of the adapter functions and auxiliary systems. All the cabling had to be refurbished and the control electronics re-assembled in the new racks. Obsolete items have been removed to obtain space and gain simplicity. Extensive testing was required thereafter and servicing of a couple of functions was necessary too. Additional refrigerated racks can be installed in the cage to accommodate the instrument control electronics.

3.2 Re-Arrangement of the Mirror Cover

This was probably one of the most impressive changes made at the 3.6-m. To reduce mirror seeing, it is essential that the mirror temperature matches the air temperature. This usually involves cooling during the day and, in some cases, ventilation when the outside temperature increases during the night. With the old configuration (the primary mirror was completely enclosed inside the centre piece) it would have never been possible to build an efficient cooling and ventilation system. For this reason, the mirror cover has been moved from its old position (a few centimetres above the mirror) to the top of the centre piece some 2 metres above the mirror. This change has several advantages:

- the space, where the cover was located, provides now for full access to the mirror surface (about 30 cm space), and could be used for forced mirror ventilation.
- there is now a direct access between the mirror and the declination axis hole, located in the centre piece. This 90-cm hole was part of the Coudé train of the telescope. It could now be used as an air duct to cool the mirror with air coming from the telescope base.

This operation required a lot of time

due to the heavy work involved (grinding off welded parts, etc.) and cleaning of the complete telescope and its environment was necessary thereafter. Most of the hardware, like motor units, drive shafts, etc. have been "recycled" and are again in use.

3.3 Elimination of M3

This point is not directly related to the improvement of the image quality but it was necessary for the relocation of the mirror cover above the centre piece. However, the 2500 kg of metal and glass that have been removed can only help to reduce telescope flexure and will improve the dynamical behaviour of the telescope. Although some difficulties were expected for the balancing of the telescope after dismantling M3, the

range of the polar counterweight could be extended by taking off the heavy cable cover (500 kg) on the delta twist of the other (West) side.

3.4 Installation of New Sensors for M1 and Mirror Cell

A study on the thermal behaviour of the dome is currently being developed by Philippe Sacre (ESO Garching) with the intention to build a simple thermal model that gives a prediction of the temperatures in the dome and on M1 as a function of external parameters. New temperature sensors have been installed on M1 and on the mirror cell together with the corresponding cabling. Displacement sensors have also been installed to measure possible movements of M1 inside the cell.

4. M1 Aluminisation and Status

A. GILLIOTTE; ESO

4.1 Aluminisation

The last aluminisation was performed in October 1994. After coating, a reflectivity of 89.5% and a micro-roughness of 60 Å was measured. These parameters were re-evaluated before the 1996 aluminisation, giving a reflectivity of 84.6% and a micro-roughness of 86 Å. These values are very good, when considering the 19 months of time between aluminisations, and these achievements have been obtained thanks to the CO₂ cleaning performed regularly during this period.

After mirror washing, the measurements were repeated, by using an Atomic Force Microscope. The reflectivity increased to 89% and the micro-roughness decreased to 65 Å. Then the standard procedure was applied: aluminium layer removal, alcohol cleaning and removal of dust particles. The coating plant was modified and improved last year; now a better vacuum pressure can be achieved than in the past, and the coating process runs in automatic mode. The aluminisation was very successful, resulting in a reflectivity of 90.5% and 59.5 Å micro-roughness.

One interesting conclusion from this set of measurements is the fact that the 3.6-m mirror coating interval may be more than 2 years, provided these figures can be confirmed in the future. This result is in agreement with the good photometric stability of EFOSC (Benetti, 1996, *The Messenger* No. 83). Also, they show the importance of a regular CO₂ mirror cleaning.

4.2 M1 Status

Although a more detailed report will be given elsewhere (Gilliotte, in prepara-

tion), some of the results can be anticipated:

1. The analysis of the mirror surface showed that no new "frosted zones" developed, when comparing the 1996 and the 1994 mirror defect maps.
2. The analysis of the mirror surface showed that the degradation of the mirror is produced by an increase of the micro-hole (digs) density. In these areas the glass looks to be more fragile and sensitive to scratches. The reflectivity in these zones is only 85% and the roughness increases to 120 Å.
3. For the first time it was possible to measure and compare the reflectivity with and without the specular reflection, with two different techniques.

The results show that: at 670 nm, the reflectivity of the "good" and "affected" regions is of 90% and 86%, the diffusion 1.1% and 8.1% respectively. At 400 nm, the diffusion increases to 1.6% in the good zones and to 17% in the frosted zones.

A roughness of 59 Å produces a diffusion within a 2 π solid angle of 1.1% whereas a value of 120 Å produces 8.1% at 670 nm. The results on the frosted zones at 400 nm indicate that reflectivity measurements in the B-UV will be needed in the future.

The previous analysis (Gilliotte, 1995, *The Messenger* No. 82) can be confirmed at the moment: frosted zones still are limited to only 2% of the mirror surface, and their contribution to the diffusion is very limited, comparable to the effects due to dust.

5. The Image Quality of the 3.6-m Telescope: Part III

S. GUIARD; ESO

In this report, in addition to the description of the work performed during the technical nights, a discussion of the current interpretation of the last measurements is given. Further investigation and confirmation is still required. Unfortunately, the nights scheduled at the beginning of August for this purposes have been lost due to inclement weather.

5.1 Checking the Lateral and Axial Mirror Supports

As highlighted in a previous report (Guisard, 1996, *The Messenger* No. 83), problems with the mirror support were discovered after the October 1994 aluminisation. This resulted in large aberrations (astigmatism, triangular and quadratic) even at zenith. All the forces of axial astatic levers were checked, they were found to be within 10 kg, except for three of the inner levers which were within 20 kg of the nominal values. The accuracy of the weighting method is about 10 kg, so that all the levers, except the three, have nominal values.

All levers have been moved several times, to ensure that any friction of the axis was eliminated, which could restrain the transmission of the force of the counterweight to the mirror.

The pneumatic lateral supports were also dismantled completely. It appeared that more than half of the supports (11 of 18) had rubber pads that were seriously damaged.

The rubber in the damaged pads was renewed. We now know that this rubber is too thick and too rigid. Problems had appeared after the October 1994 aluminisation when the rubber of all the pads were changed. More appropriate rubber has to be found. Time has been asked in November to replace the rubber on all the lateral supports.

5.2 Aberration at Zenith

At zenith, the telescope mirror is supported only by the axial supports. The lateral supports, although in contact with the mirror, should not apply any force to the mirror edge. Otherwise the mirror shape would be deformed and hence the image quality be degraded.

Abnormally high aberration at zenith has been recorded after the last aluminisation in October 1994.

In June 1996, a new set of measurements was made with the lateral supports completely loosened. For safety reasons, only the fixed points were touching the mirror edge but were not tightened. The data are summarised in Table 3 together with the results from October 1994. It can be seen that the resulting aberrations are much smaller.

TABLE 3: Aberrations

	Oct. 1994	June 1996 Loose	June 1996 Tight 0°	June 1996 10°	June 1996 20°
Astigmatism	0.40"	0.20"	0.20"	0.35"	0.50"
Triangular	0.45"	0.20"	0.20"	0.25"	0.30"
Quadratic	0.20"	0.10"	0.10"	0.10"	0.10"
Total	0.65"	0.30"	0.30"	0.45"	0.60"

After these measurements, the following steps were taken to re-establish the lateral support:

- tightening the lateral fixed points to 50 Nm and then to 70 Nm
- putting the lateral pads in contact with the mirror edge without air
- applying air pressure to the pads

Tightening the lateral fix points or pressurising the pads did not degrade the image at zenith; however, the aberration increases with larger zenith distances, as shown in Table 3. Clearly the telescope suffers from degradation and in addition the aberrations do not always return to the initial value when returning to zenith.

If the lateral supports do not keep the mirror correctly nor push it back into its normal position, stress at the contact points between the glass and the support (lateral and axial) will de-figure the mirror shape. Time has been requested at the end of November to change the rubber of the lateral pads and check the proper operation of the REOSC system.

5.3 Measuring the Spherical Aberration at the Cassegrain Focus

In the technical nights in June, measurements of the spherical aberration of the 3.6-m telescope were also performed, by using both, Antares and the Curvature Sensing method (Roddi-

er, 1993). These preliminary data show that the correct focal plane of the telescope is 12 cm below the actual focal plane.

The idea of the presence of spherical aberration at the 3.6-m telescope came out from the analysis of the Antares data, taken after 1991, whose results are summarised in Table 4. A spherical term is present, although with variable amount.

At first, noise and imprecision in the Antares measurements were suspected, but now we know that there are several reasons to believe that the Antares measurements are reliable:

1. Measurements made with Antares on other telescopes like the NTT and the 2.2-m show that the spherical aberration is smaller than 0.1". We know the quality of the images these telescopes can provide.

2. On February 9, 1996, the spherical aberration was 0.5" with Antares, a direct CCD gave a FWHM of 0.73". A seeing monitor inside the dome measured 0.5" of combined site and dome seeing. If we consider the Antares value (0.5"), the dome and outside seeing (0.5"), and the usual residual aberrations at zenith (0.3") we come up with a total image quality of about 0.7", which is what was measured with the direct CCD.

3. During June 29, 1996, intra- and extra-focal images were taken and analysed, using curvature sensing software. The analysis gave an average value of

TABLE 4: Spherical Aberration

Date	Value in nm	d80 in %	# of Measurements
21.07.91	5700	1.10"	14
22.07.91	4900	0.93"	19
24.08.93	4600	0.87"	52
19.10.94	6300	1.20"	10
21.10.94	4800	0.91"	30
24.10.94	6000	1.14"	32
21.01.95	6300	1.20"	11
22.01.95	6600	1.25"	20
23.01.95	4900	0.93"	21
09.02.95	2700	0.51"	8
06.04.96	4200	0.78"	23
28.06.96	3800	0.72"	48
29.06.96	2800	0.53"	34
30.06.96	2000	0.38"	18
01.07.96	3200	0.61"	9

0.56" of spherical aberration, similar to the 0.53" given by Antares.

4. Measurements made during May 1996 with ADONIS by P. Prado and E. Prieto showed that the spherical aberration was between 0.5" and 0.6".

In addition, during the June nights, the following measurements were done with Antares:

At the nominal focus, 0.56" of spherical aberration was found, 30 cm below the nominal position, 1.0" was measured and at 10 cm below the nominal focus, a negligible spherical was found (0.11"). Both 3rd-order calculations and computer simulations showed that, to remove 0.5" spherical at this telescope, one has to move the focal plane down by 120 mm. This coefficient (240 mm/") corresponds to what was measured by Antares in June and also corresponds to the coefficient given by Ray Wilson (237 mm/"). We know now how much we have to move the focal plane to correct a given spherical aberration. But first we have to confirm the value of the residual spherical aberration. F. Franza and B. Delabre measured 0.27" in 1982, however, we do not know the exact conditions under which this value has been obtained. Since February 1996 we have measured spherical aberrations of the order of 0.5".

Although we can now trust the Antares measurements, the apparent variability of the spherical term (see Table 4) has still to be understood. Ray Wilson suggested that this could be produced by mirror seeing. This interpretation is very appealing, but it is not easy to understand how this can be produced in practice, because these layers would be required to have the size of the pupil, and in addition, remain stable over one night. There are at least two possibilities:

(a) The mirror is enclosed in the centre piece. Stable layers of air could be formed more easily above the mirror, inducing a spherical term.

(B) There is a direct influence on the beam, at the level of the Cassegrain

adapter. One year ago, a heat source (rotator encoder) was spotted only 30 cm away from the beam inside the adapter. This source could have been a cause of "variable" spherical term. The Cassegrain hole is now insulated to shield off this heat source.

In addition, during the last months, mirror cooling has been applied, and this could explain why the "spherical" term never reached very high values. Substantially, Ray Wilson's interpretation seems very attractive; in this case the

spherical aberration would be the product of a misplacement of the focal plane, combined with a (variable) component induced by mirror seeing or air instabilities along the light path. Of course we have to confirm this by carrying out much more measurements and simulations.

There is still a lot of work to do, however the goals should be achievable. Of all the traditional 4-m-class telescopes, the 3.6-m has certainly the best intrinsic optical quality, but it does not give the best images – not yet.

6. Pointing Model

E. BARRIOS; ESO

The pointing of the 3.6-m has been erratic for a long time: pointing models were repeated quite often and an individual model was needed for each instrument. What was more worrying, the model was not stable in time.

In the last two years, several changes occurred, both from the operational and from the physical point of view. The models are now performed by starting from scratch (and are not anymore incremental); stiffening of the spider has been applied, and the new TPOINT (Wallace, 1995) software has been made available. Several pointing models have been repeated during the last year, as frequently as possible, with all instruments and top-end configurations. The results are summarised in a report (available in the WWW page of the 3.6-m+CAT TT).

Substantially, the behaviour of the telescope is quite regular, and pointing models with an RMS of less than 10" are obtained by using only a limited number of physical parameters (14), without the need of polynomial terms.

Models performed before and after the June 1996 intervention, of course,

are different, but they remain stable with time, largely independent of instrument and top-end exchanges. The parameters used are indeed the same for the 3 instruments at F/8.

Although these performances are not yet comparable with the best pointing telescopes, they are satisfactory for the instrumentation presently available at the 3.6-m telescope. Some physical limitations exist at the moment on the telescope (i.e. hysteresis in the secondary unit); however, we think that these performances can still be improved by refining the measurement technique, and by collecting enough data to search for second-order terms.

7. Acknowledgement

During this technical time at the 3.6-m telescope both shifts of the Mechanics Support Team have been involved at the same time, together with the staff of the Telescope Team, putting in a lot of effort to accomplish the mission and to cope with all the unpredictable. Special thanks shall be given here to both teams!



J. SPYROMILIO, ESO

This article is being written at the end of August during the second phase of the NTT upgrade project. I am pleased to be able to describe some of the activities undertaken while the NTT has been off-line. For those not wishing to read

much further, the short news is that we are progressing according to the detailed daily schedule with some tasks running one or two days ahead of time. In the context of the overall aims of the project and the critical question of "when

will the NTT be back on-line?" such minor variations do not have any significant impact. However, the adherence to the schedule during the hectic first couple of months suggests that we have correctly budgeted for the time needed.

So we hope that by the 1st of July 1997 the NTT can return to full service sporting its new software and hardware and also a new operations scheme.

The NTT was taken off-line on schedule on the 1st of July. The observations on the 30th of June, also known as 'last light', were in fact unfortunately clouded out. As mentioned in the previous issue of *The Messenger*, the first thing to do was the re-aluminisation of the secondary mirror. Unfortunately, although the re-aluminisation went well (reflectivity of 89.7 per cent) and performed within the time limits allocated to this task, bad weather and high winds prohibited the testing of the alignment of the system. Since the re-aluminisation was done without removing M2 from its cell, any misalignment resulting from its removal from the telescope should be small and recoverable. The decision was made to proceed with the planned activities rather than delay. The tertiary mirror will be coated in November when the whole telescope is scheduled to undergo alignment tests. These tests aim to determine whether the image elongation that sometimes is seen on the NTT is due to a misalignment and also to test the VLT alignment device and procedures.

At the time of writing, the primary mirror of the NTT is in the aluminising tank at the 3.6-m awaiting transport back to the NTT. The coating achieved on the primary seems excellent with a reflectivity of 90.1 per cent and a micro-roughness of 10 Å.

Many other activities have already been completed since the beginning of July. A large number of control subsystems have been installed and undergone preliminary testing. The fundamentals of the system look good but a significant amount of work still remains to be done. The control of the building and telescope tracking axes has been tested for basic functionality. The adapter functions (guide probes, reference unit, etc.) on side A have also undergone functionality testing. There is quite some way to go before we have tested all sub-modules and begin to integrate the complete system. It should be noted that the entire NTT electronics is undergoing modifications, and for some units substantial re-wiring is taking place. All signals from motors, amplifiers and limit switches are being checked and cross-checked against the documentation. In this context the master NTT documentation has been moved from paper drawings with notes added to them to ORCAD and AUTOCAD. This new system can be accessed from an HTML document which then allows us to access the documentation from anywhere in the NTT or the electronics lab without confusion. As we modify parts of the system, significant effort is being put into updating the documentation and producing the critical 'as built' drawings and tables.

A number of modifications and maintenance operations have also been undertaken during the first few weeks of this phase of the project. The auto-guider and other cameras in both adapters have been upgraded to VLT standard technical CCDs. This has been a non-trivial operation involving significant modifications not only to the mounts of the old cameras but also to the cable ducts to allow for plumbing of CCD heat exchange fluid. In addition the cooling of the electronics racks in the base of the telescope has undergone substantial modifications and the primary mirror cover has been refurbished. The EMMI red camera has been sent to Italy to fix a loose lens and the two silver gratings are in Garching being cleaned.

The most obvious change that visitors to the NTT notice is the furniture in the control room. The old laboratory style console has been removed along with approximately 4 kilometres of cable required to run the old displays. The new furniture which is in the same style as the NTT remote control room has been installed along with a substantial part of the computer architecture necessary for the VLT operations scheme. In this context, the four workstations involved in the operation of the NTT and associated instrumentation are now installed and running.

As has been stated many times already, one of the aims of the NTT project is to beta test the VLT control system. In this context we have in the past weeks had eight VLT staff present on La Silla learning not only about the behaviour of the control system in a real telescope environment but also in the case of some of the newer recruits to ESO the difficulties of working in remote locations and the fun of working with real hardware.

The Immediate Future

A few days after the deadline for submission of this article, we expect that most critical subsystems of the telescope shall have undergone functional tests and the integration of the system shall begin while the remaining subsystems are brought on-line. In the same period we expect that the new EMMI and SUSI software will also begin functional testing.

Around October, ESO shall be informing the members of the community who have applied and been awarded service observing time about the probability that the system can be brought to a sufficiently reliable state to start doing science in February/March 1997. The first observations shall be performed in service mode only and shall be strictly shared risks. Phase II proposal preparation tools are being finalised at this time and we hope to be delivering our first data from the new NTT in the first quarter of 1997. These observations will be performed on a best-effort basis.

The New Operations Model

In the last issue of *The Messenger* you will have seen the article by Peter Quinn describing the VLT data flow and the basics of the operations scheme. The NTT will provide the community the first opportunity to interact with the system and give feedback. The NTT project welcomes comments and suggestions by the community regarding the operations scheme and we believe that we are providing a great opportunity to the users of the VLT to influence the evolution of the system.

As opposed to conventional observing, in the new NTT we will have in addition to the telescope operator, an instrument operator assisting the observer with the details of the observing. The astronomer – whether as a visitor (classical observing) or an NTT staff member (in the case of service observing) – is then freed to worry about the decisions requiring his/her scientific expertise. As mentioned in the previous issue of *The Messenger*, a separate workstation is present in the control room to allow the astronomer to work with her/his data with the data reduction system of choice without fear of interfering with the process of data taking.

For the VLT operations scheme to be implemented on the NTT, a substantial number of new operations procedures need to be defined and coded. This work is going on mostly within the NTT team. Pipeline data reduction procedures are being written and observing templates are being specified. Observing templates form the basis for reliable and predictable operations in the new scheme. The observing template is in fact a pre-defined sequence of operations involving any combination of telescope, instrument and detector actions. The astronomer defines the parameters of this sequence and the marriage of the parameter file, and the sequence of instructions implies that as much as possible exactly what was specified will in fact be executed.

Combinations of such sequences can be grouped together in an entity called an observation block. Any given night's schedule can be expected to contain a number of observing blocks from different observing programmes but which require a similar instrumentation set-up and atmospheric conditions. A single target is observed within an observation block but there is no restriction on how many sequences are present therein. Of course, it should be obvious that if a particular observation block requires exceptional seeing and has a large number of long sequences embedded within, it will have a low probability of being successfully completed. Most observing programmes are expected to be broken down into a number of observing blocks.

The first observing blocks built and executed may well require quite some

interaction between the applicants and the operations/user support teams. As mentioned above, this will provide the users with the best way of providing feedback to ESO before we try the same scheme on the VLT. Every improvement suggested for the NTT will be directly transmitted to the VLT. This beta testing is the essence of the NTT upgrade. We aim to produce a system that is transpar-

ent to all users of the telescope whether in service or in classical mode.

Staff Movements

Two new members are welcomed to the NTT team. Erich Wenderoth, our new instrument operator, and Ricardo Schmutzer, on loan from the VLT software group until the end of the year, are

our new arrivals. Jari Roennback, who as a fellow in Garching provided support for the remote control operations and also managed the NTT WWW pages, finished his fellowship and has now left ESO. Many thanks and good luck Jari.

Jason Spyromilio
jspyromi@eso.org



La Silla – a group of small telescopes busy at work under the summer night sky.

Photograph: H. Heyer, February 1996

ESO Workshop on Science with the VLT Interferometer

A. QUIRRENBACH, *Max-Planck-Institut für Extraterrestrische Physik, Garching*

Interferometry: From Fringe Science to Mainstream Astronomy

When the coherent combination of the four telescopes of the VLT was first discussed during the design phase of the observatory, interferometry seemed to be a small field with very specialised applications. However, the reports issued by ESO's two successive advisory groups on interferometry (ESO 1989, 1992) showed already the large potential of the VLTI for a broad range of astronomical problems. This became even more apparent during the ESO Workshop on "Science with the VLT", which took place in June 1994 (see Walsh and Danziger, 1995). Several contributions to this workshop were dedicated to the interferometric mode of the VLT, and many others discussed the use of the VLTI in the context of larger multi-instrument programmes. The strong interest in interferometry expressed by astronomers working in a wide variety of fields, and the necessity to build the VLTI within tight financial constraints and optimised for the most promising scientific programmes, prompted ESO to form a new Interferometry Science Advisory Committee in April 1995. The ISAC was charged with updating the science case for the VLTI and prioritising the technical options in order to maximise the astronomical return from the interferometer. A summary of this work has been published in a previous issue of *The Messenger* (Paresce et al., 1996). At the same time ISAC served as the Scientific Organising Committee for a workshop on "Science with the VLT Interferometer", which was held at ESO's Garching headquarters from June 18–21, 1996. This workshop was aimed at presenting in more detail the ideas and views of ISAC, at gathering new developments in astronomy since 1994 and their implications for the VLTI, and at soliciting input and comments from potential users on what they expected from the VLTI. In fact, "Science with the VLTI" was perhaps the most comprehensive overview ever of the scientific questions that can be addressed with ground-based interferometry. All speakers were asked to address explicitly the question of how their project would be carried out with the VLTI, and which capabilities would be required to accomplish the scientific goals. To provide all participants with a more thorough understanding of how astronomical goals translate into technical requirements, the first morning of the

workshop was dedicated to four introductory tutorials on the fundamentals of interferometry and on the particulars of the VLTI. Many speakers who gave invited or contributed presentations during the following three and a half days came back to technical points raised in the tutorials. Indeed, almost all of them succeeded in making the connection between their aspirations and the harsh reality of instrumental limitations. In my view, this was among the great successes of the workshop: Mainstream astronomers have started to feel comfortable with talking about fringe tracking and visibility Calibration, just as if they were talking about photometric accuracy or signal-to-noise in a spectrum.

Opportunities for the VLTI, Old and New

As expressed by the choice of the title, the workshop's primary goal was a discussion of the scientific potential of the VLTI. It has been clear all the time since Michelson's and Pease's pioneering work that interferometry can be applied to a broad range of problems in stellar and Circumstellar astronomy. The capabilities of the VLTI, in particular its sensitivity and wavelength coverage, will substantially expand the range of problems that can be addressed with the instruments that are already operational. The high expectations of stellar astronomers was reflected by a large number of sessions dealing with stellar diameters and fundamental parameters of stars, imaging of stellar surfaces, binary star research, and the analysis of stellar populations and determination of proper motion in extremely crowded regions like globular clusters and the centre of the Galaxy. Observations of circumstellar matter, related to accretion or mass-loss phenomena, was another topic that received a lot of attention. Obtaining images of disks around pre-main-sequence objects is certainly one of the key scientific goals of the VLTI. Of equal importance are observations of dust disks around main-sequence stars, which range from β Pictoris-like objects down to the level of the zodiacal light in the solar system, a topic that is still good for more surprises. On the whole, however, we have a fairly clear picture of what we can expect from the VLTI for stellar astronomy, since there are well-developed models and theories that make clear predictions, and since some programmes can be direct follow-ups to current efforts at interferometers with

smaller aperture. In contrast, observing extragalactic objects with optical and near-infrared interferometry means entering completely uncharted territory. This implies that predictions of the scientific return from the VLTI are much more uncertain; on the other hand, the potential for breakthroughs in long-standing important questions is very high. Measuring the sizes of the dusty tori that are at the core of unified theories of Active Galactic Nuclei, resolving the broad line region in nearby Seyfert galaxies, determining the importance of star formation for the energy balance in Seyfert nuclei, and studying the structure of galaxies at high redshift are exciting prospects for the VLTI. Stellar and extragalactic astronomy are the two pillars on which planning for the VLTI has always rested, but there is more. There are quite a few questions concerning small bodies in our own solar system which could potentially be addressed with the VLTI. The main issue here is in which cases fringe tracking on the object itself is possible, or how suitable reference objects can be found. Among the recent developments in astronomy, the detection of brown dwarfs and extrasolar planets stands out as an event that opens a completely new area where observations with the VLTI will probably have a large scientific impact. Interferometric astrometry is a powerful method to search for Jupiter-like planets out to nearly 1 kpc, and for planets with 10 Earth masses orbiting the nearest stars. The surprising detection of a giant planet in a very close orbit around 51 Peg has established a new class of objects, which may be sufficiently bright to be detected directly with the VLTI. The VLTI could thus become the first instrument to perform spectroscopy and photometry of some extrasolar planets, and therefore to determine their temperatures, composition, and rotation periods. Some flexibility is required, of course, to incorporate the technical requirements for these challenging observations into the development plan for the VLTI.

Interferometric Life Before (and Beyond) Imaging

As a result of the workshop, we have seen an expansion of the scientific agenda of the VLTI into new areas, and refined ideas about realistic observing programmes. As a consequence, it has been realised that much, perhaps most, of the science with the VLTI can be done without "imaging". For example, there is

a lot of interest in detecting faint companions (stars at the bottom of the main sequence, brown dwarfs, giant planets) near much brighter stars. Several talks dealt with methods to do this, which involve using relative phase information, either the phase difference between two wavelength bands, or the phase difference between the primary star and a nearby reference (i.e., narrow-angle astrometry). These approaches are orders of magnitude more sensitive than synthesis imaging of the field around the primary using closure phase, and they require fewer telescopes (three are adequate, four are good). As a bonus, information on scales smaller than the resolution limit of the interferometer can be obtained. This compensates partly for the fact that the baselines of the VLTI are somewhat smaller than what one would ideally like to have. Another important point is the realisation that even in situations where synthesis imaging is the “best” method, much of the scientifically interesting information can be extracted from much more limited data, if adequate models are available. Recall, for example, the discovery of apparent superluminal motion in extragalactic radio sources, which involved fitting simple few-parameter models to data obtained with a VLBI “array” consisting of only two antennas (Whitney et al., 1971; it is very instructive to read this classical paper with 25 years of hindsight!) In many cases, a simple measurement of the size or overall geometry of an object contains much useful information. This has also been demonstrated by results from single-baseline optical interferometers, such as the I2T, G12T and Mk III instruments, which show that the H α emission region of Be stars has a disk-shaped geometry. Data of similar quality on T Tauri and β Pictoris disks, and on dust tori in Seyfert galaxies is exactly what we hope to get from the VLTI soon after “first fringes”.

The VLTI – a Community Instrument

At this point, it might be useful to recall that the VLTI is unique among the world’s interferometer projects insofar as it has been conceived within the framework of a large observatory, and with a broad community of users in mind. In contrast to the situation at all operational interferometers, the typical observer using the VLTI will not be a member of the highly specialised team that built the instrument, but rather an astronomer who needs data at milliarc-second resolution to complement his or her work with other methods. This concept of the VLTI as a community instrument will certainly enhance its scientific output, since it can capture the imagination of users from all fields of astronomy, observers and theorists alike. The broad range of topics covered at the workshop

is an encouraging indication that this process is already well on its way. However, additional ideas for applications of the VLTI are very welcome, especially in the areas of extragalactic astronomy and cosmology. Here, as in other fields, it must always be kept in mind that interferometry on its own will rarely lead to substantial progress; its real power lies in the unique capability to test predictions that have been formulated on the basis of observational work at lower angular resolution and theoretical modelling. Many projects therefore require the combination of data from the VLTI and more traditional techniques (spectroscopy, photometry, adaptive optics imaging, etc.); “one-stop shopping” at ESO will facilitate the planning of such observations tremendously. Open access to the VLTI will also ensure that programmes of all sizes can be carried out, from a snapshot of a single target (e.g., measurement of the diameter of a particular star as a function of wavelength) to long-term monitoring of large samples (e.g., astrometric surveys for low-mass companions), with detailed studies of individual key objects (such as 51Peg, α Ori, β Pic, the Galactic centre, NGC1068) ranging somewhere in between. While setting the scientific agenda for the VLTI is one important task for ESO’s user community, the equally important technical development is another. In spite of many advances in the key technologies of beam combiner design, detectors, laser metrology, vibration suppression, and instrument control, astronomical interferometry is still difficult. The workshop saw several debates among the specialists about the merits of different instrumental concepts, and about the accuracy of detailed predictions of their performance. It appears unavoidable that the VLTI will have to support both astronomical research and development of interferometric techniques, with a fairly large share of technical aspects for quite a while to come. Fortunately, ESO can rely on a number of institutes and observatories with experience in interferometry and related areas for building the “focal plane” instrumentation of the VLTI, beam combiners and fringe detectors. In short: to realise the full potential of the VLTI, ESO must draw on the astronomical *and* technical expertise available in the European astronomical community.

The Next Steps for the VLTI

Now that we have formulated our dreams about the science we want to do with the VLTI, we have to turn back to the question how we can make these dreams come true. The first important task ahead is the formulation of a prioritised instrumentation plan with realistic goals. The astronomical programmes call for instruments covering the whole wavelength range from 0.5 to 20 μ m; some

require simultaneous operation in two widely separated wavelength bands for fringe tracking and data taking. Monitoring programmes take a lot of observing time and thus need the auxiliary telescopes. To image complex objects, the auxiliary telescopes have to be combined with the four 8-m UTs, which is possible only if a sufficient number of delay lines is available. Off-source fringe tracking calls for dual star feeds and additional differential delay lines. Narrow-angle astrometry needs extremely precise metrology on top of that. The sensitivity in the visible and near-IR depends strongly on the availability and quality of adaptive optics. It is clear that we cannot get all of this from the beginning. Making the right choices about a sufficiently capable, but at the same time affordable and technically viable, “first-light” configuration will be crucial for the health of the VLTI programme. At the same time, a plan has to be drawn up how to phase in additional instruments and capabilities. In this process the balance has to be kept between relatively simple, low-cost instruments, more capable and versatile, but also more complex and more expensive solutions, and specialised techniques optimised for a single key application. The workshop proceedings will be of invaluable help for this purpose, since they will give us a good idea about the technical requirements for each scientific project. This mapping from the space of possible instrumental configurations into the space of astronomical problems that can be tackled should form the basis for discussions between astronomers and engineers about the detailed implementation plan for the VLTI. Where the mapping is still incomplete – for example in the area of solar system research – further feasibility studies are highly desirable. In parallel to the technical planning, observing strategies for short observations and for long-term programmes have to be prepared. This involves an understanding of operational aspects like calibration procedures and scheduling requirements. These issues are more complex for the VLTI than for a single telescope, because visibility measurements are strongly influenced by “dirty” atmospheric and instrumental effects, and because of the peculiarities of aperture synthesis. Some observing programmes require special preparatory work. An example is the systematic search for random associations of high-redshift galaxies and quasars with suitable foreground stars that can be used as references for fringe tracking. While planning for the VLTI is a complex process by itself, we must not forget that it is strongly influenced by outside events. Financial aspects and unexpected astronomical discoveries aside, the progress made by other interferometer projects on the ground and in space, and developments in the area of adaptive optics are the two most important factors that change the

boundary conditions for the VLTI. A number of interferometers with comparatively small aperture are already producing data or will come into operation very soon. In addition, instruments with sensitivity comparable to the VLTI (the Keck, LBT, and Magellan interferometers) may see first light soon after the VLTI. And finally, plans for interferometric space missions have been on the drawing board for quite a while. With that many contenders in the starting blocks, the competitiveness of the VLTI will depend critically on timing during all stages of its implementation. And because of its strong influence on the sensitivity, the availability of adaptive optics is an extremely important factor in this calculation.

The VLTI and Beyond

It will still take a few years until the VLTI becomes operational, and even longer before its full potential gets realised with the combination of the four 8-m telescopes using high-order adaptive optics. Nevertheless, a look ahead into the more distant future should be useful. It appears that the VLTI will be close to the limit of what can be done sensibly from the ground. Other instruments will have somewhat longer baselines, or better uv coverage, but it is difficult to envisage an affordable way of obtaining significantly more sensitivity, accuracy, wavelength flexibility or sky coverage than provided by the VLTI. On the other hand, interferometry from above the atmosphere looks very promising. Space is quiet, empty, and cold. In the absence of atmospheric fluctuations, the coherent integration time on any point in the sky is only limited by the observing time available, giving an enormous boost to sensitivity even with

moderate (1-m-class) apertures. At $\lambda \geq 2.5 \mu\text{m}$, the advantage of space is even larger, because the whole telescope can be radiatively cooled to a temperature of 40 K or so. The undistorted wavefront facilitates the calibration of the visibilities and makes advanced techniques for high-contrast observations feasible. Interferometer concepts based on “free flyers” – where each telescope is mounted on an independent small satellite – make very long baselines possible and provide superb imaging quality because the uv plane can be covered effectively. Bearing all this in mind, it seems plausible that the next big step after the VLTI will be the leap into space. Should ESO play a role in this adventure? There are very good arguments for an ESO involvement in space interferometry. First, the VLTI offers unique opportunities for the development of instrumental concepts and techniques, which have to be tested on the ground before they can be incorporated into space missions. Second, the VLTI will play an important role in defining the key scientific topics that can be addressed with space-based interferometry. And third, the efficient use of a space facility will require a user community well trained in interferometric observations. It thus appears that some coordination between ESO and ESA could be beneficial for both sides. A panel discussion with representatives of both agencies that took place during the workshop was devoted to the question of how a joint effort in the area of interferometry could work. Differences between ESO and ESA in their member nations, organisational structure, and scientific communities to be served will have to be addressed in order to define the scope and terms of a fruitful collaboration. With ESO’s VLTI back on

the track to fast implementation, and an interferometric cornerstone in ESA’s Horizon 2000+ programme, there is an enormous potential for a strong European role in the development of interferometry. Generating synergism between these programmes can only make them stronger. We can thus look forward to exciting opportunities, and to a rich harvest of astronomical results in the near future and in the decades to come. George Miley boldly predicted that the IAU will hold its third (!) symposium on “Optical Interferometry of AGN” in November 2010. I look forward to seeing his paper at that conference, and to many other results at the meetings that will be held on imaging of T Tauri disks, stellar surface features, spectroscopy of extrasolar planets . . .

Acknowledgements

All workshop participants deserve applause for their careful preparation and enthusiastic presentations. I had the pleasure of sharing with Jean-Marie Mariotti the task of summarising the workshop in the concluding talk. I hope that some of his insight has found its way into this report.

References

- ESO (1989), VLT Report No. 59.
 ESO (1992), VLT Report No. 65.
 Paresce, F., et al. (1996), *The Messenger* **83**, 14.
 Walsh, J.R., and Danziger, I.J. (1995), *Science with the VLT*, Springer-Verlag.
 Whitney, A.R., et al. (1971), *Science* **173**, 225.

Andreas Quirrenbach
 e-mail: qui@MPA-Garching.MPG.DE

Simulations of VLTI/VISA Imaging Observations of Young Stellar Objects at $2.2 \mu\text{m}$

N. AGEORGES, O. VON DER LÜHE, ESO

1. Introduction

The study of star and planet formation is one of the most exciting science goals of the VLT Interferometer. Circumstellar disks related to star and planet formation are believed to be a common feature of both young and main-sequence stars in different stages of development (e.g. Beckwith & Sargent, 1993, Backman & Paresce, 1993).

The search for direct evidence of disks around young stellar objects has been successful only recently (McCaughrean et al., 1996), although their presence has been inferred indirectly for

more than a decade. Direct detection was possible only with high angular resolution observing techniques, in particular with the HST. However, much higher resolution than available with HST is needed in order to probe the structure of these disks and to test current models which predict gaps and traces of planetesimals.

In an effort to understand the science performance of the VLTI, we have studied the potential of the VISA mode to do this kind of observations by computer simulations. Our main concern is the synthesis capability of various VISA configurations. To limit the large variety

of parameters, we have concentrated here on the study of a limited sample of disk morphologies at high angular resolution. We used the CalTech VLBI software package (Pearson, 1991) for our simulations.

2. Source Models

To make the computations more realistic we used disk parameters as derived from HST observations. The simulated object is located at 440 pc and corresponds to disk 182–332 of McCaughrean et al. (1996), with the exception that the declination is -30° . At this distance,

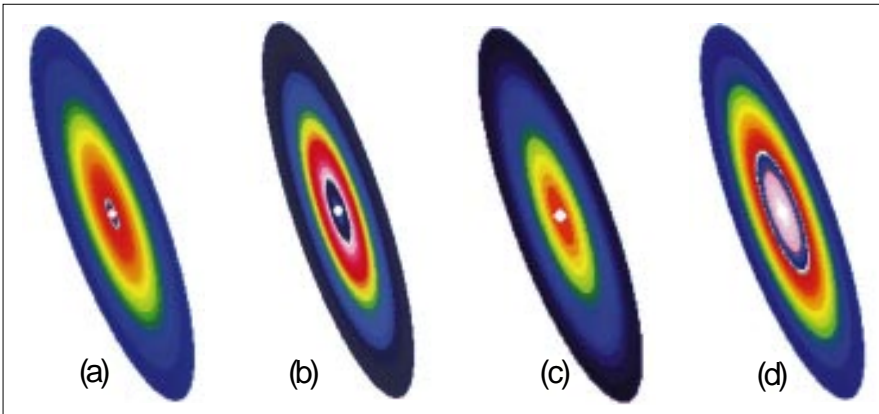


Figure 1. Simulated star + disk models: star + disk with a gap (5 AU (a); 10 AU (b), simple star + disk model (c), star + disk with a void ring (d).

the disk with a FWHM of 26 AU has an apparent extent of 60 mas. Adopting a star magnitude m_K of 9.49 and a disk luminosity of $0.5 L_*$, we constructed the 4 following models:

- (1) a featureless disk with an exponential intensity profile and a central unresolved source, viewed with an inclination angle of 75° ("star + disk" model),
- (2) a star + disk model as above with a gap of 5 AU between the star and the inner boundary of the disk,
- (3) same as before, but with a gap of 10 AU,
- (4) a star + disk system with a void between 12 and 20 AU from the star.

The VLBI package allows to model sources with various mathematical

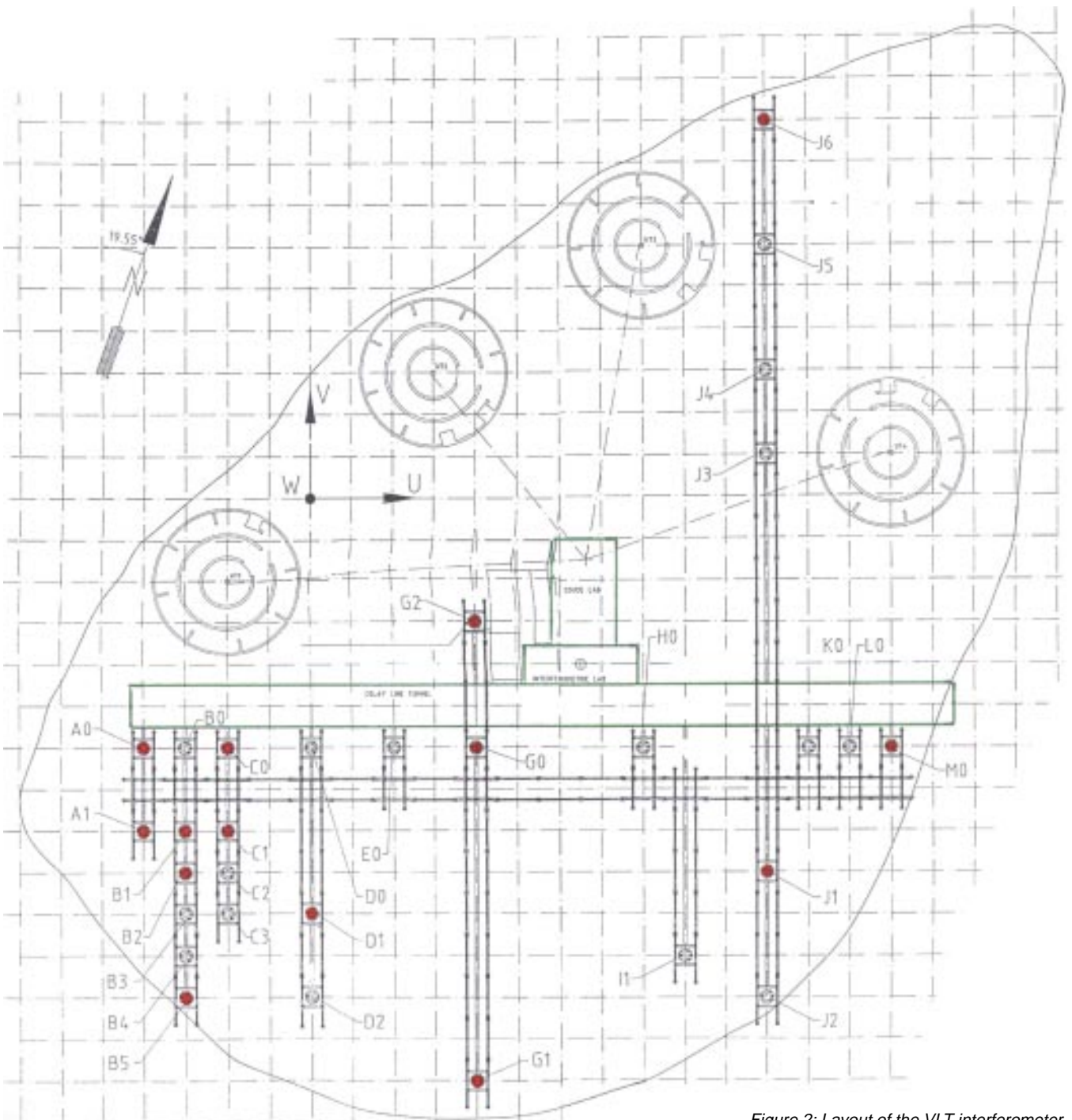


Figure 2: Layout of the VLT interferometer.

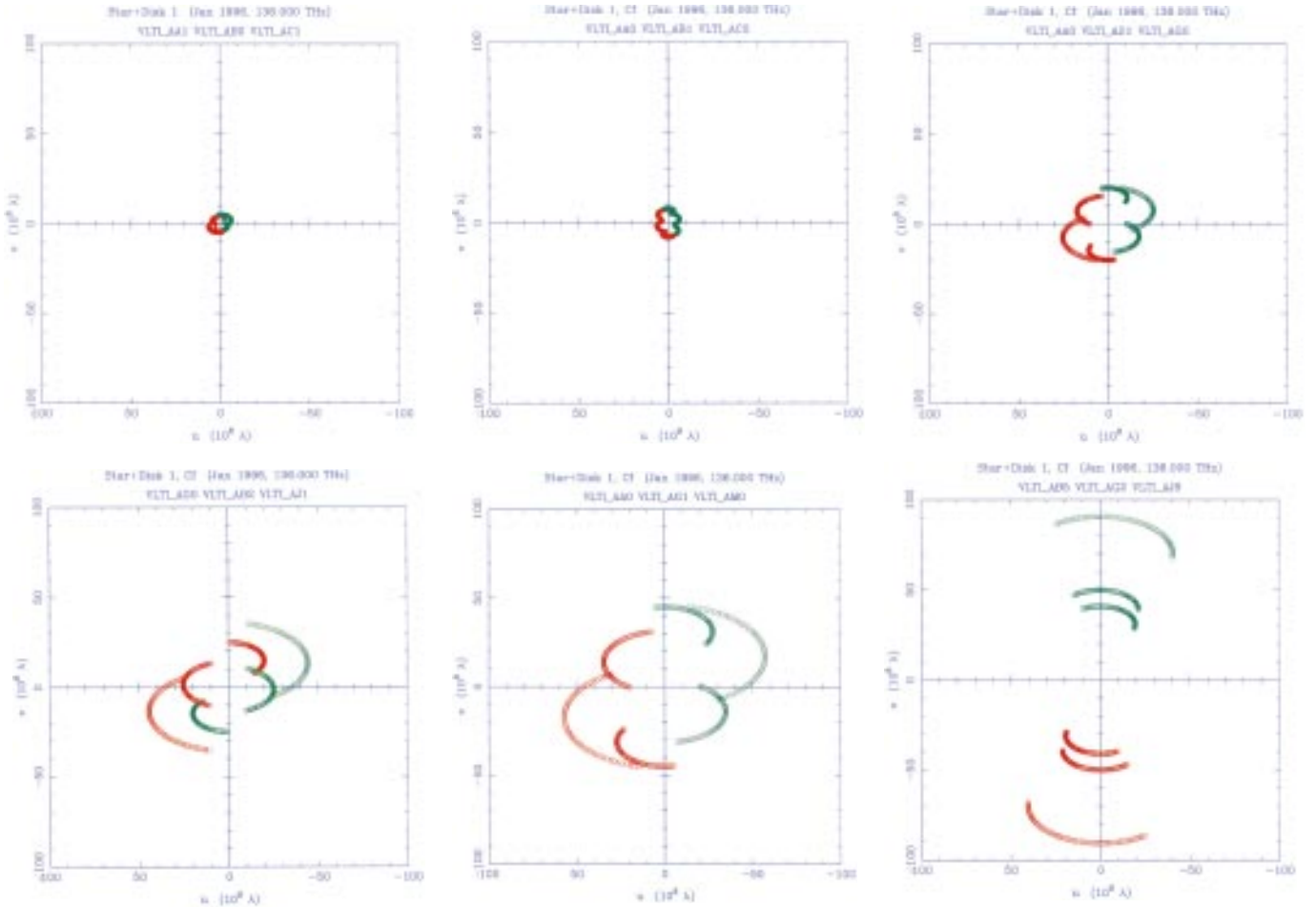


Figure 3: UV coverage from the different configurations used.

shapes, but we have used only elliptical Gaussians and uniform ellipsoids. Details of the model components are shown in Table 1.

3. Simulation of VLTI Observations

We used the actual layout (Fig. 2) for 8-m Unit and 1.8-m auxiliary telescopes of the VLT Observatory on Cerro Paranal for the modelling.

All simulations have been done for the K band at $2.25 \mu\text{m}$, using 3 auxiliary telescopes at any given time. The integration time on source is 5 minutes, which is repeated after 10 minutes; this allows for another interleaved set of reference source integrations of approximately 5 minutes. Observations are carried out between 03:00:00 and 21:00:00, with the source culminating at 12:00:00. This corresponds to a night where the source culminates at midnight. The hour angle is then limited by the zenith distance limits of the telescopes (60°). Noise sources are photon noise and a low level of detector read-out noise ($5e^-/\text{pixel}$). No other phase noise sources were accounted for.

The star with an apparent diameter of 1 mas is essentially unresolved even with the longest baselines, while the disk is clearly seen only with the shortest 8-m

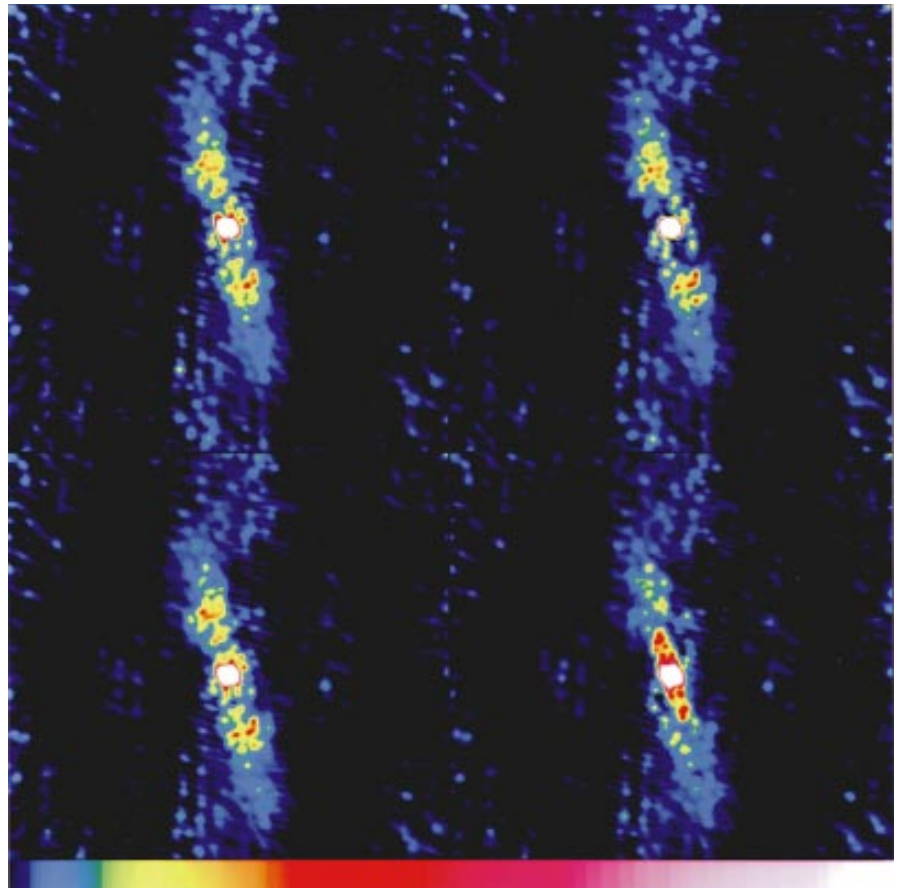


Figure 4: CLEANed images of the 4 simulated disks.

baselines between auxiliary telescopes. In fact, the disk would even be resolved with an 8-m Unit telescope with a near-infrared optimised adaptive optics system. However, the signatures of the disk features appear best at intermediate baselines of order 20 m. We therefore used six configurations of three auxiliary telescopes, the measurements of which were merged to result in a single data set which was subject to hybrid mapping and model fitting. The UV coverage of the six configurations are shown in Figure 3.

Synthetic visibility data were gridded, inverted to yield dirty maps and beams, and were subject to typically 1000 iterations of CLEAN. The resulting CLEAN maps are shown in Figure 4. We used these maps as a starting point to identify the approximate orientation and inclination angle of the disk “by eye”, as well as any discernible other feature like the central gap and the ring. From these observations, initial models for the CalTech non-linear least-squares model-fitting process were constructed. The resulting final models are then compared with the original sources.

4. Results and Discussion

Table 2 shows the parameters for the initial model (as derived from the CLEAN maps) and the iterated parameters after model fitting. These should correspond to the original parameters shown in Table 1. It also shows the agreement factors (reduced Chi-squared value for the goodness of fit

TABLE 1. Parameters of the different disk models studied. Definition of the type of components: 1 = elliptical Gaussian, 2 = elliptical disk of uniform brightness.

Flux (Jy)	Major Axis FWHM (mas)	Axial Ratio	Position Angle	Type
<i>Model 1: Star disk of uniform brightness</i>				
0.0085	1.0000	1.0000	0.0000	1
0.0042	60.0000	0.2500	20.0000	1
<i>Model 2: Star plus disk with central void (5 AU large)</i>				
0.0085	1.0000	1.0000	0.0000	1
0.0042	60.0000	0.2500	20.0000	1
-0.0001	11.3636	0.2500	20.0000	2
<i>Model 3: Star plus disk with central void (10 AU large)</i>				
0.0085	1.0000	1.0000	0.0000	1
0.0042	60.0000	0.2500	20.0000	1
-0.00035	22.7272	0.2500	20.0000	2
<i>Model 4: Star plus disk with the trace of a planetesimal between 12 and 20 AU</i>				
0.0085	1.0000	1.0000	0.0000	1
0.0042	60.0000	0.2500	20.0000	1
-0.00112	45.0000	0.2500	20.0000	2
0.00105	30.0000	0.2500	20.0000	2

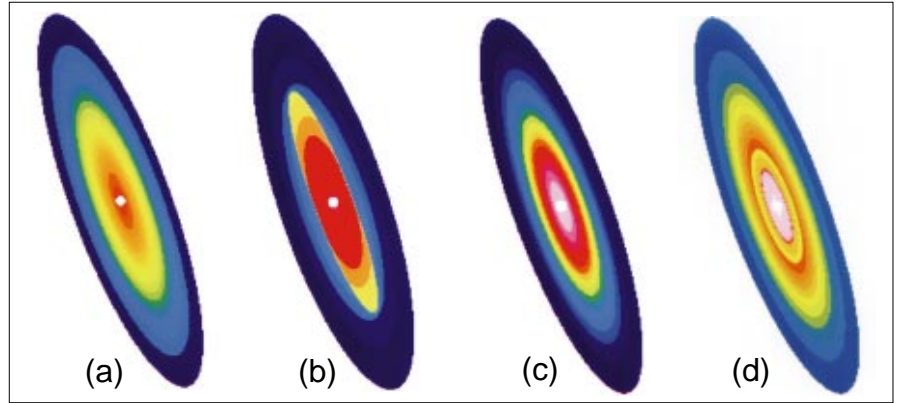


Figure 5: Results of model fitting (see Fig. 1)

between the model and the data). These numbers should be small for a good fit.

The CLEAN maps of the 10 AU gap as well as the void ring do in fact show structural differences compared to the featureless disk. For the case of a 5 AU gap, the CLEAN map is indistinguishable from that of the featureless disk. We therefore excluded this case from further discussion.

The CLEAN maps reveal that the simple approach using Fourier inversion and CLEANing is inappropriate for studying extended objects like the disk since CLEAN tries to decompose any source into a collection of point sources. At best, these maps can serve

as an input for constructing initial models, as we have done.

Initial model parameters can deviate substantially from the “true” values. In most cases studied, a reasonable input model would result in a final model which describes the actual source quite well after 40 iterations. Some parameters, in particular those related to the features in the disk, are quite sensitive. We could not obtain convergence of model fitting when entering a positive component brightness for those compo

Table 2. Parameters of the initial and iterated models.

Flux (Jy)	Major Axis FWHM (mas)	Axial Ratio	Position Angle
<i>Initial model 1</i>			
0.0100	1.0000	1.0000	0.0000
0.0070	83.8000	0.1500	30.0000
<i>Model 1: Iterated parameters, agreement factor 1.067</i>			
0.0085	1.0000	1.0000	0.0000
0.0044	60.3236	0.253451	20.1104
<i>Initial model 3</i>			
0.0100	1.0000	1.0000	0.0000
0.0100	70.8000	0.3300	13.9000
-0.0010	22.7270	0.1000	16.7000
<i>Model 3: Iterated parameters, agreement factor 1.166</i>			
0.0085	1.0000	1.0000	0.0000
0.0043	56.1651	0.25812	20.2088
-0.0005	26.2960	0.24544	19.8638
<i>Initial model 4</i>			
0.0100	1.0000	1.0000	0.0000
0.0005	74.0000	0.2000	12.7000
-0.0010	39.9000	0.2000	15.2500
0.0050	28.0000	0.2000	17.1500
<i>Model 4: Iterated parameters, agreement factor 1.203</i>			
0.0085	1.0000	1.0000	0.0000
0.0043	66.3553	0.25155	20.0408
0.0005	44.2581	0.27248	19.9609
0.0008	27.8947	0.24074	19.6639

nents which appear dark (i.e., with a negative flux) in the truth model. On the contrary, it hardly matters which initial flux is taken for the large disk component, it will always converge close to its truth value. Figure 5 shows the iterated models derived from model fitting; this should be compared to the simulated disks (Fig. 1).

Of course, this study is somewhat biased, because of the prior knowledge of the researchers, there was no "blind test". However, we made an attempt to fit the void ring model just with two components (star and large disk). Here, model-fitting convergence was slow although the two components were fairly well represented after 120 iterations. Also, the agreement factor was significantly larger (2.378). The fine structure,

like the void ring, is not recovered by the model alone, i.e. the model fitting process fits to the best the parameters that were introduced as input. It does not account for a possible further component. Nevertheless we conclude that there are some objective means which would reveal an inaccurately composed model.

We also tried reducing the number of configurations, with little encouraging results. With too few baselines, one would have been unable to identify structures in the disks without prior knowledge. Using only the long baselines, recovers only the central star – the long baselines, of course, constrain only the star. We therefore conclude that it takes quite some investment in observing time to find structures in circumstellar disks.

References

- Backman, D. E.; Paresce, F. (1993): in *Protostars and Planets III*, ed. G. Levy and J. Lunine, (Tucson University of Arizona Press), pp. 1253–1304.
 Bechwith, S.V.W.; Sargent, A.I. (1993): in *Protostars and Planets III*, ed. G. Levy and J. Lunine, (Tucson University of Arizona Press), pp. 521–541.
 McCoughrean, M.J.; O'Dell, C. R. (1996): *A.J.* **111**, p. 1977ff.
 Pearson, T. J. (1991): Introduction to the Caltech VLBI Programs, California Institute of Technology.

Nancy Ageorges
 e-mail: nageorge@eso.org



On September 19, an important milestone in the VLT project was reached: the completion of the 4th 8.2-m primary mirror blank by the Schott Glaswerke in Mainz. Following a press meeting at the Erich Schott Centre, about 100 guests gathered in the large factory hall to celebrate this achievement and to have a last look at the impressive Zerodur blank before its boat journey to France.

Photographs: H. Zodet

Resolving Nearby Galaxies into Stars

A.A. ZIJLSTRA, D. MINNITI, J. BREWER, ESO

Abstract

The combination of large-aperture telescopes and good image quality has made it possible to resolve the stellar population in many nearby galaxies. Here we present observations carried out at the NTT and CFHT, among others to study the Mira and carbon-star population in different environments, pushing the limits to outside the Local Group. One of the early results of this project has been the discovery of a population-II halo around a dwarf irregular galaxy. We discuss the possibilities for extending such studies with the VLT.

1. Introduction

With the advent of modern telescopes, the distinction between extragalactic and stellar astrophysics has become less sharp. This has long been the case for the dwarf spheroidals surrounding the Milky Way, which are so well resolved into stars that they are difficult to identify as galaxies. With the image quality nowadays routinely achieved at major telescopes, many nearby galaxies are similarly resolved into

stars. Thus, not only can the integrated properties and structure of galaxies be studied, but also directly their stellar populations.

This intrusion of stellar astronomy benefits both fields. The stellar population holds important clues to age and metallicity and thus of formation history of a galaxy. If planetary nebulae can be found, the dynamics of the old popula-

tion can also be studied (Arnaboldi et al., 1994). Star counts can determine the extent of a galaxy to much fainter levels than surface-brightness photometry (e.g. Pritchet & van den Bergh, 1994). From the other side, stellar properties and evolution can be studied in environments different from the Milky Way. Especially our understanding of stellar evolution on the Asymptotic Giant Branch, which is strongly metallicity and age dependent, has improved from extragalactic studies.

Much stellar work has been done on the LMC, with its convenient size and distance. Period-luminosity relations such as exist for Cepheids and Miras have been established and calibrated using the LMC. However, with large telescopes, these stars can now be identified at distances of several Mpc, and HST has shown itself capable of finding Cepheids at the distance of Virgo. Planetary nebulae have been found with ground-based telescopes to even larger distances. Clearly this is a field where 8-m-class telescopes can bring significant further development. Crucial are not only the large apertures, but improved seeing expected at a site such as Paranal and the move to wide-field

imaging will allow us to push stellar astronomy even further out.

In this report we will discuss recent observations obtained at the NTT and CFHT, aimed at finding and studying extragalactic AGB stars. An unexpected result of these observations has been the discovery of a population-II halo around a dwarf irregular galaxy. We discuss the carbon-star population of M31, and the goals of the NTT project. Finally,

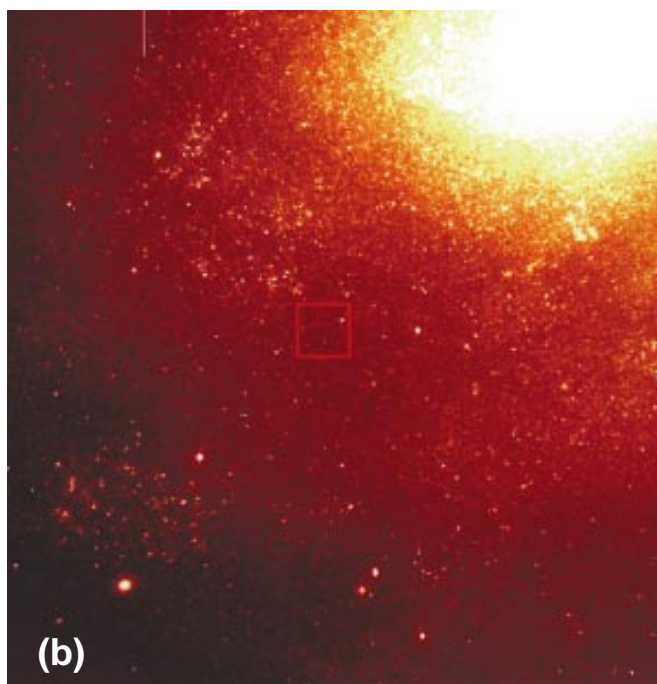
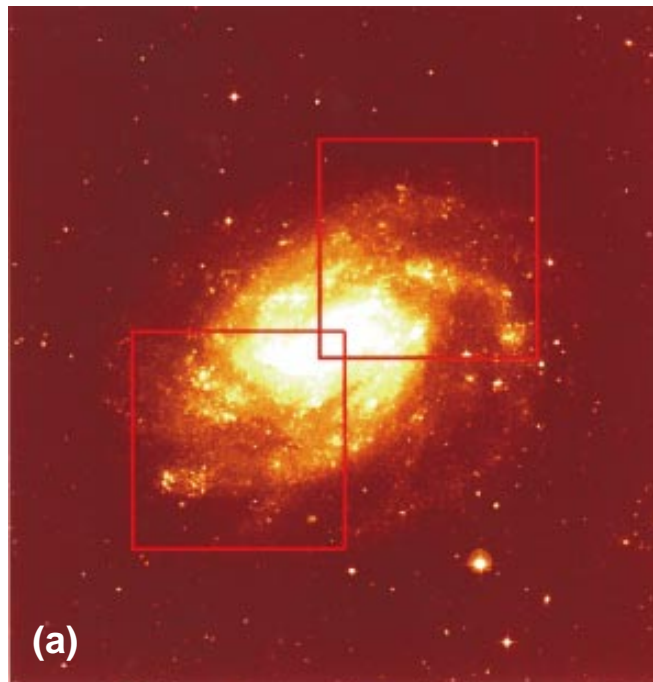
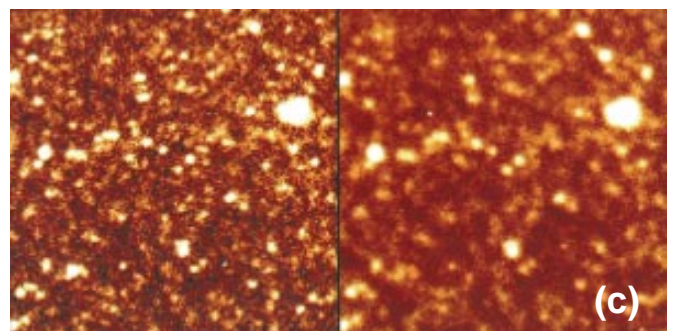


Figure 1: Panel (a) shows the dss image of NGC 300, with two EMMI fields indicated. Panel (b) shows one of these EMMI images. Panel (c) shows two epochs of the central area of panel (b): two variables near the top-right corner and bottom-left corner can be identified.



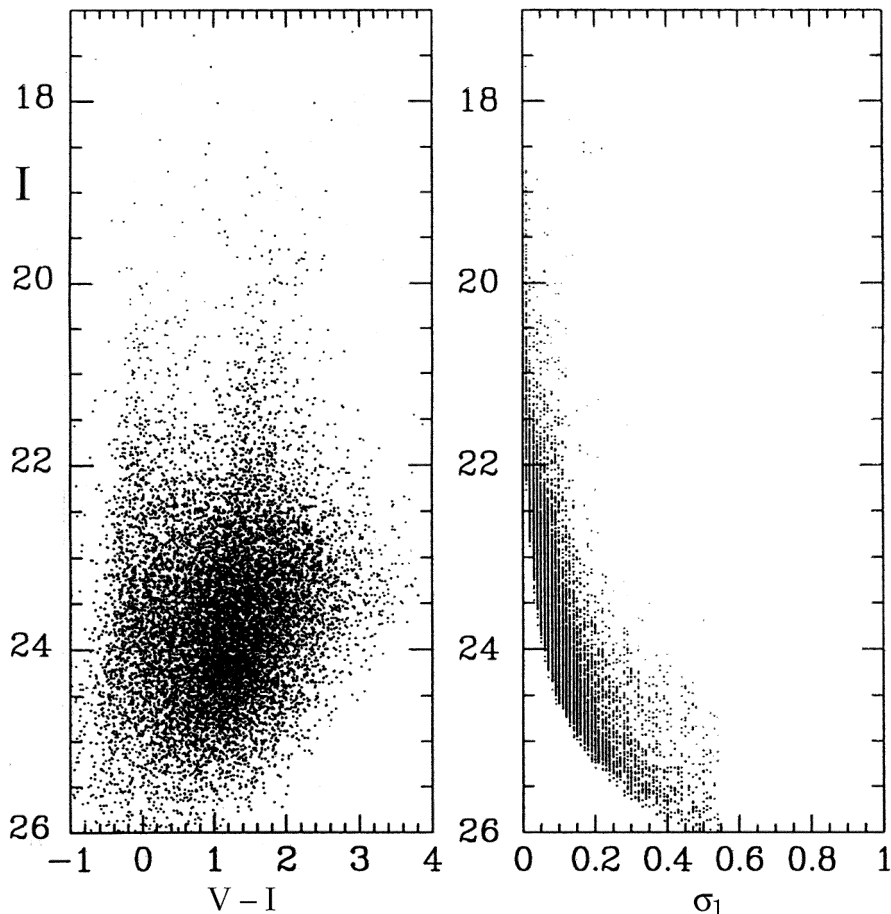


Figure 2: A colour-magnitude diagram for one EMMI field of NGC 300.

the use of the VLT for such studies is discussed.

2. Data and Project

Several galaxies in the neighbourhood of the Local Group were observed with the NTT in the V and I band. The direct aim was to find and monitor Mira variables in these galaxies, with a two-fold purpose. The first is to study the properties of the Mira variables as function of metallicity. This has proven difficult in the Galaxy where the distances to Miras are difficult to ascertain. The Magellanic Clouds (mainly the LMC) have a well-studied Mira population, but they provide a limited range in metallicity. The main uncertainty still is the phase at which AGB evolution is terminated. Mass loss is the dominant evolutionary effect on the AGB, and a phase of very high mass loss (the so-called superwind) ends the AGB, leading to the birth of a planetary nebula. The onset of the superwind is a function of the age and the luminosity and thus core mass of the star. It will also depend on metallicity, likely starting later at lower metallicity, which would cause low-metallicity stars to reach higher luminosity on the AGB. This has not yet been observationally disentangled from the dependency on age.

The second purpose is to study the period-luminosity relation of Miras. This relation has long been known and is tight especially when the K-band magnitude is used where the dispersion is only 0.13 mag. However, the metallicity dependence of the relation has been controversial. On theoretical grounds, a shift with Z of $\Delta M_{bol} = 0.73 \Delta \log Z$ at a given period is expected, but instead the PL relation in the Galaxy and the LMC appear to be highly similar (Feast, 1996, Whitelock et al., 1994). It is possible that AGB stars reach the Mira phase at different phases depending on initial metallicity, such that the total effect of Z cancels out. This was argued by Feast (1996). Studying the PL relation in various environments could potentially help solve this discrepancy.

The study of extragalactic AGB stars, especially carbon stars, has focused on galaxies within the Local Group. However, with 4-m-class telescopes they can in principle be identified out to several Mpc. We have selected a total of six galaxies which are regularly observed. Of these, the prime targets are WLM and NGC 300: we attempt to obtain data for these galaxies at every epoch. The other galaxies have less time coverage. The furthest galaxy in the sample is NGC 7793 at about 5 Mpc. WLM is a dwarf irregular at the edge of the Local Group.

NGC 300 is a large spiral at a distance of about 2 Mpc.

The I band is convenient to find the Miras since it combines the advantages of large field and good sensitivity. However, after the periods will be determined, infrared observations are needed to obtain the luminosity or K-band magnitude of the stars: in the I-band there is no obvious PL relation due to the cancellation of colour correction and luminosity. No PL relation is known for the most luminous, long-period Miras (Zijlstra et al., 1996). It is therefore important to go sufficiently deep to find the less luminous Miras which have periods of 200–400 days.

WLM fits into a single EMMI frame; for NGC 300 two pointings were used. We used DAOPHOT2 to find the stars in each frame. Figure 1a shows a dss image of NGC 300, with the two EMMI fields indicated. Figure 1b shows one of these two EMMI frames. Close to 10^5 stars could be identified in NGC 300 at a limiting magnitude of $I = 24$.

Miras will be identified based on colour (no detection is expected at V) and variability. As an example, Figure 1c shows two epochs of a small region in the central area of the EMMI field of Figure 1b. Even in this small area, two variables are clearly visible. In the full frame several hundred identifiable Miras can be expected, with an expected average I-magnitude ranging from 20 to 23. Figure 2 shows a colour-magnitude diagram for the south-east field, including a total of 15,000 stars.

For WLM, 45-minute integrations were used resulting in $I = 23.5$ at 4σ . The limit is worse in the more crowded regions: adding artificial stars at random positions, the completeness at $I = 22$ was found to drop from 90% in the outer areas to 75% in the central areas of the disk.

A colour-magnitude diagram of NGC 300 is shown in Figure 2. The main features are a red tail of AGB stars, a blue main sequence with mean colour $V-I = 0.2$, and a red supergiant sequence with $I < 20$, reaching $I \approx 16.5$. Signs for a population of blue loopers are also seen, running parallel to the main sequence, about 0.4 mag redder. The AGB is very extended, and can be traced to $V = 24.75$, and $V-I = 3.88$. Unfortunately, the present photometry is not deep enough to reach the horizontal branch of WLM. If $\Delta M_{R_{GBT-HB}} = 4.09 \pm 0.15$ this HB would be located at $I \approx 25$, accessible with HST.

Our star counts around WLM show a low-density tail, stretching considerable distances from the main body (Minniti & Zijlstra, 1996). To confirm this, two fields were observed further away from the galaxy. The total extent of the galaxy is at least 9 arcminutes along the minor axis, twice as large as the surface-brightness maps of Ables & Ables (1977).

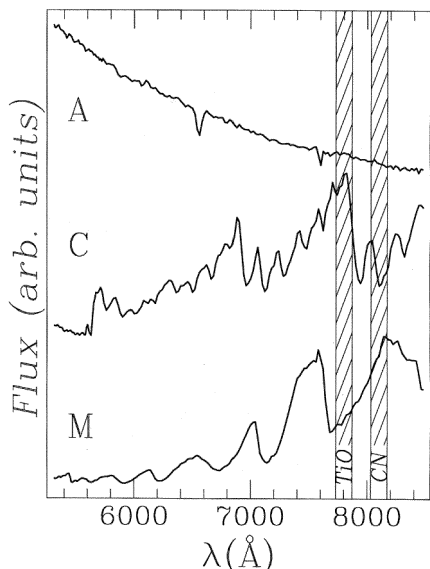


Figure 3: The upper spectrum is that of an A star, the middle spectrum a C star and the lower spectrum an M giant. Superimposed on these spectra are the bandpasses of the CN and TiO filters. Notice how the TiO filter lies on a TiO absorption band in the M star, while the CN filter lies on a CN absorption band in the C star. Data are courtesy of the Canadian Astronomical Data Centre.

3. Extragalactic Carbon Stars

The external abundances of AGB stars are changed by dredge-up following a thermal pulse. An oxygen-rich star becomes a carbon star when sufficient carbon has been brought to the surface to tie the star's oxygen up in CO. Although the internal structure of oxygen-rich and carbon-rich AGB stars is similar, their spectra differ enormously. Spectra of M-stars are dominated by bands of TiO, while, by contrast, carbon stars are dominated by bands of CN and C₂.

Palmer and Wing (1982) suggested that on account of their strong spectral features, carbon- and M stars could be distinguished by the use of narrow-band photometry. This idea was first implemented by two groups, one led by Marc Aaronson and the other by Harvey Richer. In Figures 3 and 4 we illustrate the basis of the "four-band photometric system" (FBPS). Figure 3 shows the spectrum of an A star, a carbon star, and an M star. Superimposed on these three spectra are the bandpasses of two narrow-band filters, henceforth referred to as the "CN" and "TiO" filters. The CN and TiO filters have a width of $\Delta\lambda \sim 140 \text{ \AA}$ and are centred on the CN ($\Delta\nu = +2, 8100 \text{ \AA}$) and TiO ($\Delta\nu = -1, 7800 \text{ \AA}$) absorption bands respectively. Figure 3 illustrates how the "CN" filter is positioned on a strong CN absorption band in the carbon star and pseudo-continuum in the M star, while the TiO filter is positioned on a strong TiO absorption band in the M star and pseudo-continuum in the carbon star. It can be seen from Figure 3 that: (1) the A star

will have a (CN - TiO) colour of around zero; (2) the carbon star will have a positive (CN - TiO) colour; and (3) the M star will have a negative (CN - TiO) colour. In Figure 4 we show a (CN - TiO, V - I) two-colour diagram (adapted from Richer et al., 1985) of photoelectric standards and LMC stars of known spectral type. Figure 4 demonstrates the insensitivity of the (CN - TiO) colour to early spectral types, and the bifurcation into carbon- and M stars at cooler temperatures. Indeed, the coolest carbon- and M stars show almost a *magnitude of separation* in (CN - TiO).

S stars are AGB stars in which the abundance of oxygen is similar to that of carbon. In the (CN - TiO, V - I) two-colour diagram these stars lie between the carbon- and M-star "branches", though are sufficiently scarce that no S-star "branch" is observationally seen.

FBPS surveys for AGB stars offer many advantages over surveys in which a dispersive element is used (e.g. Schmidt telescope with an objective prism). Some of these advantages are: (1) the FBPS can be used in crowded fields where spectroscopic surveys are not feasible; (2) as no dispersive element is used, the FBPS is able to reach fainter magnitudes; and (3) when used with a CCD, the FBPS gives data which are easily reduced and interpreted. On the downside, the FBPS is limited for survey work by the small field size of many CCD-based cameras. However, cameras based on large mosaics of

CCDs are starting to become common place; such cameras will allow the full utilisation of the FBPS for survey work.

The FBPS has made possible the identification and classification of AGB stars beyond the Milky Way and its dwarf companions; the most distant identified C stars are those in NGC 2403 with a true distance modulus of 27.4 (Hudon et al., 1989). More recently, the FBPS has been used at the CFHT to investigate the AGB population in M31 (Brewer et al., 1995). Five $7' \times 7'$ fields at different radial distances along M31's SW semi-major axis were observed during superb ($\sim 0.75''$) seeing conditions. In Figure 5 we show the (CN - TiO, V - I) two-colour diagrams resulting from these observations. The main results of this investigation are:

- The distance to M31 was derived using the carbon-star luminosity function, and found to be in good agreement with that derived from Cepheids. Furthermore, the carbon-star luminosity function appeared to be insensitive to differences in the star-forming history and metallicity of the fields observed.
- It is known that the ratio of carbon- to M-stars (the C/M ratio) is inversely correlated with metallicity (see, for example, Pritchett et al., 1987). The M31 observations showed that the C/M ratio tracked M31's known measured metallicity gradient, and suggested a flattening of the gradient in the outer disk.
- The correlation between the C/M ratio and galactocentric distance in

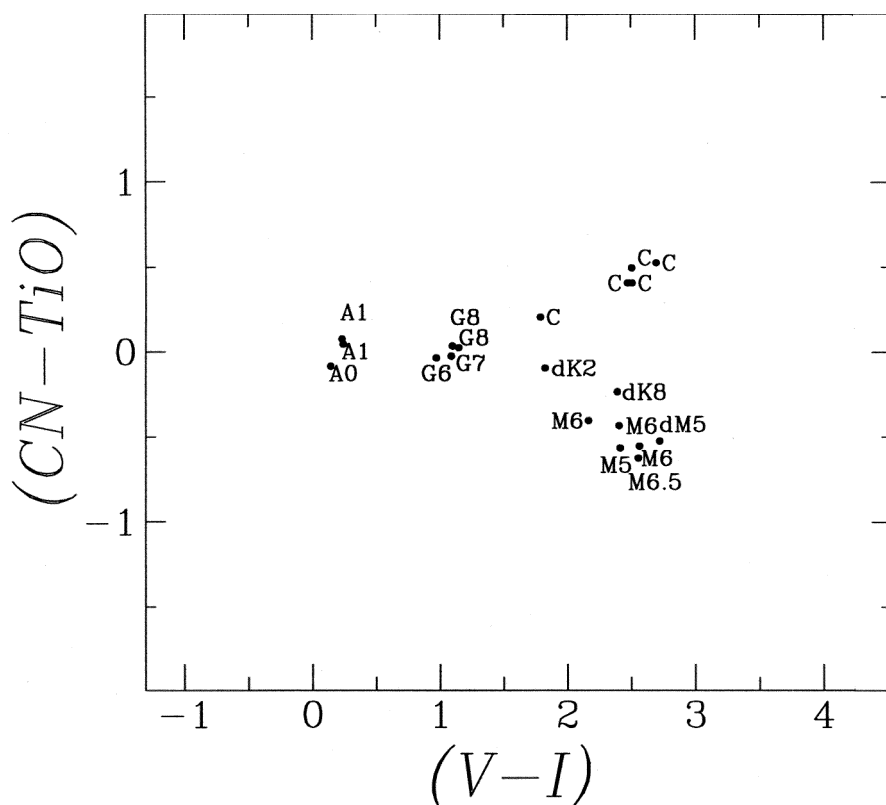


Figure 4: A plot of the (CN - TiO) narrow-band colour versus (V - I) broad-band colour for a sample of photoelectric standards and LMC stars. The data for this plot are adapted from Richer et al. (1985).

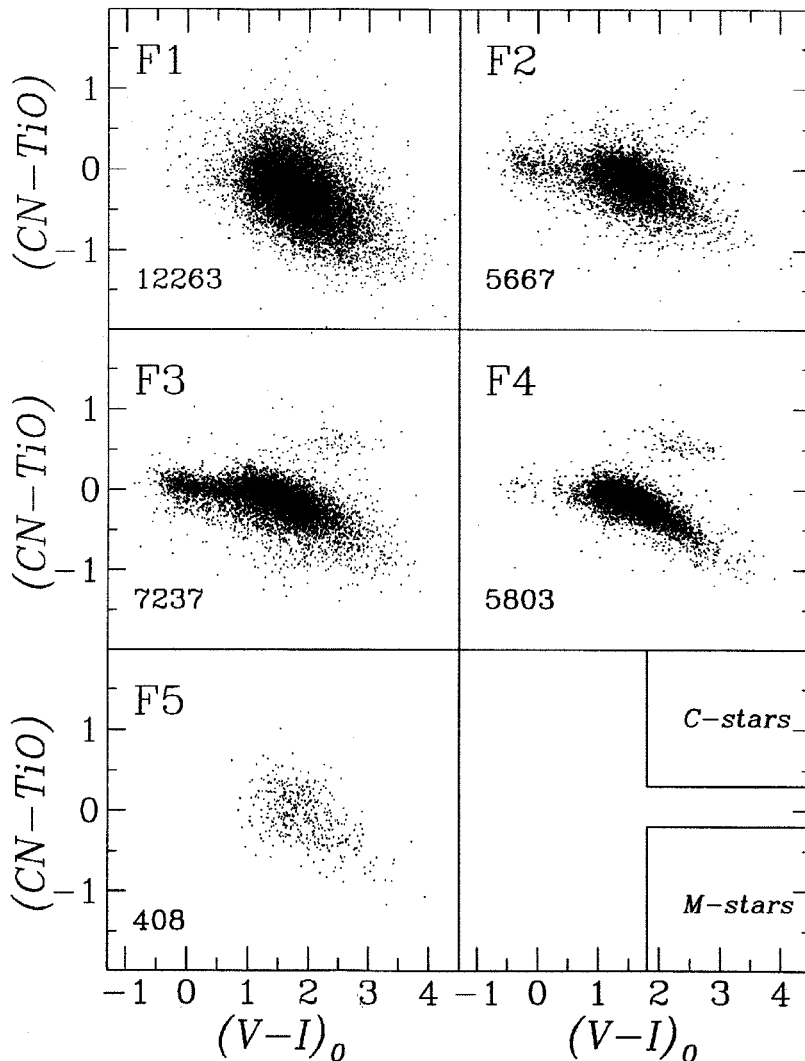


Figure 5: The labelled panels show the $(CN - TiO, V - I)$ two-colour diagrams for the five M31 fields. The number of stars measured in each field is indicated. The $(V - I)$ colour has been calibrated onto the Johnson-Cousins system and corrected for reddening, while the $(CN - TiO)$ colour has been shifted such that the mean value of $(CN - TiO)$ for stars bluer than $(V - I) = 1$ is zero. In the above labelled panels, stars with $10 < 18.5$ are excluded (such stars are likely to be foreground stars or M31 supergiants). The lower-right panel indicates where the C and M stars are expected (from spectroscopic observations) to lie in the $(CN - TiO, V - I)$ two-colour diagram.

M 31 may lead to differences in the properties of the ISM on account of the different types of grain produced by carbon- and M stars. For example, the differences observed in M31's extinction law are compatible with what would be caused by the observed C/M ratio gradient.

- The identification, and subsequent spectroscopic confirmation, of the most distant S star currently known.

Having identified the carbon- and M stars in the M31 fields, follow-up spectroscopy of some of the candidates was made using the multi-object spectrometer at the CFHT (Brewer et al., 1996). The spectra demonstrated the high reliability of the FBPS, more than 95% of suspected carbon stars were confirmed as such by spectroscopy. It also allowed for the identification of carbon stars with spectral peculiarities, such as high Li abundances and high C^{13}/C^{12} ratios.

Both of these types of spectroscopically peculiar carbon stars were found at luminosities fainter than predicted by current AGB theory. (N.B. The distance to, and consequently luminosity of, most Galactic AGB stars is unknown, making them unsuitable for comparison with theoretical AGB models).

The large aperture and expected good seeing of the VLT will be a boon for the investigation of AGB populations in Local Group Galaxies and beyond. Such studies will enhance not only our intrinsic knowledge of AGB stars, but will also shed light on areas like the spectral evolution of distant galaxies and ISM enrichment.

4. Conclusion

Clearly, there is much that can be done with the present 4-m-class telescopes: AGB stars and Miras can be

identified and studied at distances much larger than has been done so far. The NTT is useful because of a relatively large field of view and a good image quality. However, a larger field of view, such as available on CFHT, would be advantageous as illustrated by Figure 1.

For the VLT, it can be expected that the limits can be pushed to far outside the Local Group. The increase in collecting area alone significantly increases the possible distance. A second advantage can be expected from the seeing at Paranal which will allow point-spread functions of 0.4–0.5 arcsec to be routinely achieved. Together, a distance limit of 10–15 Mpc can be expected for these studies. A second advantage is the good IR quality of Paranal. For the study of Miras, it is crucial to obtain infrared photometry in addition to optical I-band photometry.

A drawback is the small field of view foreseen for the VLT. At larger distances, crowding becomes more important in the inner regions, and the outer regions should be included in the field of view. For a galaxy such as NGC 300, a good field of view would be 10 arcmin at a distance of 10 Mpc. It is important that instruments which give this field with optimum image quality will be available. This point is also strongly relevant to infrared cameras: their field of view will have to be comparable to that of the optical cameras on the VLT. Together, such instruments will keep the VLT at the forefront of extra-galactic stellar astronomy.

References

- Ables, H. D., & Ables, P. G. 1977, *ApJS*, **34**, 245.
 Arnaboldi M., Freeman, K.C., Hui, X., Capaccioli, M., Ford, H., 1994, *The Messenger*, **76**, 40.
 Brewer, J.P., Richer, H.B., & Crabtree, D.R. 1995, *AJ*, **109**, 2480.
 Brewer, J.P., Richer, H.B., & Crabtree, D.R. 1996, *AJ*, in press.
 Cook, K. H., Aaronson, M., & Norris, J. 1986, *ApJ*, **305**, 634.
 Hudon, J.D., Richer, H.B., Pritchett, C.J., Crabtree, D.R., Christian, C.A., & Jones, J. 1989, *AJ*, **98**, 1265.
 Feast, M.W., *MNRAS*, **278**, 11.
 Minniti, D., Zijlstra, A.A., 1996, *ApJ* (Letters), in press.
 Palmer, L.G., & Wing, R.F. 1982, *AJ*, **87**, 1739.
 Pritchett, C.J., Richer, H.B., Schade, D., Crabtree, D.R., & Yee, H.K.C 1987, *ApJ*, **323**, 79.
 Pritchett, C. J., & van den Bergh, S. 1994, *AJ*, **107**, 1730.
 Renzini, A. 1992, in IAU Symp. 149 on "The Stellar Populations of Galaxies", ed. B. Barbuy & A. Renzini (Kluwer: Dordrecht), p. 325.
 Richer, H.B., Pritchett, C.J., & Crabtree, D.R. 1985, *ApJ*, **298**, 240.
 Whitelock, P.A., Menzies, J.W., Feast, M.W., Marang, F., Carter, B., Robert, G., Catchpole, R., Chapman, K., 1994, *MNRAS*, **267**, 711.
 Zijlstra, A.A., Loup, C., Waters, L.B.F.M., Whitelock, P.A., van Loon, J.Th., Guglielmo, F., 1996, *MNRAS*, **279**, 32.

Albert Zijlstra
 e-mail: azijlstr@eso.org

PKS 1610–771: a Highly Reddened Quasar?

F. COURBIN ^{1, 2, 3}, D. HUTSEMÉKERS^{1*}, G. MEYLAN ²,
P. MAGAIN ^{1**}, S.G. DJORGOVSKI ⁴

¹Institut d'Astrophysique, Université de Liège, Belgium; ²ESO, Garching

³URA 173 CNRS-DAEC, Observatoire de Paris, France;

⁴Palomar Observatory, California Institute of Technology, Pasadena, USA

* Also chercheur qualifié au Fonds National Belge de la Recherche Scientifique

**Also maître de recherches au Fonds National Belge de la Recherche Scientifique

1. Introduction

About ten to twenty more or less convincing cases of gravitationally lensed quasars are presently known (Keeton & Kochanek, 1996). Most of these lensed quasars have been discovered on the basis of their apparently large absolute luminosities and high redshifts.

Following these criteria, the radio-loud highly polarised quasar PKS 1610–771, at $z = 1.710$ (Hunstead & Murdoch, 1980) was a good potential candidate. The quasar was first observed under poor-seeing conditions in August 1991 by Meylan and Djorgovski, using the ESO 3.5-m New Technology Telescope (NTT). In spite of these non-optimal seeing conditions, the object appeared double.

In April and May 1995, we were able to obtain, under much better seeing conditions, new NTT-EMMI *R* and *I* images of the field of PKS 1610771 as well as long-slit low-resolution spectra of both the quasar and its companion.

2. Not a Gravitational Lens . . .

Thanks to the relatively good seeing conditions during the nights of April 17–18, 1995 (FWHM = 0.8") and May 16–17, 1995 (FWHM = 0.9") the imaging of PKS 1610–771 not only confirmed a double point source structure, but also revealed at least three extended objects very close (closer than 2") to the line of sight (A, B and D on Fig. 1).

The slit of the EMMI red arm spectrograph was subsequently oriented along a direction joining PKS 1610–771 and its brightest point-like companion. In case of gravitational "splitting" of light by a massive object on the line of sight to the quasar, the two spectra should be essentially identical. This is not the case here. After a total of two hours of integration in low-dispersion mode (EMMI grism #1), the second point source, located 4.55" north-west of the quasar, turns out to be a late-type star.

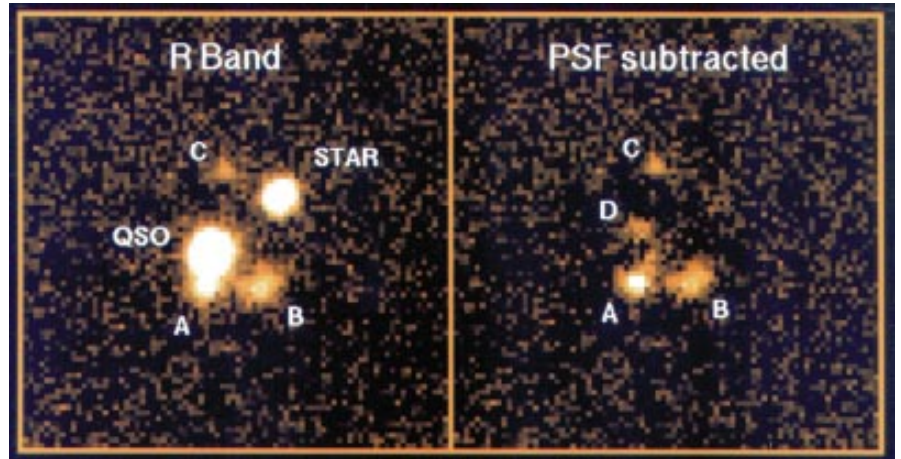


Figure 1: Left: NTT-EMMI *R* band image of PKS 1610–771 (1200-second exposure, $0.85 \leq$ seeing). The field is $20 \leq$ wide, North is up and East to the left. Right: same image, but a Point Spread Function (PSF) has been subtracted from the quasar and its companion. Three objects (A, B, D) can be seen very close (angle wise) to the QSO. The A–D fuzzy elongation appears perpendicular to the polarisation *E* vector of the quasar, suggesting their physical relation.

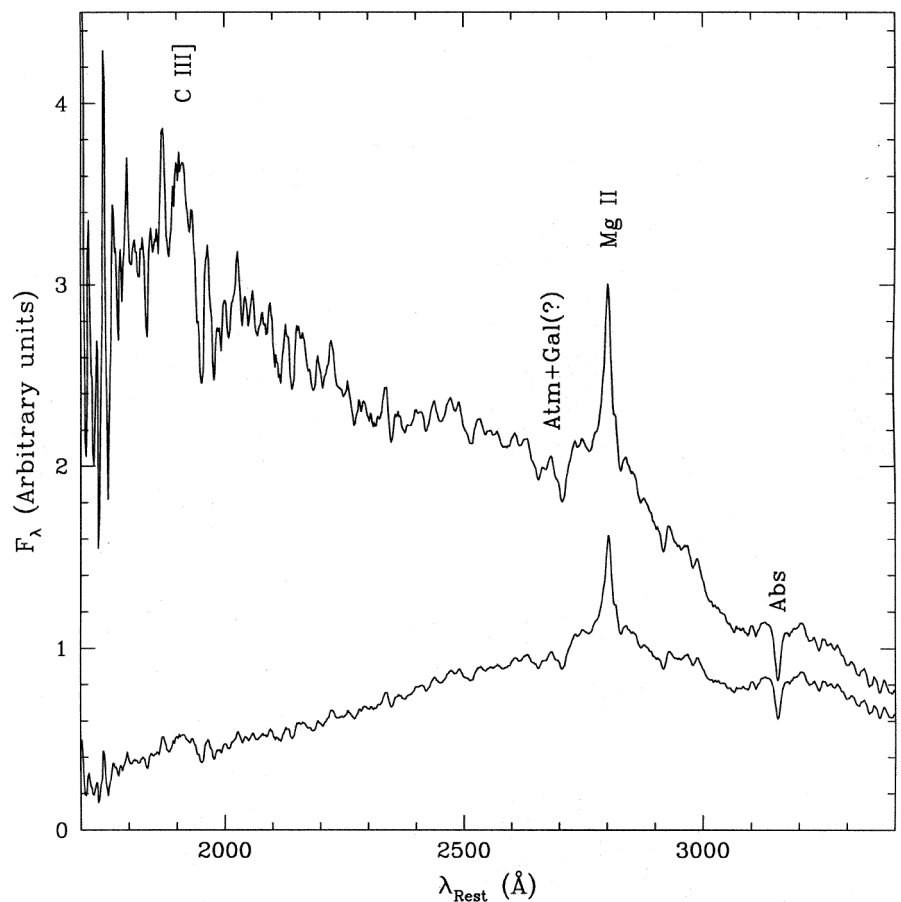


Figure 2: The spectrum of PKS 1610–771 (bottom) in the rest wavelength frame. Its unusual convex shape could be due to internal reddening, as illustrated by the de-reddened version of the spectrum (top).

3. . . . But a Surprising Object

Despite the fact that PKS 1610–771 is not a new gravitationally lensed quasar, its spectrum yields a surprise. The spectrum shows a curved continuum breaking at 7600 Å (2800 Å rest frame) (Fig. 2). In order to be sure that this unusual shape was not due to atmospheric refraction, we re-observed the quasar in May 1995 with the slit carefully oriented along the parallactic angle. The spectra of several spectrophotometric standard stars were obtained under similar conditions and used to check the accuracy of the flux calibration (see for more details Courbin et al., 1996). The results obtained confirmed our previous observations indicating that the weird spectrum shape is not due to atmospheric refraction.

Only very few quasars are known to have spectra similar to PKS 1610–771. These unusual spectra lead up to several interpretations out of which it is always difficult to draw a definite conclusion (e.g. Turnshek et al., 1994). One of the plausible scenarios which might play a role in the formation of such continuum is related to internal extinction by dust, which could affect many quasar spectra (Webster et al., 1995).

4. Internal Dust Extinction?

The reddening hypothesis was tested by performing a reddening correction of the flux-calibrated spectrum, using an SMC-like extinction law (Prévot et al., 1984) and assuming the dust at the redshift of the quasar. Figure 2 displays the result of this de-reddening, i.e., a more usual quasar spectrum. However, this certainly does not prove that reddening is responsible for the convex shape of PKS 1610–771's spectrum, but only that it is compatible with it.

In addition, we noticed that the fuzzy elongations north and south (A and D in Fig. 1) of the QSO are oriented perpendicular to the quasar polarisation angle (Impey & Tapia, 1988, 1990), as usually observed in high-redshift radio galaxies and suggesting that both objects are physically related to the quasar. This could suggest that PKS 1610–771 is a radio-loud quasar highly reddened by its host galaxy, but not completely hidden, its polarisation being due to diffusion by dust rather than synchrotron emission. In the framework of the AGN unification scheme (e.g. Urry & Padovani, 1995, Antonucci, 1993), PKS 1610–771 could be intermediate between quasars and radio galaxies.

The complete version of this study is published in Courbin et al. (1996). Surely, this scenario has to be checked in more detail on the basis of future observations, but we believe that PKS 1610–771 is a very interesting quasar to study in the context of AGN unification scheme.

References

- Antonucci R., 1993, *ARAA*, **473**, 521.
 Courbin F., Hutsemékers D., Meylan G., Magain P., Djorgovski S.G., 1996, *A&A*, in press.
 Hunstead R. W., Murdoch, H. S., 1980, *MNRAS*, **192**, 31p.
 Impey C.D., Tapia S., 1988, *ApJ*, **333**, 666.
 Impey C.D., Tapia S., 1990, *ApJ*, **354**, 124.
 Keeton C., Kochanek C.S., 1996, *Proceedings of the 173rd IAU Symposium: "Astrophysical Applications of Gravitational Lensing"*, Melbourne, Australia, eds. Hewitt and Kochanek (Kluwer), p. 419.
 Urry C.M., Padovani P., 1995, *PASP*, **107**, 803.
 Prévot M.L., Lequeux J., Maurice E., Prévot L., Rocca-Volmerange B., 1984, *A&A*, **132**, 389.
 Turnshek D.A., Espey B.R., Kopko M., 1994, *ApJ*, **428**, 93.
 Webster R.L., Francis P.J., Peterson B.A., Drinkwater M.J., Masci F.J., 1995, *Nat*, **375**, 469.

Frédéric Courbin
 courbin@astra.astro.ulg.ac.be

Two Planetary Nebulae Discovered in the Sagittarius Dwarf Galaxy

A.A. ZIJLSTRA, G. DUDZIAK, J.R. WALSH, ESO

There are currently nine dwarf spheroidal galaxies known in the near neighbourhood of the Galaxy. These small galactic systems are many times more massive than globular clusters and are gravitationally bound to the Milky Way Galaxy. The latest to be discovered was that in Sagittarius (Ibata et al., 1994, 1995), its late discovery attributable to its proximity to the Galactic Centre. It is situated at a distance of 25 kpc (Galactocentric distance 16 kpc) and is interacting with the Galaxy; with an estimated mass of $\geq 10^7 M_{\odot}$ it is perhaps the largest such local dwarf spheroidal. It contains several globular clusters, among them M 54, which may constitute its centre (Ibata et al., 1995). Until very recently the only dwarf spheroidal known to contain a planetary nebula (PN) was Fornax (distance ~ 160 kpc), discovered by Danziger et al. (1978) from on- and off-band [O III] imaging.

As part of a programme to study the kinematic properties of Galactic Centre PN, emission-line radial velocities of some 50 PN were obtained with the ESO 1.4-m Coudé Auxiliary telescope and the Coudé Echelle Spectrograph and short camera (spectral resolution

6kms⁻¹). Subsequent to the observations it was realised that several objects in the extensive objective prism surveys of PN in the Galactic Centre region were in fact in the vicinity of the Sagittarius

dwarf galaxy. Comparison of the radial velocity of these PN with that of the Sagittarius dwarf (+140 kms⁻¹ with velocity dispersion 10 kms⁻¹) showed that two objects, He 2-436 (004.8–22.7) and

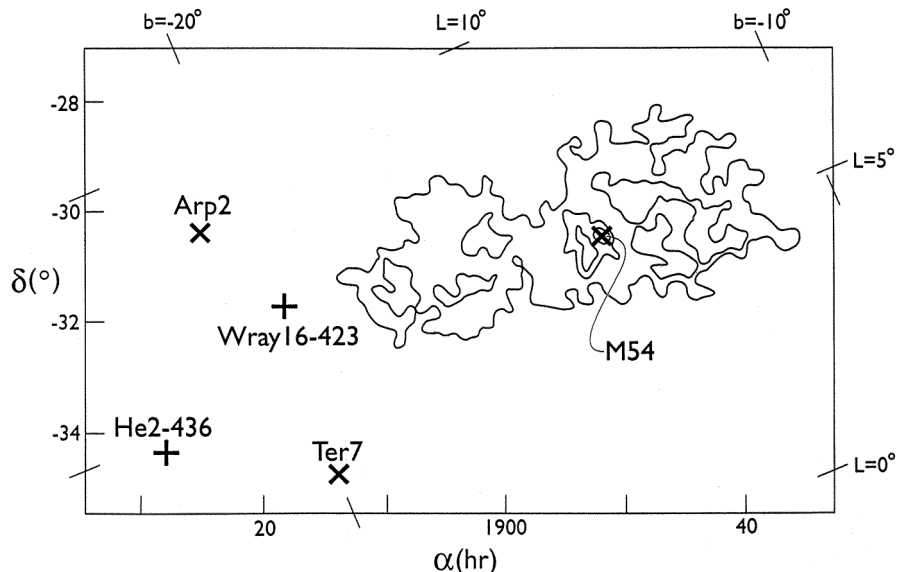


Figure 1: Sketch of the Sagittarius dwarf galaxy and the position of the two PN (pluses). The positions of three globular clusters are also shown (crosses). B1950 equatorial and Galactic coordinates are shown.

Wray 16-423 (006.8–19.8) were very probable members of this galaxy (Zijlstra & Walsh, 1996). Another PN, Hb 8, also lies in the direction of the Sagittarius dwarf galaxy, but has a very different velocity and can therefore be discounted as a member. The position of the two PN now ‘discovered’ in the Sagittarius dwarf galaxy are shown against a sketch of the galaxy in Figure 1. The two PN are situated some 5° from the core in the direction of the tidal tail found by Mateo et al. (1996). The radial velocity hardly changes from the core south-eastwards (Ibata et al., 1995); the radial velocities of the two PN are in good agreement with that expected for the dwarf galaxy.

In addition, there are two other PN which are possible members of the Sagittarius spheroidal: one, PRMG 1, has no measured radial velocity whilst the other, M 3-33, has a larger positive velocity, suggesting it is not a likely member. Table 1 summarises the properties of these PN. The expansion velocities of both He 2-436 and Wray 16-423 were measured from the full width at half maximum of the [O III]5007Å line (the lines were not resolved into two components as expected for small or unresolved nebulae) as 13 and 15 kms⁻¹ respectively. These expansion velocities are lower than the average PN expansion velocity of ~ 20 km s⁻¹, but not exceptional.

Further Observations

Following the discovery of the two PN, low-dispersion spectra were obtained during a short allocation of ESO Director’s Discretionary Time on the NTT and during scheduled time on the ESO 1.5-m. EMMI with a long slit and grism 2 (resolution 9Å) were used to obtain spectra of both He 2-436 and Wray 16-423 in May 1996 with a wavelength coverage 4000 to 8200Å. Images were also obtained with EMMI in RILD mode using [O III] and H α +[N II] filters. Further spectra for the important wavelength region below 4000Å and for wide-slit spectrophotometry were obtained on the ESO 1.5-m with the Boller & Chivens spectrograph and a coated Loral CCD (ESO # 39) in June 1996. Full details of the observations and analysis will ap-

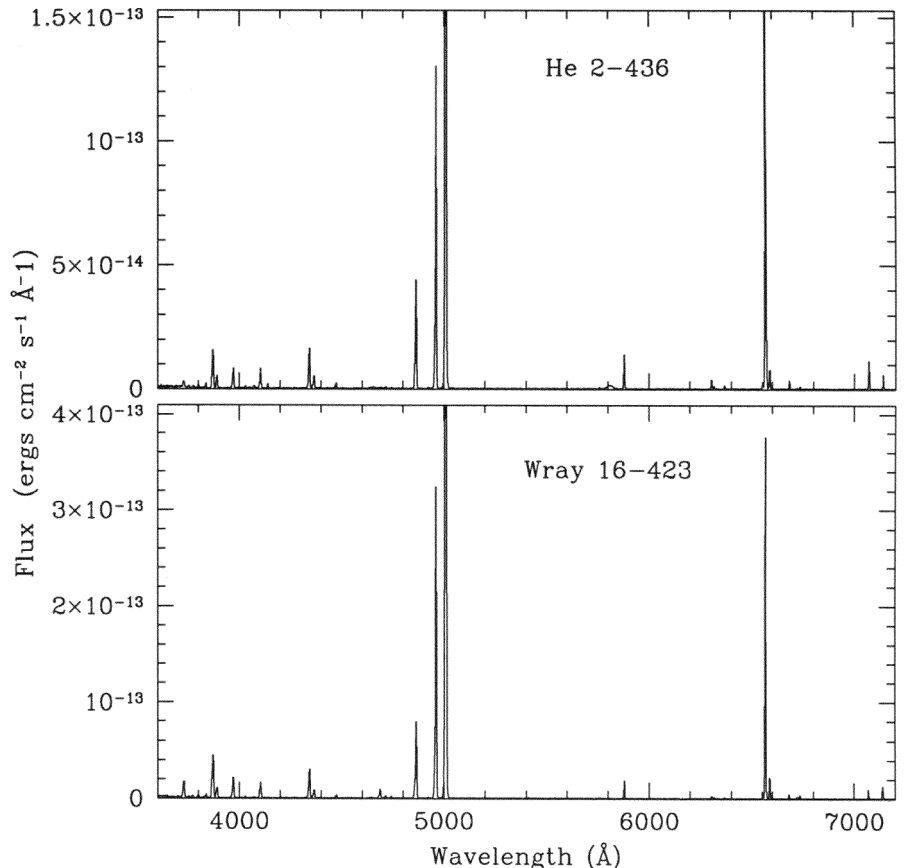


Figure 2: ESO 1.5-m observed spectra of the two PN in the Sagittarius dwarf galaxy.

pear in a forthcoming paper (Walsh et al., 1996). Figure 2 shows the low-dispersion spectra of both PN from the 1.5-m data. It is noteworthy that He 2-436 has a strong broad (stellar) C IV feature at 5807Å indicating a WC-type central star. Wray 16-423 has a very weak stellar feature at C IV. From the [O II], [O III], [N II], [S II], [Ar IV] and [Cl IV] diagnostic line ratios, the characteristic values of T_e and N_e were determined and the abundances of the light elements derived. He 2-436 is a high-density nebula with electron density $\sim 10^5$ cm⁻³, whilst Wray 16-423 has densities typical of many PN at ~ 5000 cm⁻³. Both have hot stars as measured from their Zanstra temperatures, but the central star of Wray 16-423 is the hotter and shows He II 4686Å in emission.

The seeing at the time of the NTT observations was not good (measured 1.4'' FWHM). Both PN appear to be unre-

solved on the raw images. Using stars in the frame, the PN images were restored using the accelerated Richardson-Lucy algorithm. He 2-436 was not resolved but Wray 16-423 showed an elliptical image, with major axis $\sim 1.0''$. For a distance of 25 kpc, the major axis diameter is 0.13 pc – typical of the size of PN with known distances (e.g. in the Magellanic Clouds – Dopita & Meatheringham, 1991).

Discussion

The sample of PN in dwarf spheroidal galaxies has increased by a factor 3 following the discovery of these two PN in the Sagittarius dwarf! This provides a very useful sample of PN in unique low-Metallicity environments and at known distances (derived from e.g. main-sequence fitting). Although many Galactic PN are closer, their distances are difficult to determine. The mean number of PN per solar mass in the LMC, SMC, Galactic disk and bulge (correcting for large number unseen) is about 3×10^{-7} PN M_\odot^{-1} . The corresponding value for Fornax is significantly less (a few times 10^{-8} PN M_\odot^{-1}) but is similar to that for Galactic globular clusters (based on 3 PN in 133 globulars – Jacoby et al., 1996). Taking the value for Fornax as indicative of the value for the dwarf spheroidal a mass of $\sim 4 \times 10^7 M_\odot$ for the Sagittarius dwarf is suggested, based on 2 PN. There may be more PN in the Sagittarius dwarf (and in Fornax); deep

TABLE 1. Planetary nebulae in the direction of the Sagittarius Dwarf Galaxy

Name	Designation	RA	Dec	V_{Hel}	Membership
			(J2000)	(km s ⁻¹)	
He 2-436	004.8–22.7	19 32 07.3	–34 12 33	+132.9	Probable
Wray 16-423	006.8–19.8	19 22 10.6	–31 30 40	+133.1	Probable
M 3-33	009.6–10.6	18 48 12.0	–25 28 50	+180	Possible
PRMG 1	006.0–41.9	21 05 53.5	–37 08 17		Possible
Hb 8	003.8–17.1	19 05 36.4	–33 1139	–172	Non-member

[O III] imaging surveys would be useful.

Whilst there are differences between the abundances of the two Sagittarius PN – He 2-436 has a low N abundance – the values generally bracket the abundances for the Fornax PN. The O abundances of He 2-436 and Wray 16-423 differ by only 0.08 dex and the mean of both is $12+\text{Log}(\text{O}/\text{H})=8.35$. The value for the Fornax PN is 8.5 (Danziger et al., 1978). Whilst the O/H abundances of these three PN are lower (by ~ 0.4 dex) than the average for Galactic PN, they are not as low as that of Compact Blue Galaxies ($[\text{O}/\text{H}]\sim 8.1$, e.g. Pagel & Edmunds, 1981), indicating that the PN belong to later generations of star formation. The PN can therefore be regarded as arising in an intermediate-age population and provide a unique diagnostic of the abundances of the light elements, which are difficult to determine from stellar spectra. Mateo et al., (1995) derived an Fe/H abundance of 8% compared to solar for the Sagittarius dwarf, suggesting that $[\text{O}/\text{Fe}]$ ($\log \text{O}/\text{Fe}$) is $+0.6$. Inci-

dentally, the errors on the oxygen abundance are much lower than the errors on the Fe abundance, the latter measured from the integrated stellar population. The $[\text{O}/\text{Fe}]$ value in the Sagittarius dwarf is higher than for the Galaxy and the Magellanic Clouds ($+0.45$ and -0.3 respectively, Richer & McCall, 1995), consistent with the galactic evolution models of Matteucci & Brocato (1990).

Although only three planetary nebulae have so far been confirmed in dwarf spheroidal galaxies, they clearly have a pivotal role to play in understanding the star-formation history in these dwarf galaxy systems.

References

Acker, A., Ochsenbein, F., Stenholm, B., Tyndala, R., Marcout, J., Schohn, C., 1992, *Strasbourg - ESO Catalogue of Galactic Planetary Nebulae*, ESO.
Danziger, I. J., Dopita, M. A., Hawarden, T. G., Webster, B. L., 1978, *ApJ*, **220**, 458.

Edmunds, M. G., Pagel, B. E. J., 1981, *ARAA*, **19**, 77.
Ibata, R. A., Gilmore, G., Irwin, M. J., 1994, *Nature*, **370**, 194.
Ibata, R. A., Gilmore, G., Irwin, M. J., 1995, *MNRAS*, **277**, 781.
Jacoby, G. H., Fullton, L., Morse, J., Phillips, M., 1996, paper presented at the IAU Symposium No. 180 on Planetary Nebulae, Groningen.
Mateo, M., Udalski, A., Szymanski, M., Kaluzny, J., Kubiak, M., Krzeminski, W., 1995, *AJ*, **109**, 588.
Mateo, M., Mirabel, N., Udalski, A., Szymanski, M., Kaluzny, J., Kubiak, M., Krzeminski, W., Stanek, K. Z., 1996, *ApJ*, **458**, L43.
Matteucci, F., Brocato, E., 1990, *ApJ*, **365**, 539.
Pagel, B. E. J., Edmunds, M. G., 1981, *ARAA*, **19**, 77.
Richer, M. G., McCall, M. L., 1995, *ApJ*, **445**, 642.
Zijlstra, A. A., Walsh, J. R., 1996, *A&A*, **312**, L21.
Walsh, J. R., Dudziak, G., Zijlstra, A. A., 1996, in prep.

Albert Zijlstra
e-mail: azijlstr@eso.org

The Distribution of Ionised Gas in Early-Type Galaxies

W.W. ZEILINGER¹, P. AMICO², G. BERTIN³, F. BERTOLA⁴, L.M. BUSON⁵,
I.J. DANZIGER^{6,2}, H. DEJONGHE⁷, A. PIZZELLA⁴, E.M. SADLER⁸
R.P. SAGLIA⁹ and P.T. DE ZEEUW¹⁰

¹Institut für Astronomie, Universität Wien; ²ESO-Garching; ³Scuola Normale Superiore, Pisa;
⁴Dipartimento di Astronomia, Università di Padova; ⁵Osservatorio Astronomico di Capodimonte, Napoli
⁶Osservatorio Astronomico, Trieste; ⁷Sterrenkundig Observatorium, Universiteit Gent;
⁸School of Physics, University of Sydney; ⁹Universitäts-Sternwarte München; ¹⁰Sterrewacht Leiden

1. Introduction

The presence of significant amounts of interstellar matter (ISM) in early-type galaxies has been recognised only in recent years (see Macchetto *et al.*, 1996 and references therein). The ISM appears to be more complex than in spiral galaxies. Several components have been identified so far: hot (10^7 K) X-ray gas (typical mass range $10^8\text{--}10^{10} M_\odot$), warm (10^4 K) ionized gas ($10^2\text{--}10^4 M_\odot$) and cold (< 100 K) atomic and molecular gas ($10^6\text{--}10^8 M_\odot$). The amount of X-ray gas is directly related to the optical luminosity of the galaxy (White & Sarazin, 1991) as expected in a cooling-flow picture (e.g. Thomas *et al.*, 1986). The HI content (Knapp *et al.*, 1985), dust content (Forbes, 1991) and CO content (Lees *et al.*, 1991) are found to be unrelated to the stellar luminosity in contrast to what is observed in spiral galaxies. It seems therefore that the hot ISM is a bulge-related phenomenon and the cold component is disk-related, with little interaction between the two. Recent studies revealed that the presence of dust and gas in early-type galaxies is the

rule rather than the exception (Bregman *et al.*, 1992).

There are two main sources for the observed non-stellar material: either it is coeval with the stars, resulting from stellar mass loss or it is accreted from outside in a second event in the galaxy his-

tory. Faber & Gallagher (1976) investigated how much gas may be produced by stellar evolutionary processes. Assuming a stellar mass-loss rate of $0.015 M_\odot$ year, $10^9\text{--}10^{10} M_\odot$ of gas can be accumulated over a Hubble time for a typical elliptical galaxy. In the accretion sce-

TABLE 1: Object list.

Object	RSA Type	RC3 Type	B_T	cz [km/s]	
NGC 484		SA0 ⁻	13.1	5200	imaging
NGC 745		S0 ⁺ pec	14.0	5953	imaging
NGC 1395	E2	E2	10.5	1699	imaging
NGC 1453	E0	E2-3	12.6	3933	imaging & spectroscopy
ESO 118-G34		S0 ⁰ pec	13.5	1171	imaging
NGC 1947	S0 ₃ (0)pec	S0 ⁻ pec	11.6	1157	imaging
NGC 2974	E4	E4	11.9	2006	imaging & spectroscopy
NGC 3962	E1	E1	11.6	1818	imaging & spectroscopy
NGC 4636	E0/S0 ₁ (6)	E0-1	10.4	927	imaging & spectroscopy
NGC 5846	S0 ₁ (0)	E0-1	11.0	1710	imaging & spectroscopy
NGC 6868	E3/S0 _{2/3} (3)	E2	11.7	2858	imaging & spectroscopy
ESO 234-G21		SA0 ⁰ pec	13.9	5430	imaging
NGC 7097	E4	E5	12.6	2539	imaging & spectroscopy
NGC 7302	S0 ₁ (4)	SA(s)0 ⁻	13.2	2586	imaging
IC 1459	E4	E	11.0	1691	imaging

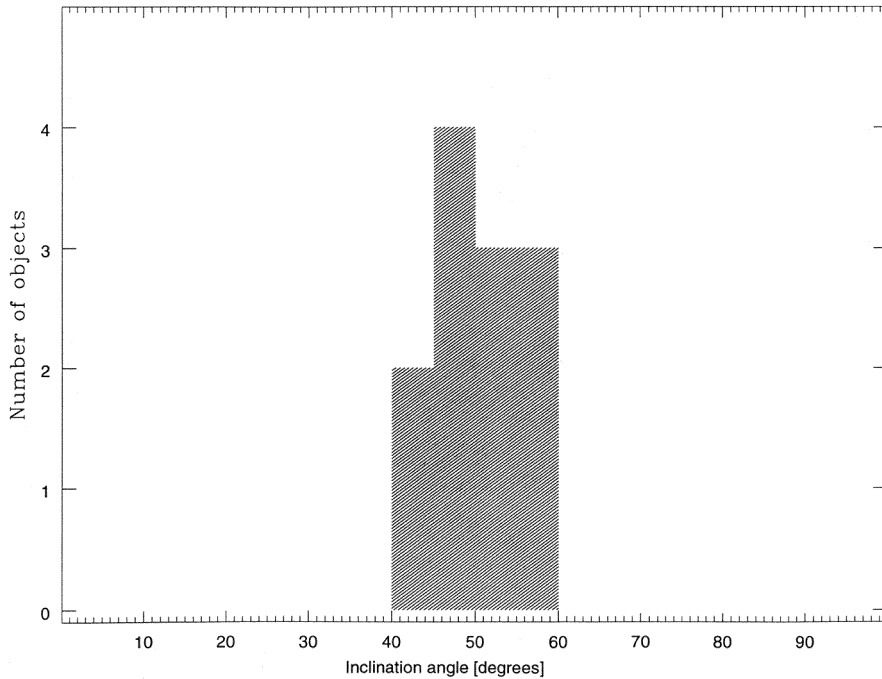
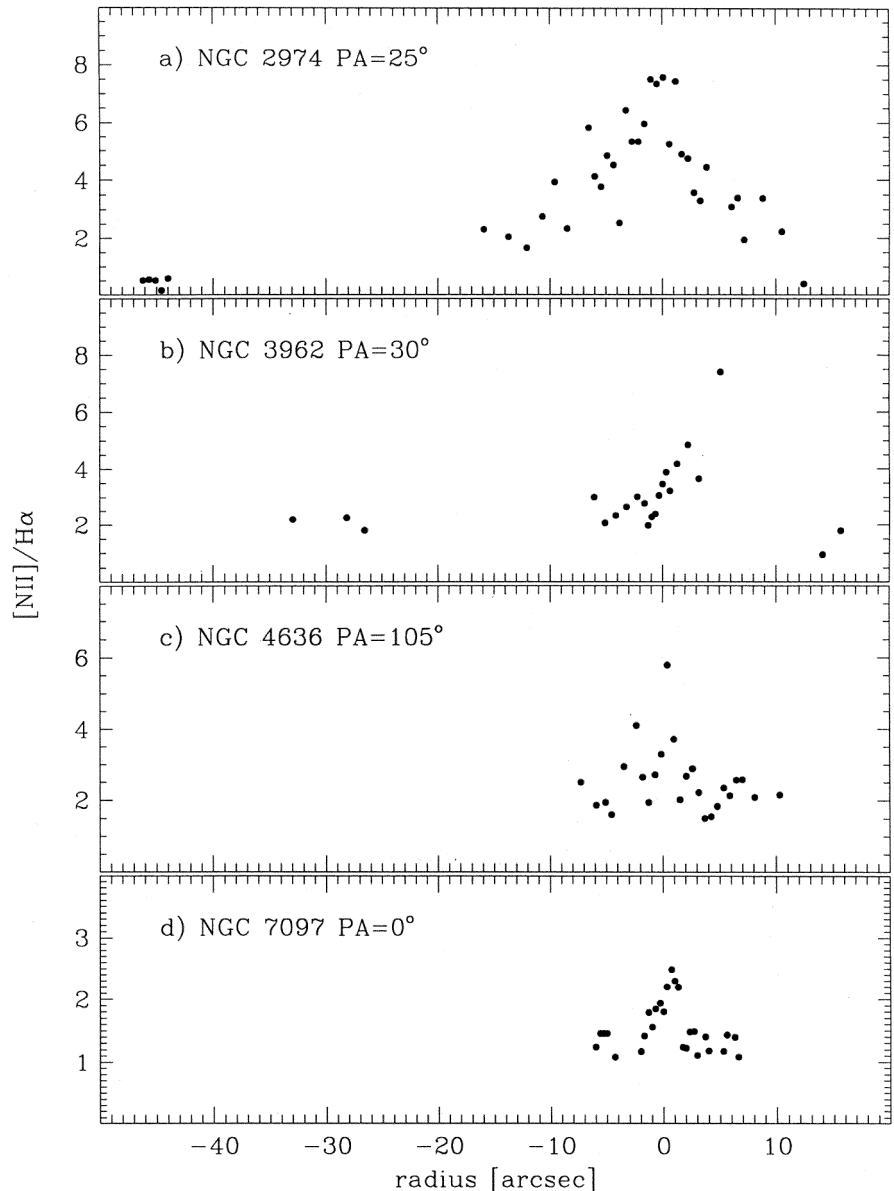


Figure 1: Distribution of inclination angles for the programme galaxies derived gas disk geometry under the assumption of a circular structure.

nario, a typical elliptical galaxy may collect up to $\approx 10^{10} M_{\odot}$ of gas over a Hubble time by interaction with its environment (Schweizer, 1983). The conspicuous class of dust-lane ellipticals are explained in this framework. A gaseous disk in an elliptical galaxy which is seen close to edge-on ($i \approx 80^{\circ}$) appears as a dust-lane crossing the stellar body (see review by Bertola, 1992) Disks which are not almost edge-on are more difficult to recognise, and can usually be detected only by the presence of emission lines which arise from the ionised gas which is associated with the dust. The key argument in favour for the external origin of the gaseous matter is that in many cases the kinematics of gas and stars are decoupled.

Physical properties of the ISM are expected to hold clues to the formation and subsequent evolution of elliptical galaxies both as dynamical systems and as aggregate of ageing stars. One approach of the ESO Key Programme “A search for dark matter in elliptical galaxies” (Bertin *et al.*, 1989) to trace the radial mass distribution was to study elliptical galaxies with embedded gaseous disks. Observations and modelling are described in a series of three papers (Buson *et al.*, 1993; Zeilinger *et al.*, 1996; Pizzella *et al.*, 1996). A sample of 15 elliptical galaxies with extended emission was selected for this study (Table 1). Narrow-band imaging in the light of the [N II]+H α lines carried out at the ESO/MPI 2.2-m telescope was used to study the distribution of the ionised mat-

Figure 2: Relative [N II]/H α flux ratios as function of distance from the galaxy centre for four programme galaxies. ▶



ter. A subsample of six objects, which have the most disk-like gas distribution, was selected for long-slit spectroscopy at the ESO 3.6-m and ESO/MPI 2.2-m telescopes in order to map the gas velocity field. The photometric and kinematic results were then used to constrain the intrinsic shape and mass distribution of the host galaxy.

2. Physical Properties of the Ionised Gas

The ionized gas is usually confined to the inner regions of the galaxy extending typically 5–15'' from the nucleus. The distribution of the gas appears to be regular. The isophotal major axes of the stellar and gaseous components are frequently misaligned. The isophotes of the gas disks are found to be significantly flatter than those of the stellar distribution supporting the model of an inclined disk. The surface brightness profiles of the gaseous disks closely follow an $R^{1/4}$ law with an effective radius smaller than the one of the stellar component. This is

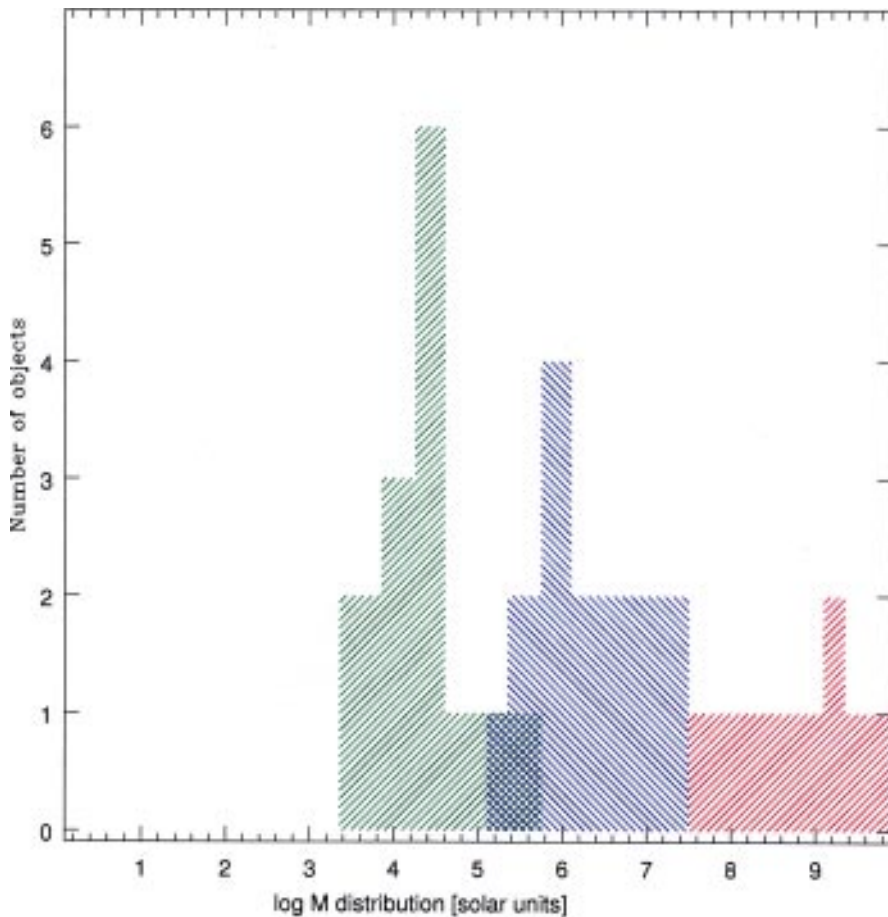


Figure 3: Mass distribution of the three ISM components of the sample galaxies: dust (blue histogram; data from Knapp *et al.* 1989), ionised gas (green histogram; data from Buson *et al.* 1993) and X-ray gas (red histogram; data from Roberts *et al.* 1991).

part of the galaxy are interpreted as high-velocity dispersions indicating a dynamically rather hot gas component. The kinematic data in the central parts of the galaxy (typically $R < 4''$) are certainly affected by seeing. The lines are blurred and consequently velocity gradients are lowered and lines become broadened. Simulations showed that seeing effects may produce an artificial increase of the velocity dispersion to a maximum of 150 km/s. The observed peak velocity dispersions are however in the range of 200–250 km/s. This could be evidence for a pressure-supported gas in central regions of the galaxy (*e.g.* Bertola *et al.*, 1995).

The spectra of all the sample galaxies are characterised by LINER-type emission indicating nuclear activity as described by Demoulin-Ulrich *et al.*, (1984). The typical $[N II]/H\alpha$ ratios found are ≥ 2 in the central parts of the galaxy (Fig. 2). Hot stars can therefore be ruled out as the only sources of ionisation. A similar conclusion was reached by Phillips *et al.* (1986) for “normal” early-type galaxies. Comparing the radio continuum emission of the programme galaxies with a complete sample, it turns out that galaxies with ionised gas disks have radio powers typically 10–15 times higher than “normal” ellipticals. This would suggest that an active nucleus contributes to the ionisation of the gas disk as is also the case for more powerful FR II radio galaxies (Baum & Heckman, 1989)

in contrast to the distribution of neutral hydrogen in spiral galaxies, where the density profile of the gaseous disks obeys an exponential law with a scale length usually larger than that of the stellar disk (see Wevers, 1984, Kennicutt, 1989). The distribution of inclinations of the sample was derived assuming that the disks are fundamentally flat structures of circular shape. The inclinations range between 45° to 60° (Fig. 1). The lack of face-on disks ($i \approx 0^\circ$) is due to the fact that the disk is a low-surface-brightness structure and therefore can hardly be seen against the bright background of the galaxy. On the contrary, galaxies with edge-on disks ($i > 75^\circ$) will appear as a dust lane due to the absorbing matter associated with the gas.

The observed gas kinematics is found to be consistent with the picture of the ionised gas being distributed in regular disk-like structures. The rotation pattern follows closely the geometry of the line-emitting region. The presence of large emission-line widths in the central

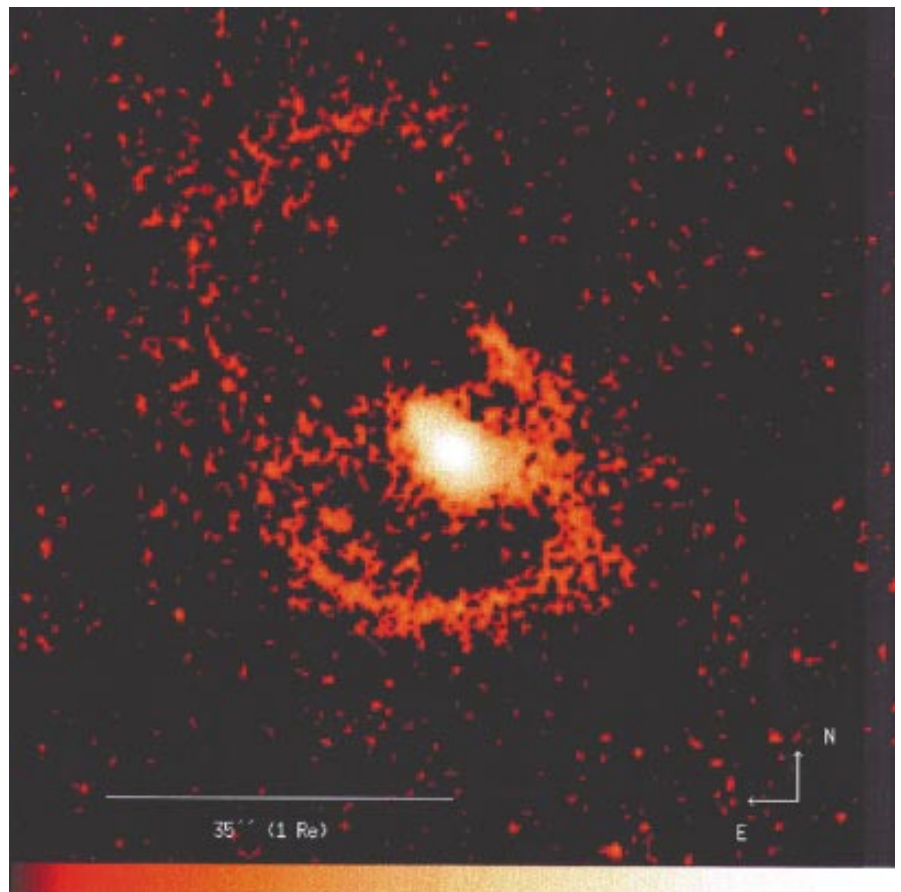


Figure 4: Narrow-band image of NGC 3962 in the light of the $[N II]+H\alpha$ emission lines obtained at the ESO/MPI 2.2-m telescope with a typical seeing of $\approx 1.1''$. The image reveals two distinct ionized gas components: an inner disk-like structure and an outer arc-like structure.

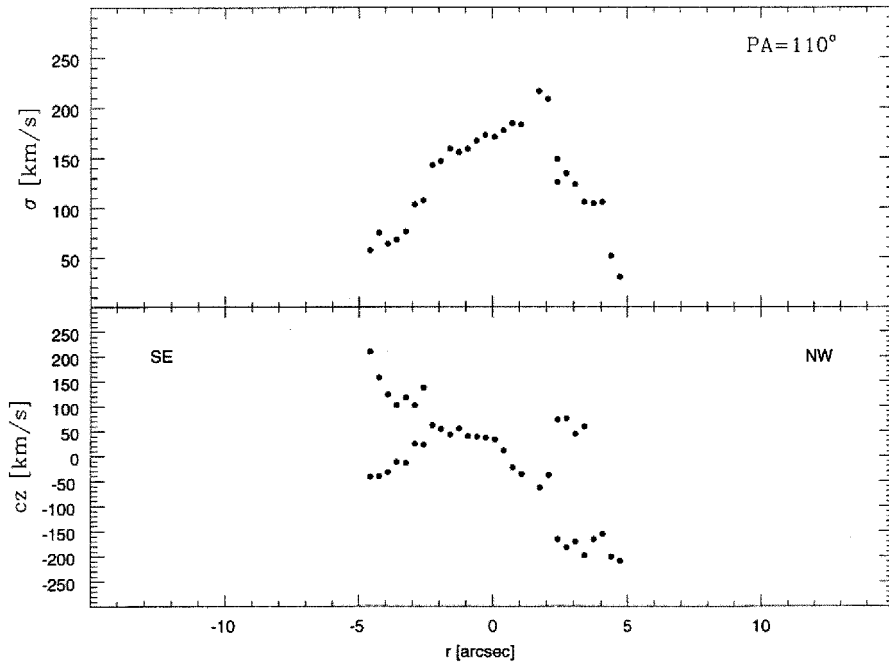


Figure 5: Ionised gas kinematics of NGC 6868 derived from the $[N II] \lambda 6583.4 \text{ \AA}$ line. The spectrum was obtained at the ESO/MPI 2.2-m telescope equipped with EFOSC2. The typical seeing was $\approx 1''$ during the exposure. The lower panel displays the radial velocity curve. In the upper panel the velocity dispersion profile is shown.

The mass distributions of the different phases of the ISM are displayed in Figure 3. The median mass of the X-ray gas is $\approx 1.5 \times 10^9 M_{\odot}$. A median dust mass of $8 \times 10^5 M_{\odot}$ was derived using IRAS measurements as indicator for the cold ISM component. If the dust/gas ratio of the Galaxy applies also to the sample galaxies the median H I mass would be of the order $8 \times 10^7 M_{\odot}$. The median mass of the ionised gas is only $6 \times 10^4 M_{\odot}$ which, however, would be about 10–100 times higher than in “normal” early-type galaxies of similar optical luminosity. The ionised gas is probably closely related to the cold (atomic and molecular) component of the ISM as also suggested by Macchetto & Sparks (1992). Under this assumption the ionised gas would contribute significantly less than 1% to the total mass of the cold component. The kinematics of the ionized gas would consequently be dominated by the underlying cold gas disk and the amount of ionized gas which is seen will depend on the number of ionised photons available rather than on the amount of gas present. This would also explain why the gas velocity field is regular despite a morphology which in some cases appears disturbed.

The analysis of the observational material revealed a number of peculiarities strongly supporting the view that significant amounts of gas result from external accretion. NGC 3962 exhibits two distinct gas structures: an elongated central disk-like component and an arm-like structure extending from the major axis of the inner gas disk (Fig. 4). The line of nodes of the two components are significantly misaligned. In NGC 6868 two

counter-rotating gas components were discovered (Fig. 5).

3. Gaseous Disks as Probe for the Galactic Potential

The programme galaxies for the modelling were selected as the cases where we established the presence of a regular disk, settled in the potential of the host galaxy (Christodoulou *et al.*, 1992; Katz & Rix, 1992). The gas should then occupy the simple closed orbits of the potential. Earlier work used circular orbits in spherical potentials to model the observed gas kinematics (Caldwell *et al.*, 1986 in the case of NGC 7097). Bertola *et al.*, (1991) used triaxial mass models with a separable potential to model the observed gas kinematics of NGC 5077. These models incorporate the proper shape of the galaxy and allow an exact analytic description of the velocity field, but correspond to density profiles with finite density cores. As a result, the elliptic closed orbits become very elongated in the central region and are unlikely to give the correct description of the gas motions there. In the

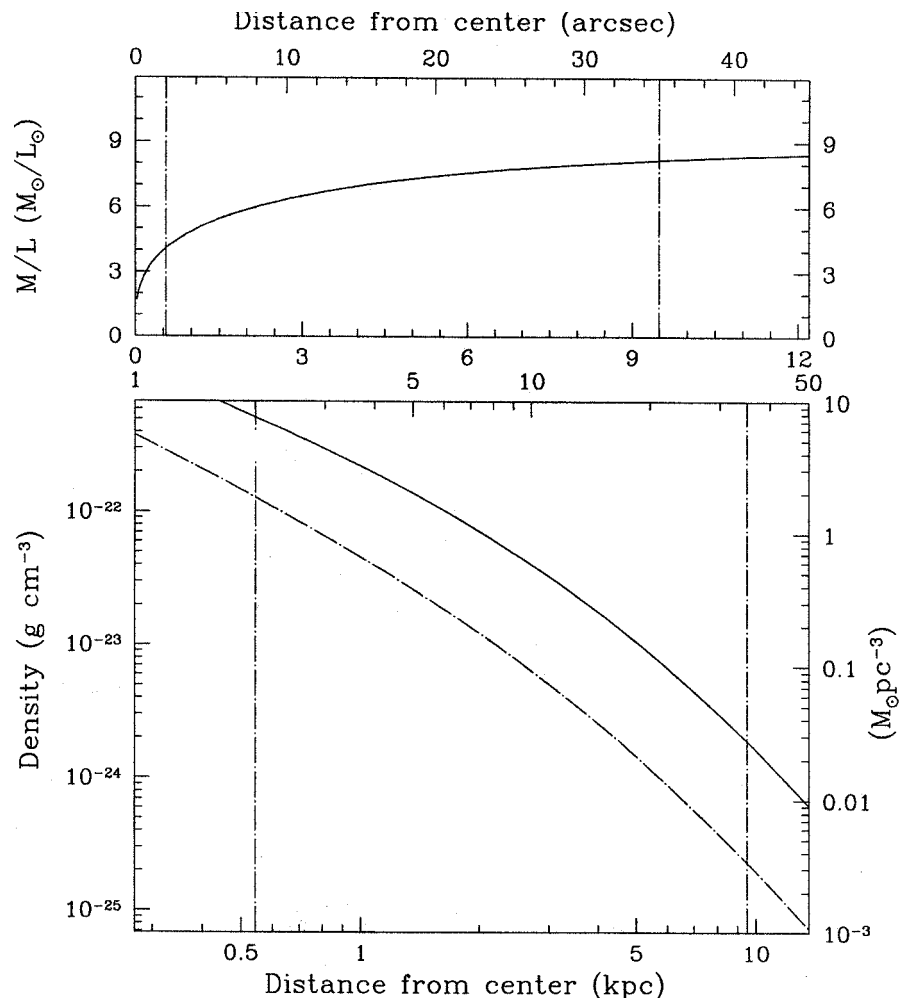


Figure 6: NGC 5077: lower panel: Mass (full line) and light (long-dashed line) density profiles. upper panel: local M/L_B ratio as a function of radius. The vertical lines define the regions where the modelling results are valid. The inner limit is defined by the seeing while the outer limit is given by the last observed kinematical data point. H_0 is 50 km/s/Mpc.

present study, a family of non-rotating triaxial mass models was used with a central density cusp as observed in the centres of many ellipticals (Crane *et al.*, 1993). These models allow for variations of ellipticity and position angle of major-axis isophotes. They are described in detail by de Zeeuw & Carollo (1996).

Out of the original sample only three galaxies (NGC 1453, NGC 2974 and NGC 7097) turned out to be suitable for modelling. In the remaining objects either presence of several gas components or non-regularities in the velocity field preclude modelling with the gas settled on simple closed orbits. The data of NGC 5077 were also modelled to be compared with the results of Bertola *et al.* (1991). The new model is found to be in reasonable agreement, but better constrained due to the more restrictive geometry (allowing for isophotal twisting). The modelling yielded for NGC 2974 and NGC 7097 that the gas moves on a plane perpendicular to the intrinsic minor axis while in NGC 1453 and NGC 5077 the gas occupies a plane perpendicular to the intrinsic major axis of the galaxy. This would also support the view of the external origin of the gaseous matter.

The resulting mass and light density profiles together with the radial trend of the local M/L_B ratio of NGC 5077 is displayed in Figure 6 as an example for the whole sample. The derived M/L profiles do not show significant radial variations. The M/L ratio seems to be higher for objects of higher optical luminosity. A mean value of $M/L \approx 5 M_\odot/L_\odot$ within $1 R_e$ was derived for the sample. This suggests that the central regions of elliptical galaxies are essentially dominated by luminous matter while dark matter becomes dynamically important only in the range of $2-3 R_e$; in this region, however, one has to use the information provided by the stellar kinematics (*e.g.* Saglia *et al.*, 1993; Bertin *et al.*, 1994; Carollo *et al.*, 1995) or resort to other tracers of the gravitational field (Bertola *et al.*, 1993). The use of X-ray data, which extend out to typically $\approx 7 R_e$ is not straightforward (*c.f.* Bertin *et al.*, 1993), although a recent combination of ASCA and ROSAT

data allowed more precise constraints on the mass distributions for NGC 720 and NGC 1332 (Buote & Canizares, 1997).

The ionised gas proves to be a good tracer of the potential of the host galaxy when compared with stellar kinematical results as in the case of NGC 2974 (Cinzano & van der Marel, 1994).

Acknowledgements

A.P. acknowledges support from a *Acciaierie Beltrame* grant. R.P.S. acknowledges the financial support by the Deutsche Forschungsgemeinschaft under SFB 375. W.W.Z. acknowledges the support of the Hochschuljubiläumstiftung der Stadt Wien (project H-112/95).

References

- Baum, S.A. & Heckman, T., 1989, *Astrophys. J.*, **336**, 69.
 Bertin, B., Bertola, F., Buson, L.M., Danziger, I.J., Dejonghe, H., Sadler, E.M., Saglia, R.P., Vietri, M., de Zeeuw, P.T. & Zeilinger, W.W., 1989, *The Messenger*, **56**, 19.
 Bertin, G., Bertola, F., Buson, L.M., Danziger, I.J., Dejonghe, H., Sadler, E.M., Saglia, R.P., de Zeeuw, P.T. & Zeilinger, W.W., 1994, *Astron. Astroph.*, **292**, 381.
 Bertin, G., Pignatelli, E. & Saglia, R.P., 1993, *Astron. Astroph.*, **271**, 381.
 Bertola, F. 1992 in "Morphological and Physical Classification of Galaxies" ed. Longo, G. *et al.*, p. 115.
 Bertola, F., Bettoni, D., Danziger, I.J., Sadler, E.M., Sparke, L.S. & de Zeeuw, 1991, *Astrophys. J.*, **373**, 369.
 Bertola, F., Pizzella, A., Persic, M. & Salucci, P., 1993, *Astrophys. J.*, **416**, L45.
 Bertola, F., Cinzano, P., Corsini, E.M., Rix, H.W. & Zeilinger, W.W., 1995, *Astrophys. J.*, **448**, L13.
 Bregman, J.N., Hogg, D.E. & Roberts, M.S., 1992, *Astrophys. J.*, **387**, 484.
 Buote, D.A. & Canizares, C.R., 1997, *Astrophys. J.*, in press.
 Buson, L.M., Sadler, E.M., Zeilinger, W.W., Bertin, G., Bertola, F., Danziger, I.J., Dejonghe, H., Saglia, R.P. & de Zeeuw, P.T., 1993, *Astron. Astroph.*, **280**, 409.
 Caldwell, N., Kirshner, R.P. & Richstone, D.O., 1986, *Astrophys. J.*, **305**, 136.
 Carollo, C.M., de Zeeuw, P.T., van der Marel, R.P., Danziger, I.J. & Qian, E.E., 1995, *Astrophys. J.*, **441**, L25.

- Cinzano, P. & van der Marel, R.P., 1994, *Mon. Not. R. astr. Soc.*, **270**, 325.
 Crane, P. *et al.* 1993, *Astron. J.*, **106**, 1371.
 Christodoulou, D.M., Katz, N., Rix, H.W. & Habe, A., 1992, *Astrophys. J.*, **395**, 113.
 Demoulin-Ulrich, M.H., Butcher, H.R. & Boksenberg, A., 1984, *Astrophys. J.*, **285**, 527.
 Faber, S.M. & Gallagher, J.S., 1976, *Astrophys. J.*, **204**, 365.
 Forbes, D.A., 1991, *Mon. Not. R. astr. Soc.*, **249**, 779.
 Katz, N. & Rix, H.W., 1992, *Astrophys. J.*, **389**, L55.
 Kennicutt, R.C., 1989, *Astrophys. J.*, **344**, 685.
 Isnapp, G.R., Turner, E.C. & Cunliffe, P.E., 1985, *Astron. J.*, **90**, 454.
 Knapp, G.R., Guhathakurta, P., Kim, D.-W. & Jura, M., 1989, *Astrophys. J. Suppl.*, **70**, 387.
 Lees, J.F., Knapp, G.R., Rupen, M.P. & Phillips, T.G., 1991, *Astrophys. J.*, **379**, 177.
 Macchetto, F. & Sparks, W.B., 1992 in "Morphological and Physical Classification of Galaxies" ed. Longo, G. *et al.*, p. 191.
 Macchetto, F., Pastoriza, M., Caon, N., Sparks, W.B., Giavalisco, M., Bender, R. & Capaccioli, M., 1996 *Astron. Astroph.*, in press.
 Phillips, M.M., Jenkins, C.R., Dopita, M.A., Sadler, E.M. & Binette, L., 1986, *Astron. J.*, **91**, 1062.
 Pizzella, A., Amico, P., Bertola, F., Buson, L.M., Danziger, I.J., Dejonghe, H., Sadler, E.M., Saglia, R.P., de Zeeuw, P.T. & Zeilinger, W.W., 1996 *Astron. Astroph.*, submitted.
 Roberts, M.S., Hogg, D.E., Bregman, J.N., Forman, W.R. & Jones, C., 1991, *Astrophys. J. Suppl.*, **75**, 751.
 Saglia, R.P., Bertin, B., Bertola, F., Danziger, I.J., Dejonghe, H., Sadler, E.M., Stiavelli, M., de Zeeuw, P.T. & Zeilinger, W.W., 1993, *Astrophys. J.*, **403**, 567.
 Schweizer, F., 1983, IAU Symp. **100**, p. 319.
 Thomas, P.A., Fabian, A.C., Arnaud, K.A., Forman, W. & Jones, C., 1986, *Mon. Not. R. astr. Soc.*, **222**, 655.
 Wevers, B.M.R.H. 1984, Ph.D. diss., University of Groningen.
 White, III, S. & Sarazin, C.L., 1991, *Astrophys. J.*, **367**, 476.
 de Zeeuw, P.T. & Carollo, C.M., 1996, *Mon. Not. R. astr. Soc.*, in press.
 Zeilinger, W.W., Pizzella, A., Amico, P., Bertin, G., Bertola, F., Buson, L.M., Danziger, I.J., Dejonghe, H., Sadler, E.M., Saglia, R.P. & de Zeeuw, P.T., 1996, *Astron. Astroph.*, in press.

Werner Zeilinger
 e-mail: wzeil@doradus.ast.univie.ac.at

The Challenging Type Ia SN 1991bg in the Virgo Galaxy NGC 4374

M. TURATTO^{1,2}, S. BENETTI¹, E. CAPPELLARO², I.J. DANZIGER^{1,3}, P.A. MAZZALI³

¹European Southern Observatory;

²Osservatorio Astronomico di Padova; ³Osservatorio Astronomico di Trieste, Italy

The long-standing effort in studying type Ia Supernovae (SN Ia) has been motivated in part by their use as distance indicators. Several publications

have recently been devoted to the absolute calibration of SN Ia up to the distance of the Virgo cluster using the Cepheids discovered by HST in the

SN parent galaxies. It is now commonly believed that the average absolute magnitude of SN Ia at maximum is close to $M_B = -19.5$, while the average

intrinsic colour is $(B - V) \approx 0.0$ (Tammann et al., 1996).

Nevertheless, it is also recognised that SN Ia are not strictly identical: most SN Ia exhibit a small scatter both in absolute magnitudes and colours. Given the accuracy of modern observations, this scatter cannot be attributed to photometric errors (Patat et al., 1996). This scatter reduces the reliability of SN Ia as standard candles unless a relation is found between the luminosity and some other observational parameter. Indeed, Phillips (1993) and Hamuy et al. (1995) have found a linear relation between the absolute magnitude, M_B , and the rate of decline in the first 15 days past maximum, $\delta(m)_{15}$. Most SNe with $\Delta(m)_{15}$ in the range $1.1 < \Delta(m)_{15} < 1.8$, conform to this relation, but there are exceptions, e.g. SN 1994D (Patat et al., 1996).

Another serious problem has been posed by the discovery of a few SN Ia showing large deviations from the average behaviour. The most extreme among these objects is SN 1991bg in NGC 4374. A spectrum of this SN taken soon after discovery (Benetti et al., 1991) showed most of the typical features of SN Ia, but also some distinct peculiarities. The unusual characteristics motivated the inclusion of this SN among the high priority targets of the ESO Key Programme on SNe. Using five different telescopes (including also the Asiago Observatory 1.8-m) we obtained spectra on 20 nights and photometric measurements on 28 epochs, spanning the period from discovery to eighteen months later.

Whereas a detailed discussion of the results of this remarkable observational effort will appear in two forthcoming papers (Turatto et al., 1996, Mazzali et al., 1996), here we emphasise the most interesting conclusions.

The first striking peculiarity of SN 1991bg is its faint luminosity: the apparent magnitude at maximum was $B_{max} = 14.75$, about 2.5 mag fainter than that of the two other SN Ia discovered in the same galaxy, SN 1957B and 1980I. In addition, the colour was very red: $(B - V)_{max} = 0.74$ instead of the typical value $(B - V)_{max} = 0.0$. In principle the faint magnitude and the red colour could indicate the presence of strong reddening in the parent galaxy, but this is not expected, since NGC 4374 is an elliptical galaxy. In the spectra, at about 5890\AA only a weak interstellar absorption is present. This can be attributed to NaI D within the Galaxy and is consistent with the small galactic extinction in the direction of NGC 4374. Adopting the distance modulus to NGC 4374 obtained with the Surface Brightness Fluctuation method ($\mu = 31.09 \pm 0.30$, Ciardullo et al., 1993), and accounting for a galactic reddening of $E(B-V) \sim 0.05 \pm 0.02$, we obtain for SN 1991bg an absolute magnitude $M_B = -16.54 \pm 0.32$. Even if one assumes for NGC 4374 the Cepheid distance to NGC

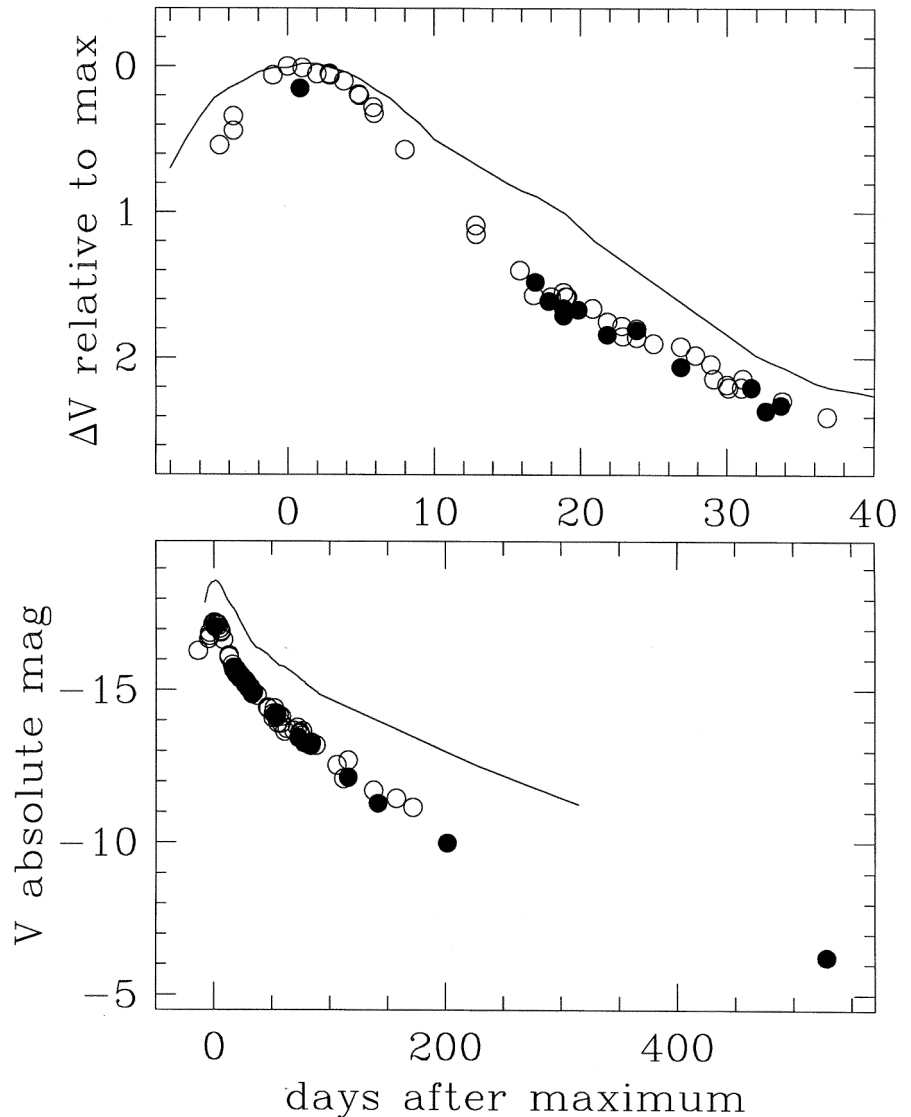


Figure 1: Comparison of the V light curve of SN 1991bg with that of the normal SN Ia 1992A. In the upper panel, the fast luminosity evolution of SN 1991bg near maximum light is emphasised. In the lower panel, the comparison of the absolute magnitudes shows that SN 1991bg was about three times fainter at maximum and, because of the more rapid evolution, the difference increases to a factor 5 on day 200. Filled symbols are our measurements and open symbols are measurements from Filippenko et al. (1992) and Leibundgut et al. (1993). At early epochs the agreement between the different sources is good, but it becomes poor as the SN fades. Since the zero point is the same (the local sequences coincide), the inconsistency is attributed to the measuring technique. We measured the magnitudes using the point spread function fitting with Romafot and with Snoopy, a package for SN photometry developed by F. Patat.

4639, which is considered to be located on the far side of the Virgo cluster (25 Mpc, Tammann et al., 1996), SN 1991bg remains 2 mag fainter than the average value for SN Ia.

Additional photometric peculiarities are the very narrow light curve and the steep luminosity decline, $\beta_B = 14.7 \text{ mag} \times (100d)^{-1}$, to be compared with a typical value $\beta_B = 12 \text{ mag} \times (100d)^{-1}$ as measured for SN 1992A (Fig. 1). Moreover, the I light curve shows no sign of the secondary maximum which is normally seen in other SN Ia about 3 weeks after the primary one. The rapid evolution is indicative of a small mass of the ejecta. In fact, a small mass implies a less efficient trapping of the γ -rays from the radioactive decays and a more rapid decrease of

temperature than in “normal” SN Ia. As a consequence, the photosphere recedes faster in mass co-ordinates, and a steep luminosity decline is observed.

Owing to the extensive coverage in several photometric bands, it was possible to obtain the *uvoir* bolometric luminosity for SN 1991bg. At maximum, this was $\log L = 42.20 \text{ erg s}^{-1}$, i.e. about 3 times fainter than the “normal” SN Ia SN 1992A ($\log L = 42.65$, Suntzeff, 1996). In the scenario where the SN light curve is powered by the radioactive decay of ^{56}Ni – ^{56}Co – ^{56}Fe , there is a direct relationship between the luminosity at maximum and the amount of ^{56}Ni produced in the explosion, although the actual estimate of the mass of radioactive material may vary by as much as 50% depending

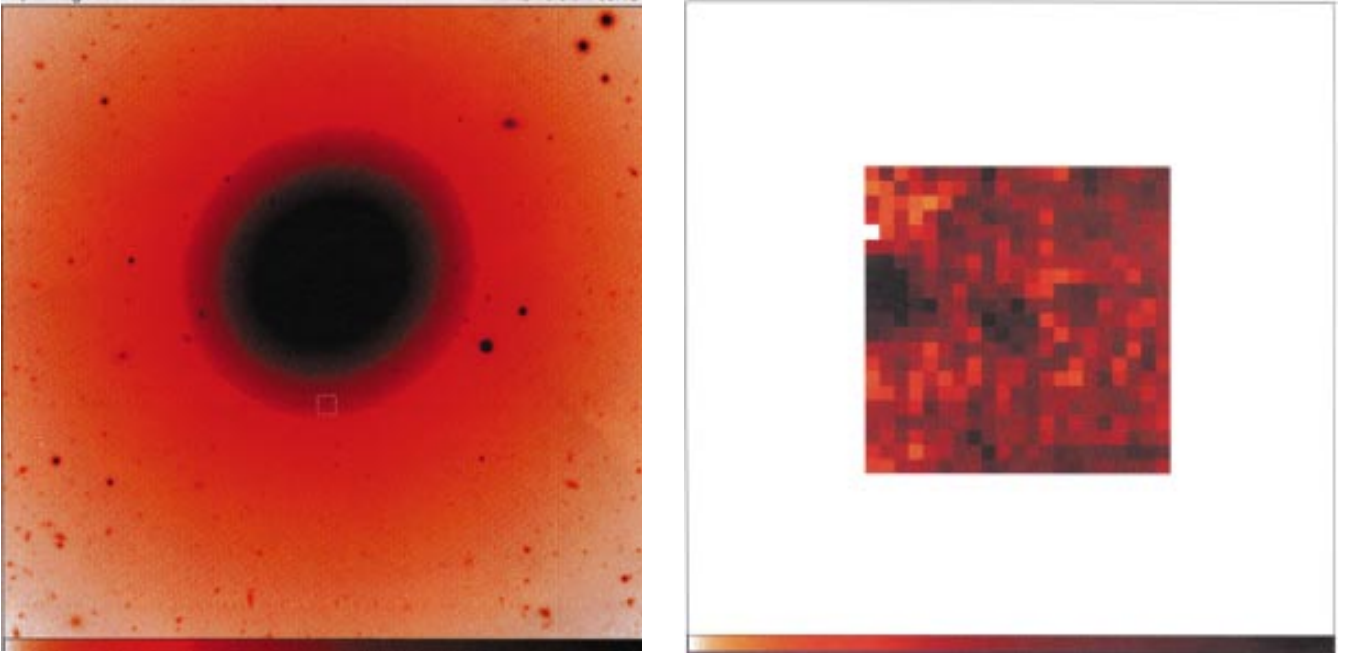


Figure 2: Co-added V image of NGC 4374 (left) obtained on May 26, 1993 (i.e. 530 days after maximum) at the NTT (+EMMI) (total exposure 170 min.). The location of SN 1991bg is marked. The SN region is enlarged and background subtracted on the right panel. Though the seeing was not exceptional (~ 1.15 arcsec), the SN was detected at $V = 24.95 \pm 0.40$.

on the explosion mechanism. If we adopt the so-called “standard model”, where normal SN Ia produce about $0.6 M_{\odot}$ of Ni, then SN 1991bg produced only about $0.2 M_{\odot}$.

Theoretical models of both early- and late-time spectra suggest that not only the Ni mass is small ($\sim 0.1 M_{\odot}$), but that the ejected mass was also small: $\sim 0.6 M_{\odot}$ compared to $1.4 M_{\odot}$ for “normal” SN Ia. Assuming that no remnant was left over, this indicates that SN 1991bg was the result of the explosion of a sub-Chandrasekhar mass progenitor.

Focusing on the spectra, SN 1991bg shows most of the typical SN Ia features due to intermediate-mass elements, in particular the strong Si III $\lambda 6355$ absorption, although with noticeable differences in the relative line intensities. The most distinctive peculiarities are the presence of an absorption between 4200 and 4500 Å, attributed to Ti II, and the low expansion velocity of the photosphere, $v_{max} = 9700 \text{ km s}^{-1}$ instead of about $v_{max} = 12,000 \text{ km s}^{-1}$ measured for SN 1992A.

The fast photometric evolution of SN 1991bg has its spectral counterpart in the early appearance of the nebular lines. Already on day 34 a relatively narrow emission line appeared at a rest frame wavelength of about 5900 Å. Because of the close coincidence in wavelength, the line was identified with the Na I D line, but in the light of the spectral modelling of Mazzali et al. (1996) we propose a significant contribution from [Co III] $\lambda 5890\text{--}5908$.

The ESO observations are especially interesting for the description of the late-time behaviour of SN 1991bg. Even at late epochs the fading rate continues to be significantly faster than those of all

other well-observed SN Ia. For instance in the V band the luminosity decline rate between 70 and 200 days was $2.7 \text{ mag} \times (100d)^{-1}$ while typical rates for SN Ia are about $1.5 \text{ mag} \times (100d)^{-1}$. With the observation shown in Figure 2 we were able to detect the SN 530 days after maximum. This last point indicates that luminosity decline slowed down significantly and became consistent, within the errors, with the radioactive decay of ^{56}Co to ^{56}Fe ($0.98 \text{ mag} \times (100d)^{-1}$). Assuming for day 530 the same spectral distribution as on day 203, the corresponding *vvoir* bolometric luminosity was $\log L \sim 38.0 \text{ ergs s}^{-1}$.

The latest spectral observation of SN 1991bg was secured 203 days after maximum. This is compared in Figure 3 with SN 1992A at a similar epoch. Contrary to previous claims, the same features are present in both spectra, although they are definitely narrower in SN 1991bg. The narrow width of the lines makes the identification of the related atomic transition easier than in normal SN Ia. The identifications are shown in Figure 3 and are based on the modelling presented in Mazzali et al. (1996). All lines find satisfactory identifications with forbidden lines of Fe-group elements, with one exception. In previous work this line was measured at 6570 Å in the galaxy rest frame and hence identified with H α . Actually the correct wavelength (obtained averaging the positions measured in three spectra) is $6590 \pm 5 \text{ Å}$. Although we cannot rule out the possibility of high-velocity blobs emitting redshifted hydrogen lines, according to our spectral modelling we suggest the identification with [Co III] $\lambda 6578$ as a possibility.

All observations indicate a scenario in which an under-energetic explosion took place in a low-mass progenitor. The weaker explosion provided less kinetic energy and a smaller amount of radioactive ^{56}Ni which in turn provided less energy to the light curve than in most SN Ia.

The existence of this unusually faint SN Ia immediately raises the question how many of these explosions occur. So far, few other SN Ia with some of the characteristics of SN 1991bg have been observed, namely SNe 1986G, 1991F and 1992K, but none of them as extreme as SN 1991bg. On the other hand, it is known that overluminous SN Ia also exist, the best example being SN 1991T (cf. Ruiz-Lapuente et al., 1992, Phillips et al., 1992, Mazzali et al., 1995).

In the context of the use of SN Ia as distance indicators, one should take care to use only those SNe which did not show photometric or spectroscopic peculiarities. Hence one should use only those SNe for which good signal-to-noise observations and an adequate temporal and spectral coverage are available.

However, when detailed modelling will be available for a good sample of SNe, it might become possible to establish diagnostic criteria correlating spectral properties and luminosity. At that point, thanks to an individual spectrophotometric calibration there may be no “peculiar” objects, but only a sequence of SNe, all of them useful as distance indicators. Some early results in this direction have already been obtained (e.g. Hoflich & Khokhlov, 1995) but much still has to be done from both the observational and the theoretical point of view.

References

- [1] Benetti, S., Cappellaro, E., Turatto, M., 1991, *IAUC* 5405.
- [2] Ciardullo, R., Jacoby, G.H., Tonry, J.L., 1993, *ApJ* **419**, 479.
- [3] Filippenko, A.V., Richmond, M.W., Branch, D., Gaskell, C.M., Herbst, W., Ford, C.H., Treffers, R.R., Matheson, T., Ho, L.C., Dey, A., Sargent, W.L.W., Small, T.A., Bruegel, W.J.M., 1992, *AJ* **104**, 1543.
- [4] Hamuy, M., Phillips, M.M., Maza, J., Suntzeff, N.B., Schommer, R.A., Aviles, R., 1995, *AJ* **109**, 1.
- [5] Hofflich, P., Khokhlov, A.M., 1995, *ApJ* **457**, 500.
- [6] Leibundgut, B., Kirshner, R., Phillips, M.M., et al., 1993, *AJ* **105**, 301.
- [7] Mazzali P.A., Chugai, N., Turatto, M., Lucy, L., Danziger, I.J., Cappellaro, E., Della Valle, M., Benetti, S., 1996, *MNRAS* in press.
- [8] Mazzali P.A., Danziger, I.J., Turatto, M., 1995, *A&A* **297**, 509.
- [9] Patat, F., Benetti, S., Cappellaro, E., Danziger, I.J., Della Valle, M., Mazzali, P., Turatto, M., 1996, *MNRAS* **278**, 111.
- [10] Phillips, M.M., 1993, *ApJ* **413**, L105.
- [11] Phillips, M.M., Wells, L.A., Suntzeff, N.B., Hamuy, M., Leibundgut, B., Kirshner, R.P., Foltz, C.B., 1992, *AJ* **103**, 1632.
- [12] Ruiz-Lapuente, P., Cappellaro, E., Turatto, M., Gouiffes, C., Danziger, I.J., Della Valle, M., Lucy, L.B., 1992, *ApJ* **387**, L33.
- [13] Suntzeff, N.B., 1996, in *Supernova and Supernova Remnants*, McCray, R. & Wang, Z., ed., Cambridge University Press, Cambridge, p.41.
- [14] Tammann, G.A., Labhardt, L., Federspiel, M., Sandage, A., Saha, A., Macchetto, F.D., Panagia, N., 1996, in *Science with the Hubble Space Telescope II*, eds. Benvenuti, P., Macchetto, F.D. & Schreier, E.J., STScI/ST-ECF Workshop, p. 9.
- [15] Turatto, M., Benetti, S., Cappellaro, E., Danziger, I.J., Della Valle, M., Gouiffes, C., Mazzali, P., Patat, F., 1996, *MNRAS* in press.

Massimo Turatto
e-mail: mturatto@eso.org

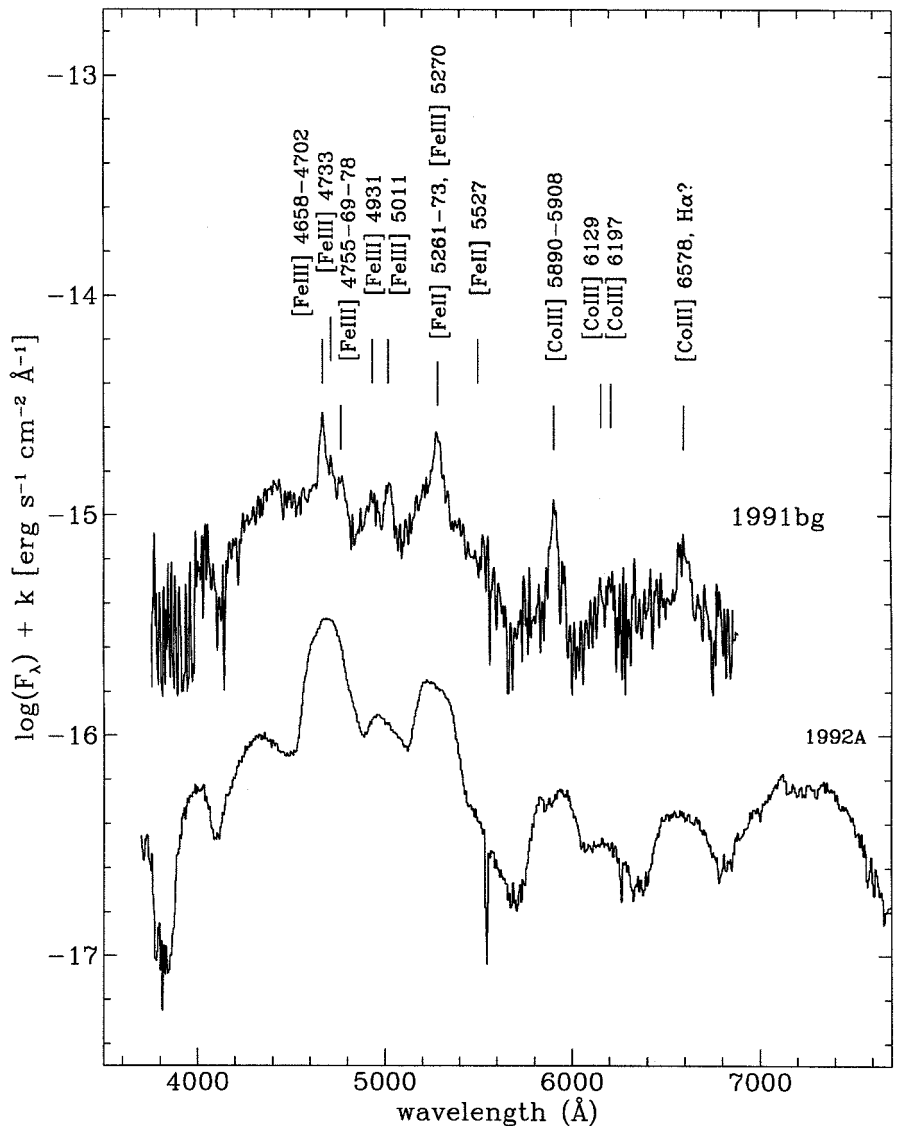


Figure 3: Comparison of the late spectra of SNe 1991bg (203 days) and 1992A (227 days), both obtained with EFOSC1 at the 3.6-m telescope. The identifications of the main emission lines are based on the NLTE models by Mazzali et al. (1996).

Long-Slit Echelle Spectroscopy at the NTT

R.L.M. CORRADI¹, A. MAMPASO¹, M. PERINOTTO²

¹Instituto de Astrofísica de Canarias, Tenerife, Spain

²Dipartimento di Astronomia e Scienza dello Spazio, Università di Firenze, Italy

During our recent observing run at La Silla (April 26–28, 1996), we had the chance to experiment successfully a previously unexplored capability of the NTT: high-dispersion spectroscopy using the full slit length of EMMI.

The EMMI-REMD (REd Medium Dispersion) spectroscopic mode is provided with three echelle gratings (#9, #10, and #14), which give spectral resolving powers of 7700, 28,000, and 60,000, respectively, for a slit width of 1" and the actual Tek 2048 × 2048 CCD #36. These gratings are normally coupled to a grism which acts as a cross-disperser to obtain

conventional multi-order echelle spectroscopy. The closeness of adjacent orders, while providing a large total spectral coverage, limits the usable slit length to a few arcseconds. For several astrophysical applications, however, it would be highly desirable to have a longer slit. This can be obtained by taking off the cross-disperser, and isolating one echelle order by means of a narrow-band filter mounted in the filter wheel unit (see the *ESO Operating Manual* No. 15, Zijlstra et al., 1996, for more details). In this way, one can take advantage of the full length of the EMMI-REMD slit (6 arc-

min!), and work at very high spectral and spatial resolutions ($R \leq 70000$, with a spatial scale of $0.27'' \text{ pix}^{-1}$, matching excellent seeing conditions which are not infrequent at the NTT).

With this configuration, the spectral coverage is of course limited to few manometers by the width of the narrow-band filter, and normally includes one or few spectral features. It is, however, a very powerful combination for many applications which concern the observation of extended objects with narrow spectral features, such as Galactic HII nebulae, and possibly external galaxies.

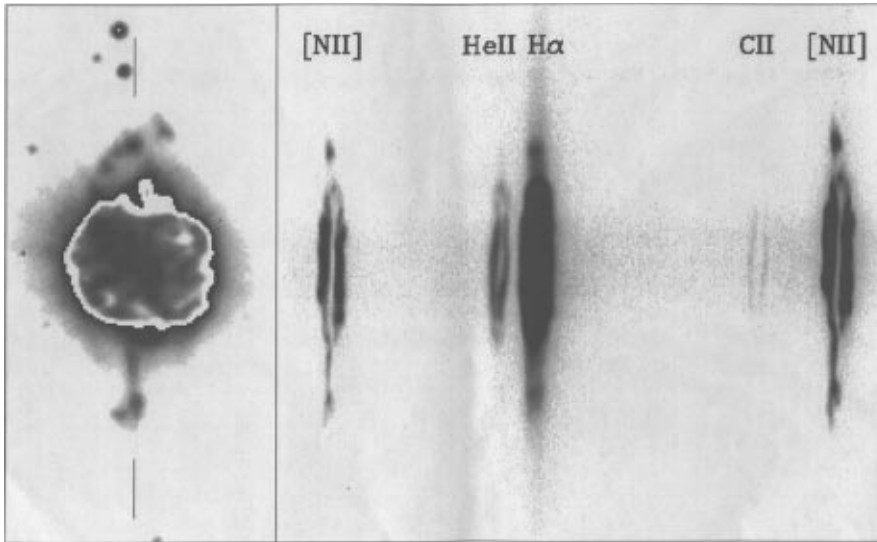


Figure 1. To the left, a [NII] image of the planetary nebula NGC 3918, rotated in order to have the adopted slit position (indicated by short lines on either side of the object) aligned with the vertical direction. Different intensity cuts have been used for the inner and outer part of the nebula. Intensity levels are on a logarithmic scale. The total extension of the figure in the vertical direction is 1 arcmin. On the same spatial scale, in order to facilitate comparison with the image, we present to the right the raw long-slit echelle spectrum of the object. The spectral region from 654.5 to 658.7 nm is displayed, corresponding to about 1000 pixels.

A limitation of this observing mode is the relatively small number of narrow-band filters available at EMMI, which however include the following important spectral features in the study of emission-line regions: He I at λ 447.1 nm, He II 468.6, H β , [O III]500.7, H α , [N II]654.8,658.3, [S II]671.6,673.1, and [S III]953.2. Some simple test should however be done in order to check if all these filters have a suitable FWHM to isolate the selected spectral range without overlapping with neighbouring orders. Another problem to be taken into account is that the filter efficiency at a given wavelength changes along the slit. This limits the accuracy of relative flux calibration along the slit, but it should not be too serious for relatively broad filters.

A rapid excursion to other European observatories shows that long-slit echelle spectroscopy can be performed at the ORM Observatory in the Canary Islands (using the 4-m WHT telescope +UES spectrograph or the 2.6-m NOT+IACUB), as well as at the Anglo-Australian Observatory (4-m AAT+ UCLES). At ESO, the 3.6-m+CASPEC is also provided with a similar capability. None of these instrumentations, apart from IACUB at the NOT, can however provide the spatial resolution of the NTT, and in any case none of them have such a remarkably long slit. In addition, and unlike the above-mentioned instrumentations, EMMI can be switched from the high-resolution spectroscopy mode to imaging or low-dispersion spectroscopy in a short time. This is very useful, for instance, for precise positioning of the target into the slit. These properties make the NTT+EMMI a unique instrument of this kind.

Our run at the NTT of past April was part of a programme aimed at investigating the nature of low-ionisation micro-

structures in planetary nebulae (PNe). Extensive imaging surveys of PNe (e.g. Schwarz et al. 1992) fully illustrate the bewildering variety of shapes that characterises this class of objects. Besides the presence of typical large-scale components (cores, shells, halos, bipolar lobes), PNe show very interesting microstructures which are enhanced in the light of low-ionisation species such as [N II], [S II], or [O I]. Some of these small-scale structures have been studied in detail by Balick and collaborators (1993, 1994), and found to be one of the most puzzling components of PNe. They usually appear in the shape of radially symmetrical pairs of knots, ansae or filaments, move supersonically through the ambient gas, and are nitrogen (only) enriched. None of the models presently available can fully account for their observed properties or can even explain their existence. We have recently identified (Corradi et al., 1996) several new candidates of this kind in 23 PNe, by using the emission-line images of Schwarz et al. (1992), and dividing the H α + [N II] frames by the [O III] ones. In the ratio maps, these ionisation features stand out clearly.

In an attempt to understand these structures, the basic piece of information is the detailed kinematics of the nebulae. As typical expansion velocities of planetary nebulae range between 10 and 30 km s⁻¹, a high spectral resolution is required in order to resolve their various kinematical components. For the purposes of our project, the possibility of obtaining long-slit spectra at $R \sim 60,000$ is therefore a very appealing one. For this reason, during the first afternoon of our observing run, we made a quick test and decided to carry on our programme with the following configuration: EMMI-REMD mode with the echelle grating #14 plus

the “broad” H α filter ESO #596, whose central wavelength and FWHM are of 656.8 and 7.3 nm, respectively. This combination isolates the spectral region containing the nebular emission lines of H α and both the [N II]654.8,658.3 collisionally excited lines. Some contamination from the same spectral lines from an adjacent order is present but does not overlap with the region of interest. Note that, having removed the cross-disperser, the spectrum appears as a conventional grating long-slit spectrum (which in fact is), with the spatial and spectral directions perpendicular to each other (apart from the usual slit distortions) as opposite to the characteristic inclined echelle multi-order spectra.

An example of a real exposure obtained during our observations is presented in Figure 1. This is a median average of three 10-min spectra of the PN NGC 3918, whose [N II] image is also presented in the left side of the figure. The slit was positioned through the collimated structures which are visible outside the main body of the nebula. Note that these features are bright in the [N II] emission, fainter in H α and invisible in He II. The velocity field is quite complex, showing an irregular shell-like expansion in the inner body of the nebula, and articulated structures with apparently low velocities (which, however, can be due to projection effects) in the collimated features. A detailed analysis of these data, coupled with low-resolution spectra to study the physical conditions and chemistry, will hopefully allow us to better understand the nature of these puzzling components of PNe, and shed new light on the very complex mass-loss phenomena which characterise the last stages of stellar evolution.

This was likely the first time that NTT+EMMI was used in this “high-dispersion long-slit” mode, and the results were indeed so good that we very much look forward to observing again with the same configuration, hopefully soon after the NTT Big Bang is completed. We conclude by warmly thanking Albert Zijlstra for the excellent support at the telescope and especially for encouraging us to try and use this “new” powerful capability of the NTT.

References

- Balick, B., Rugers, M., Terzian, Y., Chengalur, J.N.: 1993, *ApJ* **411**, 778.
- Balick, B., Perinotto, M., Maccioni, A., Terzian, Y. Hajian, A.: 1994, *ApJ* **424**, 800.
- Corradi, R.L.M., Manso, R., Mampaso, A., and Schwarz, H.E.: 1996, *AA*, in press.
- Schwarz, H.E., Corradi, R.L.M., Melnick, J.: 1992, *AAS* **96**, 23.
- Zijlstra, A.A. Giraud, E., Melnick, J., Dekker, H., D’Odorico, S.: 1996, EMMI & SUSI, *ESO Operating Manual* No.15, Version No. 3.0.

Romano L.M. Corradi
e-mail: rcorradi@iac.es

Performances of COMIC, the New Infrared Camera for ADONIS

O. MARCO ^{1, 2}, F. LACOMBE ², D. BONACCINI ³

¹Université Paris 6; ²Observatoire de Paris-Meudon; ³ESO Adaptive Optics Group

1. Introduction

COMIC is a new 1–5 μm high-resolution camera dedicated to the ESO adaptive optics system ADONIS, developed by a group from Meudon Observatory, in collaboration with the Grenoble Observatory. The 128×128 HgCdTe/CCD array detector is optimised in the 3–5 μm range. Two image scales are available: 36 mas/pixel (for J, H, short-K and K) and 100 mas/pixel (for L, L' and M), leading to fields of view of 4.5×4.5 arcsec and 12.8×12.8 arcsec, respectively.

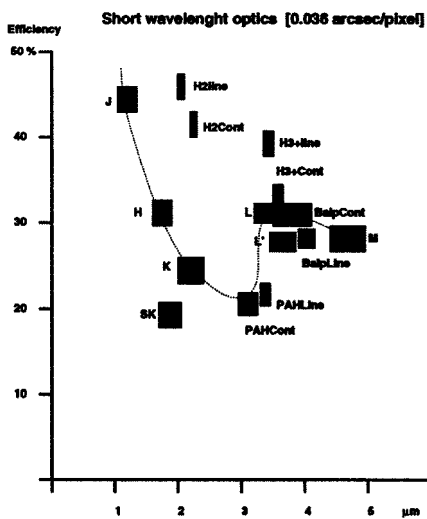


Figure 1: Efficiency for all the filters, with the short wavelength optics. The rectangles indicate the bandwidth (horizontally) and the measurement error (vertically).

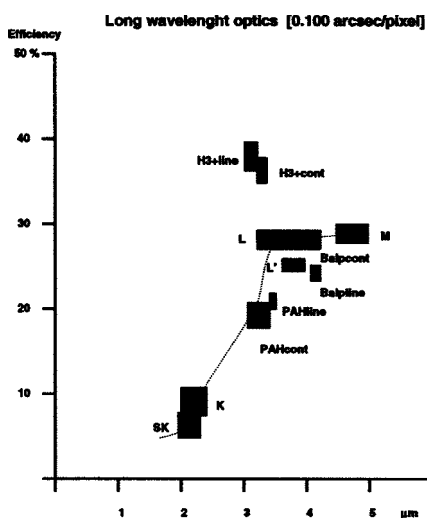


Figure 2: Efficiency for all the filters, with the long-wavelength optics. The rectangles indicate the bandwidth (horizontally) and the measurement error (vertically).

Several narrow-band filters are also available: H₂ 1-0 S(1), PAH, H3+, Br α and 2 CVF (1.2–2.5 μm and 2.4–4.8 μm with a spectral resolution of 60). It can be used in conjunction with a polarimeter unit. The measured dark current of 2000 e⁻/s/pixel at the operating temperature of 77 K allows long exposure times at short wavelengths ($\lambda < 3$ μm), as the limiting factor is the read-out noise (1000 e⁻ RMS). This camera is used at the F/45 output focus of the adaptive optics system ADONIS on the ESO La Silla 3.6-m telescope.

The quantum efficiency ranges from 60 % at 1.2 μm to 40 % at 4.5 μm . The full efficiency (including the detector and the optics) for all the filters available with COMIC (with the theoretical bandwidth and for a transmission of 1) is presented in Figure 1 for the short-wavelength optics, and in Figure 2 for the long-wavelength optics. The detector pixels have a size of 43 μm , with a pitch of 50 μm , which gives a filling factor of 74 % not reported in Figures 1 and 2.

2. The Technical Run

The COMIC technical run took place on the 3.6-m telescope with the ADONIS adaptive optics system from 1 to 5 November 1995. The adaptive optics correction was performed on the standard stars, which were chosen bright enough to provide a good signal-to-noise ratio, and an optimum wavefront correction. Standard stars, of different brightness, were observed sequentially at J, H, K, L, L' and M. For all of them, at any wavelength, we used a chopping mode: sky (OFF) positions were always taken at symmetric positions with respect to the star (ON). The distance between ON and OFF positions was always of 10", so as the star was at the field centre of the ON position, there was no contribution from the star on the OFF position. The detector integration time per frame (DIT) was taken as long as possible at long wavelengths (L', L or M), to make sure we were observing in background limiting performances (BLIP) conditions. At short wavelengths, it was reasonably

long (2 to 4 seconds), but short enough to allow an eventual analysis of background fluctuations, thermal at K, or due to the air glow at J or H.

3. Observing Procedure

As this infrared camera ranges from 1 to 5 μm , the best way to observe depends on the limiting performance factors.

At short wavelengths (J, H, K), the dark current dominates the background. The detector integration time (DIT) from which the detector is limited by the dark current is:

$$T_{\text{dark limited}} = 2 \times \frac{RON^2}{DC}$$

where RON is the read-out noise and DC the dark current. Based on the integration tests in Meudon, we find $T_{\text{dark limited}} = 1000$ s, which means that the images are RON limited at these wavelengths. As there is a large dynamic, one can have long-exposure images, but to keep the adaptive optics correction as good as possible (the seeing is changing with short time scales), we advise a maximum detector integration time of 30 s (see Table 1).

At long wavelengths (L, L', M), the instrumental emission dominates upon the dark current. The minimum time to be in background-limited performances (BLIP) condition is:

$$T_{\text{BLIP}} = 2 \times \frac{RON^2}{BG}$$

where BG is the thermal background from the instrument and the sky. We report in Table 1 the time T_{BLIP} and the maximum exposure time, corresponding to the detector saturation.

4. Imaging Performances

Based on the data from the technical nights in November 1995, we derive the imaging performances with that camera and ADONIS, under realistic observing conditions. We compute the limiting magnitude for two kinds of sources, point-like and extended. For the first

TABLE 1: Observing limitations for the standard bands.

Band	J	H	K	L	L'	M
Limitation	RON	RON	RON	BLIP	BLIP	BLIP
T_{BLIP} (ms)				500	260	150
T_{max} (s)	30	30	30	7	3.5	1.5

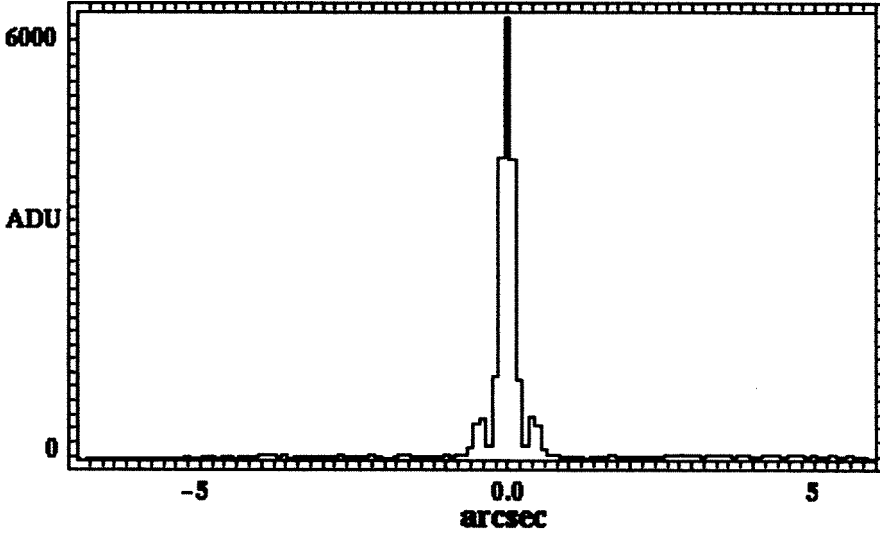


Figure 3: Cut of the bright star HR 8720 in the M band with ADONIS and COMIC. The strehl ratio is 61% for an integration time of 0.5s.

TABLE 2.

Band	J	H	K	L	L'	M
Z_0	18.6	18.4	17.8	17.7	17.2	15.7
dZ_0	0.17	0.21	0.22	0.16	0.12	0.44

one, we take into account the correction quality (which is measured by the Strehl ratio), and for the second one the pixel size and the detector filling factor.

4.1 The zero point

For any band, the zero point is defined as the star magnitude which corresponds to a detected flux of 1 ADU/s at an airmass = 0:

$$Z_0 = 2.5 \times \log(F_0[\text{ADU/s}])$$

Using the mean known extinction coefficients for La Silla, a conversion factor is derived from the flux measurement in circular apertures for the standard stars. The signal is taken as the mean (temporal) value of the flux integrated in given diaphragms for each star, and the noise is taken as the temporal fluctuations of the same quantity.

From the signal/noise ratio, we derive the photometric accuracy of the Zero point determination:

$$dZ_0 = 2.5 \times \frac{dF_0}{F_0}$$

Knowing the airmass and the atmospheric absorption, one can then compute any magnitude for a given wavelength λ and for a detector integration time as:

$$m_\lambda = Z_0 - 2.5 \times \log(F_\lambda [\text{ADU/s}])$$

$$- M [\text{airmass}] \times K_\lambda [\text{Mag/airmass}]$$

The results are summarised in Table 2:

4.2 The limiting magnitudes

Since different users will observe different kinds of objects (point-like or extended), looking for different photometric accuracy, we decide to derive the limiting magnitude:

1. from the noise equivalent power on one pixel, which is called the noise equivalent magnitude (NEM)
2. for a point-like source
3. for an extended source

As ADONIS is expected to provide a good correction, we compute all the limiting magnitudes at the angular resolution limit and for a signal-to-noise ratio of 5. As for the zero point, the results are given for an airmass = 0.

4.2.1 Evaluating the NEM

To evaluate the NEM, we compute the standard time deviation for each pixel. We take a spatial average of it, outside the circular aperture where the star is, of course. This, we assume, is repre-

sentative of the limiting power we can detect for a given DIT on one pixel, with that camera and under the given observing conditions:

$$NEM_{DIT} = Z_0 - 2.5 \times \log \left(\frac{\text{noise[ADU]}}{DIT[s]} \right)$$

To derive the limiting magnitude after a longer observing time, we extrapolate this result to a typical time of 15 minutes, taking into account that:

- at short wavelengths, we increase the DIT to a typical value of $T_{max} = 30$ s where the signal/noise ratio increases as DIT (RON limited), and then we co-add N images for which signal/noise increases as \sqrt{N} :

$$NEM_{900s} = NEM_{DIT} + 2.5 \times \log \frac{T_{max}}{DIT} + 2.5 \times \log \sqrt{\frac{900}{T_{max}}}$$

- at long wavelengths, this will be done by coadding N frames, and the signal/noise ratio increases as \sqrt{N} since the background is the limiting factor (BLIP conditions):

$$NEM_{900s} = NEM_{DIT} + 2.5 \times \log \sqrt{\frac{900}{DIT}}$$

This gives the noise equivalent magnitude corresponding to the noise equivalent power, for one pixel, for a signal/noise ratio of 1, and for an equivalent integration time T_{eq} of 15 minutes. We then scale it to a signal/noise ratio of 5.

All the results are given in Table 3.

4.2.2 Point-like sources

We have calculated the NEM for 1 pixel. There are two factors decreasing the limiting magnitude for a point-like source:

1. All the energy is not in only one pixel because of the diffraction, and there is a detector filling factor of 74 %. The pixel sampling is fixed by the two optics available, which leads to an oversampling in K, M, . . . We compute this diffraction dilution coefficient (DDC) as (E. Gendron, 1995, PhD, Université Paris 7):

$$DDC = \frac{\pi}{4} \times \frac{1 - o^2}{u^2}$$

where

Table 3: Limiting Magnitudes, $\frac{S}{N} = 5$, $T_{eq} = 900$ s.

Band	NEM	Point source		Extended source Mag/arcsec ²
		Mag	Strehl %	
J	16.8	13.0	30	9.3
H	16.9	12.5	30	9.4
K	16.5	11.8	40	9.0
L	13.9	10.7	50	8.6
L'	13.5	10.1	50	8.2
M	11.6	7.7	50	6.3

$\sigma = 0.47$ (cold diaphragm occultation)

$u = \frac{\lambda}{D}$ [pixel units] D = primary mirror diameter.

2. Diffraction theory indicates that for a *perfect* PSF, with a Strehl Ratio of 1, and without any central occultation, 84% of the energy is in the central core, i.e. within 2.44 FWHM diameter, 45.6% within the core FWHM diameter. When an adaptive optics servo-loop is aiming at diffraction-limited images, residual errors are present which leave higher energies in the surrounding halo of the long-exposure PSF, and less energy in the central core: when the Strehl ratio is less than 1, the energy is spread on more pixels. Therefore, we calculate the limiting magnitude for a significant Strehl ratio, based on our experience.

We calculate the limiting magnitude for a given sampling and a given Strehl ratio, but not as a function of the FWHM which is not the relevant information for such an estimation: for a Strehl ratio of about 30 %, the FWHM is the same as the Airy pattern of the instrument, but the image is not the theoretical one, as the correction can still be improved.

Assuming that, we estimate the equivalent magnitude of the star as:

$$m_{\text{lim}}[\text{Mag}] = \text{NEM} + \Delta m_{\text{sampling}} + 2.5 \log(\text{Strehl})$$

where

$$\Delta m_{\text{sampling}} = 2.5 \log 0.74 + 2.5 \log \text{DDC}$$

4.2.3 Extended sources

For an extended source, we need to scale the NEM to the pixel size, taking into account the filling factor:

$$m_{\text{lim}}[\text{Mag}/\text{arcsec}^2] = \text{NEM} + \Delta m_{\text{sampling}} + 2.5 \log(\text{Pix}_{\text{scale}})^2 [\text{arcsec}^2]$$

where

$$\Delta m_{\text{sampling}} = 2.5 \log 0.74$$

5. Conclusion

The main characteristics of the COMIC detector, as measured during the acceptance tests in Meudon and during the commissioning run in November 1995 show that this camera, in conjunction with the adaptive optics system ADONIS, is fully adapted to imaging operation in the 1–5 μm spectral band. The large dynamic range of the detector allows long exposure time imaging at all wavelengths, which is possible regarding the good quality of the images provided by the

adaptive optics system. A new software, including real-time facilities such as shift-and-add, dead pixels removal, sky subtraction and flat fielding, statistics (S/N, histogram, diaphragm photometry), 3D view, zoom, one pixel versus time, batch sequences, automatic log-book, ..., allows the astronomers to evaluate and improve in real time the scientific output of their observations.

The first astronomical object observed with COMIC, the bright ($M_v = 5.40$) solar type star 51 Pegasus, clearly demonstrates the excellent imaging quality of ADONIS with the COMIC camera (see *The Messenger* No. 82, December 1995). The Figure 3 clearly demonstrates the excellent imaging quality of ADONIS with the COMIC camera, on the star HR 8720: the Strehl ratio is up to 60%, and the diffraction limit is achieved, in the M band, under a median seeing condition (not better than 1.5").

Additional information is available on the ESO WEB site where under Adaptive Optics/Adonis there is an updated description of the instrumentation: www.hq.eso.org/aot/adonis/adonis.html#comic

O. Marco

e-mail: marco@hplyot.obspm.fr

OTHER ASTRONOMICAL NEWS

5th ESO/OHP Summer School in Astrophysical Observations

Observatoire de Haute-Provence, France, 15–26 July 1996

M.-P. Véron, CNRS – Observatoire de Haute-Provence; P. Crane, ESO

The 5th ESO/OHP Summer School was hosted again at the Observatoire de Haute-Provence from 15–26 July. The school which has so far only been offered bi-annually, selects 18 of Europe's most promising young doctoral students in astronomy. Courses of lectures, observations and analysis form the intellectual menu. These are aimed at the



Figure 1: As in past years, the official group photo is taken during the break in the talk by Ray Wilson. The organisers are still trying to explain this occurrence. From left to right in the first row: Ray Wilson, M.-P. Véron, K. Eriksson, V. D'Odorico. Second Row: A. Fishburn, W. Gacquer, O. Barziv, N. Christlieb, D. Russeil, G. Dudziak, H. Gleisner, E. Pompei, C. Laffont, and C. Moutou. Third row: P. Crane, T. Stanke, A. Mathieu, M. Dennefeld, R. Voors, P. Royer, J.M. Perrin, J. Fynbo, S. Darbon, P. Goudfrooij, L. Kaper, B. Geiger, H. Schmidt. Missing: Torsten Böhm.



Figure 2: Torsten Böhm explains the vagaries of data reduction systems (or is it French keyboards?) to Norbert Christlieb, Céline Laffont, and Pierre Royer

process of extracting astrophysically digestible results from photons harvested at the telescopes.

The OHP observatory is exceptionally well equipped to provide the ingredients of success for the school. The three main telescopes which are reserved for the students have state-of-the-art instruments and detectors. The site is well placed to provide a proper mix of clear skies and other facilities (proper nourishment, other sustenance, access to recreation, etc.). It is perhaps the other options which provide the ambience which insures that the various items on the menu form a coherent whole and inspire the students, their tutors, and all around to pursue the tasks at hand with vigour and enthusiasm.

The basic ingredients for the school were unchanged from previous years. Students are formed (not divided) into groups of three, and each group is assisted by a tutor. The tutors helped the students prepare observing programmes for both imaging and spectroscopy. The telescopes and instruments were prepared carefully according to the requirements of the programmes, and the observations were performed, data were obtained and analysed.

The tutors this year were: Torsten Böhm, Paul Goudfrooij, and Lex Kaper from ESO; Denis Gillet, Sergio Ilovaisky, both of whom have participated in previous years, Jean-Marie Perrin and Stephan Darbon from OHP. There is no doubt that the success of the school is very much a result of their efforts. Indeed, this has been confirmed to us by the students themselves.

T. Böhm led C. Laffont, N. Christlieb and P. Royer in a study of Herbig Ae/Be stars. With the AURELIE spectrometer, they monitored such a star to look for

spectral line variability of “active” lines which are a good indicator for the presence of a magnetically structured stellar atmosphere. At the 1.2-m telescope, they observed a young open cluster in several colours in order to classify the stars in the HR diagram.

D. Gillet led J. Fynbo, C. Moutou and E. Pompei in a study of the β Cephei star BW Vul in an attempt to distinguish between Stark broadening introduced by the passage of the compression wave and shock emission during the line-doubling phase. They used the AURELIE spectrometer to measure variations in the H β line. Their imaging project was to see if the small migrating bump reported in the light curve of XX Cygni is real or an artifact.

The group (O. Barziv, W. Gacquer and T. Stanke) led by P. Goudfrooij observed some S0 galaxies in imagery to study their (B–I) colour gradients and in spectroscopy, at the 1.93-m telescope with CARELEC, to measure metallicity gradients, using the M_{92} index.

S. Ilovaisky led V. d’Odorico, G. Dudziak and H. Gleisner in a search for an optical counterpart for ROSAT X-ray sources. They used the 1.2-m telescope to obtain multi-colour images of the X-ray fields, in order to select possible optical candidates. Using CARELEC, they then obtained low-dispersion spectra of the candidates. The spectra were searched for peculiar spectral features which would identify the optical counterpart of the X-ray source.

Under the guidance of L. Kaper, A. Mathieu, H. Schmidt and R. Voors tried to find out by imaging the field at H α with a narrow-band filter if the high-mass binary Cygnus X1 is a run-away system with an associated bow shock. At the 1.93-m telescope they have mapped a strong nebular emission line as a func-

tion of the distance from the blue variable star P Cygni.

J.-M. Perrin and S. Darbon led K. Eriksson, B. Geiger and D. Russeil in a search for extended red emission (ERE) fluorescence in the compact H II region Sh 61. Initially, interference filter images were obtained at the 1.2-m telescope in order to find the possible location of the ERE. Subsequently, low-dispersion spectra of these regions were taken with CARELEC.

The other major ingredient in the school was a series of invited lectures on topics related to observations, instrumentation, detectors, and other closely associated topics. Ray Wilson gave a stimulating lecture on the design criteria of modern telescopes and the progress that has been made in the last few years. Guy Monnet gave a comprehensive overview of instrument designs and the regions of parameter space that they fill. Michel Dennefeld described optical detectors and emphasised the physical processes and limitations of CCDs. Poul-Eric Nissen presented an overview of high-resolution spectroscopy in which he described design criteria for an echelle spectrograph, and showed some results that can be obtained. Jean-Paul Sivan’s lecture was aimed at low-resolution spectroscopy and its applications to the determination of density, temperature and abundances in various types of emission-line nebulae, to rotation curves of galaxies or to the measurements of quasar redshifts. Hermann-Josef Röser talked about imaging and photometry. His comprehensive lecture reviewed and consolidated a large number of topics partially covered by other lectures, and went on to show some real results. Richard Hook gave an overview of how computers are used in astronomy for data analysis and of some of the major software efforts in astronomy. He also described some techniques for resolution enhancement. Finally, but actually initially (although not planned that way) Michel Mayor described his own work done on site at OHP in which he discovered the first extra-solar planet around a normal star.

Of course, there were some sweet parts to the school. A Sunday excursion to the gorges du Verdon provided an opportunity to view some of the surrounding country side. This included a short stop in Moustier Sainte-Marie, a small village nestled in the side of a mountain and famous for its pottery. The trip continued on with a nice picnic at the Lac de Sainte-Croix. After the picnic, a large number of people rented paddle boats or canoes to go into the Gorges. The highlight of this was an unplanned and only marginally accidental swimming event which occurred when one group capsized in their canoe.

All schools of this sort must end, and this one did too! On the final day, each group of students presented a summary of their results. Although the analysis

techniques had for the most part just been learned, all groups presented interesting and in some cases potentially publishable results. This is no small achievement considering that most peo-

ple were entirely new to the scientific subject, the observing process, and the data analysis.

Although this school has not yet achieved the reputation of some other

schools in France, the organisers thought that each student would nevertheless appreciate the "Cordon Lavande" they received and which certifies their achievements.

ANNOUNCEMENTS

ESO Director General Reappointed

Following an Extraordinary Council Meeting on 13 September 1996, to consider the Contract of the Director General, the ESO Council extended the current mandate of Professor Riccardo Giacconi as Director General to 31 December 1999.

Professor Giacconi became Director General of ESO on 1 January 1993, after a 12-year term as Director of the Space Telescope Science Institute in Baltimore. While a Professor at Harvard University, he directed the Einstein X-ray Observatory. His early career achievements include the discovery of X-ray stars and the development of the first all-sky X-ray satellite observatory Uhuru.

PERSONNEL MOVEMENTS

(15 July – 30 September 1996)

International Staff

ARRIVALS

EUROPE

CUBY, Jean-Gabriel (F), Infrared Instrumentation Specialist
 STEINER, Katjuscha (D), Administrative Clerk Personnel
 KARBAN, Robert (A), Software Support Engineer
 PIEPER, Holger (D), Short-term Student

CHILE

PANTIN, Eric (F), Fellow
 BYSTRÖM, Rune (S), Associate SEST

DEPARTURE

EUROPE

HINTERSCHUSTER, Renate (D), Draughtswoman
 CLEMENTS, David (GB), Fellow

Local Staff Chile

ARRIVALS

RIVERA, Andres (RCH), Optical Detector Engineer

New ESO Scientific Preprints

(July–August 1996)

1158. D. Minniti et al.: High Dispersion Spectroscopy of Giants in Metal-Poor Globular Clusters. II. Oxygen and Sodium Abundances. *ApJ*.
 1159. G.A. Wade et al.: An Analysis of the Ap Spectroscopic Binary HD 59435. *AA*.
 1160. N.S. van der Bliik, J. Manfroid and P. Bouchet: Infrared Aperture Photometry at ESO (1983–1994) and Its Future Use. *AA*.
 1161. S. Hubrig and G. Mathys: The λ 3984 Feature in Late-B Spectroscopic Binaries. *AA*.
 1162. P.A. Mazzali et al.: Properties of the Be Stars in the Field of the SMC Cluster NGC 330. *AA*.

1163. D. Minniti et al.: Background Giants in the Field of the Globular Cluster M22: Kinematics of the Galactic Bulge. *A.J.*
 1164. S. Heathcote et al.: Hubble Space Telescope Observations of the HH47 Jet: Narrow Band Images.
 1165. M.-H. Ulrich: The Narrow Variable Components of C IV in NGC 4151 from 1981 to 1987. *M.N.R.A.S.*
 1166. D.L. Clements and W.J. Couch: Candidate Primeval Galaxies in the Hubble Deep Field. *M.N.R.A.S.*
 1167. R.A. Méndez and W.F. van Altena: Galactic Structure Towards the Open Clusters NGC 188 and NGC 3680. *A.J.*
 1168. S. Savaglio et al.: The Shape of the Ionising UV Background at $z \sim 3.7$ from the Metal Absorption Systems of Q0000–2619. *AA*.
 1169. F. Courbin et al.: Sub-Arcsecond Imaging and Spectroscopy of the Radio-Loud Highly Polarized Quasar PKS 1610–771. *AA*.
 1170. A.F.M. Moorwood: Starburst Galaxies. *Space Science Reviews*.
 1171. A.A. Zijlstra and J.R. Walsh: Two Planetary Nebulae in the Sagittarius Dwarf Galaxy. *AA*.
 1172. I.N. Reid et al.: Starcounts Redivivus II: Deep Starcounts with Keck and HST and the Luminosity Function of the Galactic Halo. *A.J.*
 1173. M.-H. Ulrich and K. Horne: A Month in the Life of NGC 4151: Velocity-Delay Maps of the Broad-Line Region. *M.N.R.A.S.*
 1174. G. De Marchi et al.: The Density Profile of 47 Tucanae. *ApJ Letters*.
 1175. F. Comerón, G.H. Rieke and M.J. Rieke: Properties of Low Mass Objects in NGC 2024. *ApJ*.
 1176. I. Rüedi et al.: Magnetic Field Measurements on Moderately Active Cool Dwarfs. *AA*.
 1177. Lin Yan and J.G. Cohen: A Spectroscopic Survey for Binary Stars in the Globular Cluster NGC 5053. *AJ*.
 1178. L.N. da Costa et al.: The Mass Distribution in the Nearby Universe. *ApJ Letters*.
 1179. R.A. Méndez et al.: Starcounts in the Hubble Deep Field: Constraining Galactic Structure Models. *M.N.R.A.S.*
 1180. D.L. Clements and A.C. Baker: Misclassified Merging Ultraluminous Infrared Galaxies. *AA*.
 1181. H. Boehnhardt, J. Babion and R.M. West: An Optimized Detection Technique for Faint Moving Objects on a Star-Rich Background. A Search for the Nucleus of Comet 46P/Wirtanen. *AA*.
 1182. R. Ottmann, T.A. Fleming, L. Pasquini: ROSAT All-Sky Survey Observations of Pop II Field Binaries: X-Ray Activity of Old, Metal-Poor Stellar Coronae. *AA*.
 1183. S. Moehler, U. Heber, G. Rupprecht: Hot HB Stars in Globular Clusters – Physical Parameters and Consequences for Theory. III. NGC 6752 and Its Long Blue Vertical Branch. *AA*.
 1184. P. Molaro, P. Bonifacio, F. Castelli, L. Pasquini: New Beryllium Observations in Low-Metallicity Stars. *AA*.

ESO, the European Southern Observatory, was created in 1962 to . . . establish and operate an astronomical observatory in the southern hemisphere, equipped with powerful instruments, with the aim of furthering and organising collaboration in astronomy . . . It is supported by eight countries: Belgium, Denmark, France, Germany, Italy, the Netherlands, Sweden and Switzerland. It operates the La Silla observatory in the Atacama desert, 600 km north of Santiago de Chile, at 2,400 m altitude, where fourteen optical telescopes with diameters up to 3.6 m and a 15-m submillimetre radio telescope (SEST) are now in operation. The 3.5-m New Technology Telescope (NTT) became operational in 1990, and a giant telescope (VLT = Very Large Telescope), consisting of four 8-m telescopes (equivalent aperture = 16 m) is under construction. It is being erected on Paranal, a 2,600 m high mountain in northern Chile, approximately 130 km south of Antofagasta. Eight hundred scientists make proposals each year for the use of the telescopes at La Silla. The ESO Headquarters are located in Garching, near Munich, Germany. It is the scientific, technical and administrative centre of ESO where technical development programmes are carried out to provide the La Silla observatory with the most advanced instruments. There are also extensive facilities which enable the scientists to analyse their data. In Europe ESO employs about 200 international Staff members, Fellows and Associates; at La Silla about 50 and, in addition, 150 local Staff members.

The ESO MESSENGER is published four times a year: normally in March, June, September and December. ESO also publishes Conference Proceedings Preprints, Technical Notes and other material connected to its activities. Press Releases inform the media about particular events. For further information, contact the ESO Information Service at the following address:

EUROPEAN
SOUTHERN OBSERVATORY
Karl-Schwarzschild-Str. 2
D-85748 Garching bei München
Germany
Tel. (089) 320 06-0
Telex 5-28282-0 eo d
Telefax (089) 3202362
ips@eso.org (internet)
ESO::IPS (decnet)

The ESO Messenger:
Editor: Marie-Hélène Demoulin
Technical editor: Kurt Kjär

Printed by
Druckbetriebe Lettner KG
Georgenstr. 84
D-80799 München
Germany

ISSN 0722-6691

ESO Proceedings Still Available

A number of proceedings published by ESO are still available. To permit you to complete the series or simply to inform you about any volume that you may have missed, we reproduce here a list of some recent ESO proceedings.

No.	Title and year of publication	Price
50	ESO/OAT Workshop "Handling and Archiving Data from Ground-based Telescopes", 1994	DM 35.—
51	Third CTIO/ESO Workshop on "The Local Group: Comparative and Global Properties", 1995	DM 50.—
52	European SL-9/Jupiter Workshop, 1995	DM 80.—
53	ESO/ST-ECF Workshop on "Calibrating and understanding HST and ESO instruments", 1995	DM 60.—
54	OSA/ESO Topical Meeting on "Adaptive Optics", 1996	DM 80.—

Contents

R. Giacconi: Chilean Senate Ratifies Agreement with ESO	1
---	---

TELESCOPES AND INSTRUMENTATION

S. Stanghellini: The M1 Cell-M3 Tower of the VLT – Design Overview and Manufacturing Progress	2
T. Andersen: VLT System Engineering Group Moving Ahead	6
Bo Reipurth: KODAK Technical Pan 4415 Film at the ESO Schmidt Telescope	8

THE LA SILLA NEWS PAGE

L. Pasquini, U. Weilenmann: News from the 3.6-m Upgrade Project	9
J. Fluxá, S. Guisard, G. Ihle: Report on the Technical Time in June 1996 ...	10
A. Gilliotte: M1 Aluminium and Status	11
S. Guisard: The Image Quality of the 3.6-m Telescope: Part III	12
E. Barrios: Pointing Model	13

NEWS FROM THE NTT: J. Spyromilio	13
--	----

SCIENCE WITH THE VLT/VLTI

A. Quirrenbach: ESO Workshop on Science with the VLT Interferometer	16
N. Ageorges, O. von der Lühe: Simulations of VLT/VISA Imaging Observations of Young Stellar Objects at 2.2 μ m	18

REPORTS FROM OBSERVERS

A.A. Zijlstra, D. Minniti, J. Brewer: Resolving Nearby Galaxies into Stars	23
F. Courbin, D. Hutsemékers, G. Meylan, P. Magain, S.G. Djorgovski: PKS 1610–771: a Highly Reddened Quasar?	27
A.A. Zijlstra, G. Dudziak, J.R. Walsh: Two Planetary Nebulae Discovered in the Sagittarius Dwarf Galaxy	28
W.W. Zeilinger, P. Amico, G. Bertin, F. Bertola, L.M. Buson, I.J. Danziger, H. Dejonghe, A. Pizzella, E.M. Sadler, R.P. Saglia, P.T. de Zeeuw: The Distribution of Ionised Gas in Early-Type Galaxies	30
M. Turatto, S. Benetti, E. Cappellaro, I.J. Danziger, P.A. Mazzali: The Challenging Type Ia SN 1991bg in the Virgo Galaxy NGC 4374	34
R.L.M. Corradi, A. Mampaso, M. Perinotto: Long-Slit Echelle Spectroscopy at the NTT	37
O. Marco, F. Lacombe, D. Bonaccini: Performances of COMIC, the New Infrared Camera for ADONIS	39

OTHER ASTRONOMICAL NEWS

M.-P. Véron, P. Crane: 5th ESO/OHP Summer School in Astrophysical Observations	41
--	----

ANNOUNCEMENTS

ESO Director General Reappointed	43
Personnel Movements	43
New ESO Scientific Preprints	43